Alma Mater Studiorum - Università di Bologna

SCUOLA DI SCIENZE

Dipartimento di Chimica Industriale“Toso Montanari”

Corso di Laurea Magistrale in

Chimica Industriale

Classe LM-71 - Scienze e Tecnologie della Chimica Industriale

Self-Assembly of Colloidal Particles

a Combination of Experimental and Simulation Approaches

Tesi di laurea sperimentale

CANDIDATO

DAVIDE DERELLI

RELATORE

Prof. ROBERTO BERARDI

CORRELATORE

Prof. ALFONS VAN BLAADEREN

Sessione III

Anno Accademico 2018-2019

All the experimental results described in the present thesis were obtained under the supervision of Prof. Alfons VAN BLAADEREN *within the Soft Condensed Matter & Biophysics (SCMB) group*
Debye Institute for Nanomaterials Science
Department of Physics
UNIVERSITY OF UTRECHT

There is no way around the hard work. Embrace it.
Roger Federer

Acknowledgement

First of all, I would like to thank Prof Alfons van Blaaderen who supervised me during the project. Not only he happily accepted me in the Soft Condensed Matter group, but during our various meetings he provided me of guidance and useful advices for the understanding of the topic and the acquisition of meaningful results. Thank you also to Prof Roberto Berardi for supervising me during the oral defence of the present work.

Special thanks to my daily supervisors Chris Kennedy, who introduced me to the synthesis of colloidal particles and the handling of the confocal microscope, and Robin van Damme, who helped me with the simulation inquiry and provided me the computer code for actually performing the simulation experiments.

I am grateful to Fabian for giving me appropriate advices for the synthesis of silica rods and Jessi for suggesting an effective method to circumvent the struggles connected with the spherical-confinement self-assembly procedure. Thank you to everyone in the SCM&B group for the absolutely welcoming, collaborative and enjoyable environment. In particular, I would like to mention Naveed, Rama, Carmine, Anna, Gabriele, Pepijn, Stijn and Albert.

Finally, thank you so much to all friends of the student room: Danisha, Sander, Sandra, Rutger, Bertjan, Dagney and Anan for the nice, friendly and relaxed atmosphere and for providing me of their support during the sometimes frustrating ups and downs of active research.

Abstract

In this project, self-assembly behaviour of colloidal particles was investigated by a combination of both computer simulations and experimental approach. In particular, a Brownian Dynamics algorithm was used to simulate either steep-repulsive spheres or spherocylinders in a shrinking spherical confinement. In accordance with literature, in the former case packed spheres were shown to crystallize into a distinctive icosahedral structure. In the latter study, spherocylinders clearly revealed a local tendency to form smectic layers. After the synthesis of micro-sized fluorescent-labelled silica spheres and rods, particle self-assembly in a spherical confinement was experimentally explored. While our selected method widely produced well-defined spherical supraparticles, it generally failed in inducing crystalline or liquid-crystalline ordering. This outcome was supposed to emerge due to fast compression of particles inside the confinement. In the last part of the project, Brownian Dynamics simulations of mixtures of rods and spheres in a spherical confinement were performed. Our preliminary investigation unveiled a modest tendency for rod-rich mixtures to form a binary smectic configuration. However, same-shape phase separation prominently occurred for increasing fractions of spheres. Notably, a quantitative analysis on the simulated configurations was accomplished by introduction of a novel binary smectic local order parameter.

Sommario

Questo progetto di ricerca si è incentrato sullo studio del self-assembly in spherical confinement di particelle colloidali tramite l'impiego combinato di simulazioni al computer e di metodologie sperimentali. In particolare, simulazioni rispettivamente di sfere e sferocilindri sono state effettuate con l'impiego di un algoritmo di tipo Brownian Dynamics. Analogamente a quanto riportato in letteratura, nel primo caso le sfere sono state osservate cristallizzarsi in una caratteristica struttura di forma icosaedrica a causa della pressione esercitata dal confinamento. Nel secondo caso, gli sferocilindri hanno rivelato una chiara tendenza a disporsi localmente in domini di tipo smetico. A seguito della sintesi su scala micrometrica di particelle colloidali fluorescenti, è stato esplorato sperimentalmente il comportamento di self-assembly di sfere e rod in spherical confinement. Se da un lato il metodo utilizzato si è dimostrato adatto alla produzione di supraparticelle dalla forma ben definita, in generale questo non ha condotto alla realizzazione di fasi cristalline o liquido-cristalline. La ragione di questo risultato è stata attribuita alla presumibilmente elevata velocità di compressione applicata dal confinamento. Nell'ultima parte del progetto, simulazioni di tipo Brownian Dynamics sono state impiegate per lo studio del self-assembly di miscele di rod e sfere confinate nella cavità sferica. Questo studio preliminare ha rivelato una modesta tendenza per sistemi concentrati di rod a formare una configurazione di tipo binary smectic. Tuttavia, aumentando la frazione di sfere nel sistema è stata osservata una separazione della miscela in base alla forma delle particelle constituenti. Infine, relativamente alle dinamiche analizzate è stato proposto un nuovo parametro d'ordine locale adatto alla determinazione quantitativa del grado di realizzazione della fase binary smectic.

Table of Contents

Chapter 1

Introduction

Although the word *colloid* might not be familiar to the common public, examples of colloids are spread around us in our daily life, for instance in the form of milk, shaving foam, paint or toothpaste. Coming from the greek word $\kappa\acute{o}\lambda\lambda a$ meaning *glue*, the term was introduced by the Scottish scientist Thomas Graham, who is regarded as "the father of the colloid chemistry" after his studies on colloidal diffusion and separation through dialysis [1]. A colloidal system can be defined as a dispersion of a certain substance as discrete parts called *colloids*, with size ranging from several nm to few μm, in a second phase, called a *continuum phase*, which is different either in composition or state of matter. Thus milk could be regarded as a colloidal system where liquid droplets of fat globules are dispersed in water, paint is a dispersion of solid particles (for instance titanium oxide) in a liquid solvent, while in a foam the dispersed phase consists of gas bubbles immersed either in a solid or in a liquid phase.

Due to their widespread applications, colloids have always attracted significant attention from the industrial world, with the wide spectrum of interests ranging from increasing the cleaning power of a soap or a detergent, to formulating a cosmetic more suitable for a sensitive skin, or even to creating a chocolate bar which better melts in your mouth, giving rise to a wider range of flavours. In regard of formulating more sustainable chemical products, a big effort in recent decades has been made to produce more environmental friendly paints, for instance by developing water-based paints, or by eliminating the use of the solvent at all, such as in electrostatic spray painting or in powder coating methods [2].

Other than technological significance, colloids attract a prominent interest from a scientific point of view as they can be regarded as a model system for understanding the thermodynamic behaviour of atoms and molecules. Like atoms and molecules, colloids experience continuous random motion, which is caused by the multiple collisions of the dispersed phase

with the molecules of the solvent. This interesting behaviour was first revealed by another Scottish scientist, the botanist Brown, by observing pollen grains suspended in water [3]. On the other hand, being far bigger in size than atoms and molecules, colloidal dispersions move comparatively slowly and can be observed in real space using relatively simple microscopy techniques such as confocal microscopy or even brightfield microscopy [4].

In addition to real space imaging, dramatic improvements in the comprehension of colloids systems have been achieved using computer simulations. Indeed, the availability of increasingly faster computer processors makes computational techniques a fundamental tool, not only for testing the validation of a given theory but also for performing computer experiments, which in same cases may eventually turn out be more convenient, quick or controllable than "real" experiments.

The aim of this thesis is to examine a specific colloidal systems, consisting of micron-sized silica particles suspended in a liquid phase. Particularly, my project involved both real experiments and computer simulations for the study of the self-assembly of shaped-defined particles in a spherical shrinking confinement. Self-assembly is the incredibly fascinating process which makes a randomly dispersed system assume an organized and ordered configuration due to the sum of all the complex forces which govern its behaviour. A spherical confining system could be experimentally achieved by creating a water-in-oil emulsion and by slowly decreasing the water droplet size through evaporation of the water phase (Figure 1.1). The outcome of this process may thus lead to supraparticles formed by colloidal particles arranged in an ordered configuration.

The present study involved the synthesis of rod-shaped and spherical silica particles, assembly in spherical confinement and observation of the final configuration of the system through confocal microscopy and scanning electron microscopy (SEM). In addition to real-space quantitative observation, computer simulations involving Brownian Dynamic (BD) algorithms have been employed in order to have more insight to the dynamic self-assembly process. By modelling the colloidal particles interactions with a simple hard-particle model (particles which do not overlap), we may eventually illustrate the formation of a ordered phase by simply considering the concept of entropy [5].

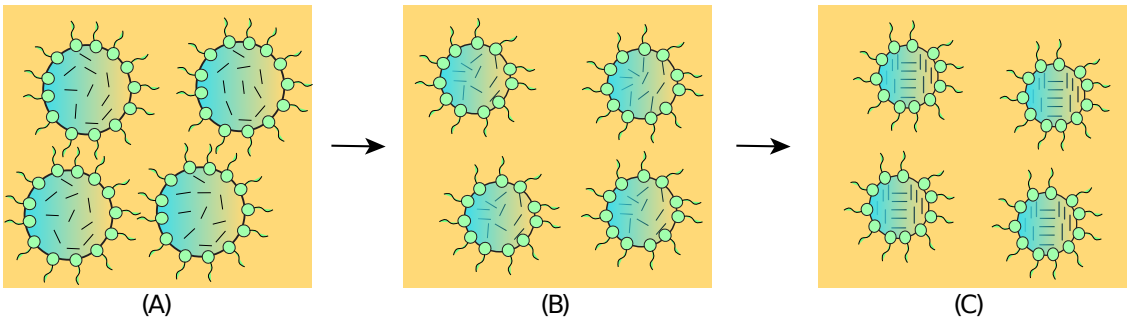

Figure 1.1: Scheme of the shrinking spherical confining conditions as experimentally explored in the present thesis. After preparation of a water-in-oil emulsion containing colloidal particles (**A**), water content is slowly evaporated so to increase particle concentration inside the water droplets (**B**). The method may in turn induce the *self-assembly* of particles in ordered strusture (**C**), thus resulting in supraparticles which may be eventually isolated and collected for further studies.

Chapter 2

Theoretical background

2.1 Main forces of a colloidal system

A wide range of complex forces determines the actual dynamics of colloidal systems. Although entire books have been written on the topic, this section will consist in a general overview of the main forces playing a role in the final configuration, namely Van der Waals forces, the electric double layer effect, Brownian motion and gravity [6].

2.1.1 Van der Waals forces

Van der Waals forces are a set of distance-dependent relatively weak forces emerging from complex electrostatic interactions between atoms, molecules or particles. Charges on two contiguous molecules, for instance, can result in either an attractive or repulsive interaction. Depending on whether both of the molecules or just one of those present a fixed non-uniform charge distribution, the Van der Waals net forces are dominated either by the Keesom multipole-multipole forces, or by the Debye induction forces. However, also uniformly charged molecules can experience an interaction potential, namely London dispersion interactions, which are always attractive and decrease with the sixth power of the distance [7]. This force, which arises from quantum mechanical considerations, can also be qualitatively explained with the formation of transient dipole moments.

Being constituted by atoms and molecules, colloidal particles also experience Van der Waals interactions. The Dutch scientist Hugo Christiaan Hamaker first developed a theory for calculating the dominating London dispersion forces for larger bodies than molecules [8]. Based on his theory, the attractive potential between two bodies in vacuum takes the form:

$$U = \frac{A_H f}{D^n} \tag{2.1}$$

Where A_H is the Hamaker constant, which depends on the material constituting the two bodies, f depends on the geometries of the two bodies at distance D and n is an integer below 6. For instance, the potential between two flat surfaces is:

$$U = \frac{A_H}{12\pi D^2} \tag{2.2}$$

Colloidal particles involved in the present study may also be modelled by using the Hamaker theory, with the additional consideration that particles are immersed in a medium. In general, the effect of the medium results in a decreased attraction between contiguous bodies, so that in some cases it may turn out become repulsive. However, it has been shown that if the interacting bodies are made of the same material, as it is for silica in this work, the net force is always attractive.

2.1.2 Electric double layer and DLVO theory

Silica surfaces immersed in a polar solvent are charged. This aspect depends on the fact that amorphous silica always includes silanol groups at the surface, which can eventually dissociate following the reaction $-SiOH \rightleftharpoons -SiO^- + H^+$. The behaviour of a charged surface immersed in a solvent was studied by Helmholtz, and then by Stern, Gouy and Chapman [9]. Those studies eventually contributed to formulate a theory known as the *Electric Double Layer (EDL) theory*, which models the charged surface as having an electric field able to attract opposite charged ions from the solvent itself [10]. The net outcome is so that a negatively charged surface emerges surrounded by a diffuse layer of positive charges, whose thickness can be expressed by the Debye length (k^{-1}) [11]:

$$k^{-1} = \sqrt{\frac{\epsilon\epsilon_0 k_B T}{2c_0 e^2}} \tag{2.3}$$

where ϵ and ϵ_0 are respectively the relative and absolute permittivity constants, k_B is the Boltzmann's constant, T is the absolute temperature, c_0 is the concentration of ions in the solvents and e is the fundamental electric charge. Although equation 2.3 is strictly valid only for planar surfaces and low potentials (Debye-Huckel Approximation), we can however deduce that the Debye length decreases in the case the concentration of the ionic species increases.

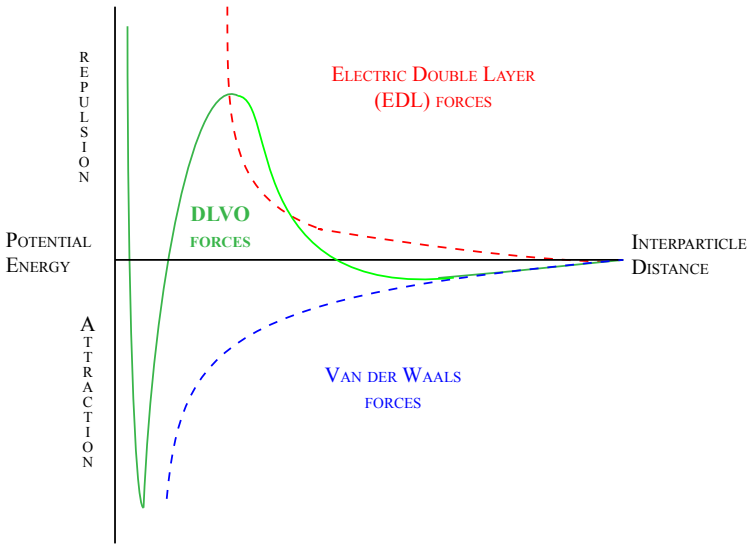

Figure 2.1: Energy potential diagram of interacting colloidal particles according to DLVO theory. DLVO forces arises as the net effect of both repulsive Electric Double Layer (EDL) and attractive Van der Waals forces

The resulting effect of the electric double layer is in stabilizing the colloidal system from aggregation. In fact, when colloidal particles approach each other so closely that both double layers overlap, an electrostatic repulsion arises. On the other hand, Van der Waals forces, briefly described in the previous section, are known to cause always an attractive interaction in the case of colloids. The net effect of these opposite forces on a colloidal system was explained by the DLVO (Derjaguin, Landau, Verwey, Overbeek) theory, named after the scientists who contributed to formulate it [12, 13]. In particular, the (repulsive) potential depending on the formation of the electric double layer can be expressed by:

$$U = Ce^{-k^{-1}D} \tag{2.4}$$

where C is a constant and D is the distance between two colloidal particles. As we have shown in the previous section (equation 2.2), the Van der Waals (attractive) potential for flat surfaces directly depend on D^{-2}. The resulting interaction strongly depends on the coefficient of the two potentials, which in turn result from a complex range of factors, for instance on the geometry of particles, properties of the media and ionic concentration in the solvent. Despite this complexity, for the systems under study the distance-dependent

potential typically takes the form as showed in Figure 2.1.

Generally, the repulsive electric double layer forces prevail at long distances and a barrier of potential energy prevents particles from approaching too close one to the other. However, if the colloidal particles are forced to come closer, they might go over the energetic barrier and find a local minima of the potential, so that the Van der Waals component stabilizes them at close distance.

According to the goal of the present thesis and after attempting the self-assembly of particles in a shrinking spherical confinement, we will take advantage of the attractive component of the interaction potential to freeze the final structure of the system. The ultimate outcome of this process will turn out be a supraparticle constituted by many colloidal particles, which we may eventually be able to collect and isolate for further use or studies.

2.1.3 Brownian motion

The world of tiny things is constantly under fast motion. This assumption was already demonstrated in 1860, when starting from statistical thermodynamics consideration, James Maxwell obtained that the probability distribution of velocities of an ideal gas was equal to [14, 15]

$$p(v) = \left(\frac{m}{2\pi k_B T}\right)^{\frac{3}{2}} e^{-\frac{mv^2}{2k_B T}} \tag{2.5}$$

Where m is the mass of the particle (or molecule), k_B is the Boltzmann constant and T is the absolute temperature. This distribution is known as the *Boltzmann-Maxwell distribution*. We may get an idea about the magnitude of this phenomenon at molecular scale, for instance by considering nitrogen (the primary component of air) at room temperature (300 K). It is easy to show that in the proposed case the most probable velocity for gas molecules is around 422 m/s. It fallows that at any moment of our life, our body immersed in the atmospheric environment constantly experience a really huge number of collisions with bodies moving at around 1500 Km/h! Although astonishing, our daily life seems not to be particularly affected by this condition due to the nanoscopic size of molecules.

That is not the case for colloids. Due to their far smaller size, the difference between the number of molecular collisions on opposite sides of the particle would cause it to constantly move back and forth in a completely random dynamic. This theory, which was first formulated by Albert Einstein and later experimentally verified by Jean Baptiste Perrin, let us to express the so called *diffusion equation* for a number N of particles moving from the

origin [16, 17]:

$$\rho(x,t) = \left(\frac{N}{4\pi Dt}\right) e^{-\frac{x^2}{4Dt}} \tag{2.6}$$

Where ρ is the particle concentration at certain position and time and D_t is the mass diffusivity (expressed in m^2/s). We can therefore conclude that the second moment of the distribution, usually referred simply as the mean squared displacement or Brownian motion, is given by:

$$\overline{x^2} = 2tD_t \tag{2.7}$$

The most important consequence of the continuous Brownian random motion of colloids is that they can assume any kind of position (and orientation) in time, so that the entire system can explore all possible configurations. As a consequence, if the system has an adequate amount of time to equilibrate, it will likely be able to reach the most stable configuration. According to our objective, our work will consist of tuning the conditions of the system so that it successfully equilibrates to form a stable configuration which may eventually turn out being an ordered one.

2.1.4 Gravity

Not being as small as atoms and molecules, the dynamics of colloid is consistently affected also by gravity. In general, the gravitational force experienced by a body can be expressed as $F(x) = mg$, where m is calculated as $m = V\delta\rho$, with V the volume of the body and $\delta\rho$ its density difference with the surrounding environment. Due to the gravitational force, particles of a colloidal suspension constantly move in the direction of the applied gravitational field, thus generating a flux of particles. By considering the *fluctuation-dissipation theorem* (FDT), it could be demonstrated that the drag force opposing the motion of particle generates a thermal fluctuation, and thus a Brownian diffusional motion. Assuming the diffusional flux and the drift flux are in equilibrium the *Einstein-Smoluchowski relation* could be eventually obtained to relate the diffusional constant D to the mobility μ [18]:

$$D = \mu k_B T \tag{2.8}$$

The *terminal velocity* reached when gravitational and diffusional effects are in equilibrium can be expressed as:

$$v_t = \frac{Dmg}{k_B T} \tag{2.9}$$

In the case of particles of spherical shape, the value of μ can be found by solving the *Stokes equation* at low Reynold's number:

$$\mu_t = \frac{1}{6\pi\eta R} \rightarrow D_t = \frac{k_\mathrm{b} T}{6\pi\eta R} \tag{2.10}$$

$$\mu_r = \frac{1}{8\pi\eta R^3} \rightarrow D_r = \frac{k_b T}{8\pi\eta R^3} \tag{2.11}$$

where η is the dynamic viscosity of the system and D_t and D_r refer to the translational and rotational diffusion coefficient.

For a more detailed explanation of the derivation of *Einstein-Smoluchowski relation* and the terminal velocity formula see *Appendix A*.

In the case of rods, translational and rotational diffusional coefficients are given by [19]:

$$D_t = \frac{k_B T ln\left(\frac{L}{D}\right) + \nu}{3\pi\eta_0 L} \quad \text{and} \quad D_r = \frac{3k_B T ln\left(\frac{L}{D}\right) + \varepsilon}{3\pi\eta_0 L^3} \tag{2.12}$$

where L and D are the length and the diameter of the rod, η_0 is the solvent viscosity and ν and ε are the end corrections. These depends on the aspect-ratio of the particles and may be estimated by [20]

$$\nu = 0.312 + 0.565\frac{D}{L} - 0.100\left(\frac{D}{L}\right)^2 \tag{2.13}$$

$$\varepsilon = \text{-}0.662 + 0.917\frac{D}{L} - 0.050\left(\frac{D}{L}\right)^2 \tag{2.14}$$

2.2 Phase behaviour of hard particles

Hard particles one of the first systems ever studied by using computer simulation techniques [21]. A *hard particle* is essentially a impenetrable particle, which means that the pairwise interaction potential is infinitely repulsive in case of overlap and zero otherwise:

$$U(i,j) = \begin{cases} \infty, & \text{if i and j overlap.} \\ 0, & \text{otherwise.} \end{cases} \tag{2.15}$$

A so defined potential evidently appears very convenient for both theoretical and computational studies. However, more than a simple model, the hard particles system has also

been shown to be suitable for the description of strongly repulsive atoms and colloids. In fact, despite the wide range of forces acting on a colloidal systems (see Section 2.1), if the repulsive barrier between two particle is steep enough, as shown in Figure 2.1, interaction between two particles can be simply modelled by assuming they do no overlap. As a consequence, hard-sphere studies are often involved in investigating the behaviour of colloidal systems. Conversely, colloids itself are usually regarded as the experimental analogous of an hard spheres systems and employed to empirically validate theories formulated by using this simple model [22].

One of the main focus of research involving hard particle has been to understand their phase behaviour, which means their abilities to form different physically distinctive form of matter. For instance, ice, liquid water and vapour are all composed by the same compound, water itself, but have completely different macroscopical properties. In the case of hard spheres, it has been shown that they form a lyotropic system, which means that their phase behaviour depends only on the concentration of the particles and not, for example, on the temperature. The phase formation is therefore determined only by entropic reasons.

In general, a system reaches it equilibrium by minimizing the Helmholtz free energy (A):

$$A = U - TS \tag{2.16}$$

where U is the potential energy and S is the entropy of the system. In the case of not overlapping hard particles, U is always zero and the free energy of the system is only determined by its entropy, which is usually defined as:

$$S = k_B \ln W \tag{2.17}$$

where k_B is the Boltzmann's constant, while W is the number of all possible microscopic configurations. For hard particles, the number of states accessible to the system are determined by the volume into which each particle can freely diffuse without bumping in an other particle. It follows that for a collection of hard particles, maximizing the entropy of the system corresponds to increasing the *free volume* available for each particle. This behaviour may conversely induce hard particles to form ordered structures, since an apparent decrease of the entropy is eventually compensated by an increase of the *free volume* available to each particle immersed in the ordered configuration.

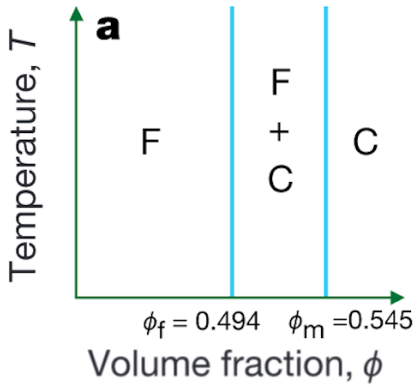

Figure 2.2: Phase diagram of a hard-spheres system. Note that in the case of not-overlapping spheres the phase behaviour depends only on the volume fraction and not on the temperature. Taken from [26]

2.2.1 Phase behaviour of hard spheres

It has been demonstrated both theoretically and by using computer simulations that a system of hard spheres can undergo a transition from a fluid to a crystal phase by increasing the particle concentration [22–24] (Figure 2.2). The transition from a completely disordered fluid phase to a more ordered one can be explained by an increase of the free volume. In bulk systems, hard spheres have been shown to crystallize in closed packed structure, such as the face-centred-cubic (FCC) crystal, which maximizes the entropy at high densities and long ranges [22, 25].

2.2.2 Phase behaviour of hard spherocylinders

The phase behaviour of anisotropic particles may attract more interest compared to spherical particles due to their possibility to display both positional or orientational order. Silica rods in particular are regarded as real models for hard spherocylinders [27]. These systems have been shown able to form ordered phases which are somewhat in between liquid and crystal and therefore called *liquid crystal phases*. Some of the possible liquid crystal phases could be the *nematic*, with orientational order, as all rods point in the same direction or *smectic*, which displays a 1D positional order in addition to orientational order, so that rods order into layers [28]. A smectic system could also further be distinguished by whether it forms layers with (*Smectic A*) or without (*Smectic B*) hexagonal intra-layer ordering. Remarkably, the spherocylinder phase behaviour strongly depends on the aspect ratio L_{cy} (which is defined as the ratio between the length of cylindrical part of the spherocylinder and its diameter),

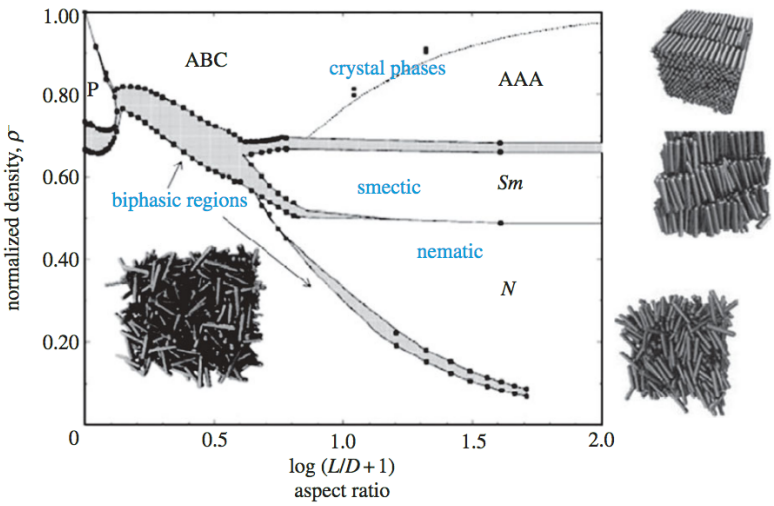

Figure 2.3: Phase diagram of a system of hard-spherocylinders. Compared to Figure 2.1, the anisotropy in the particle shapes gives the system an additional degree of freedom and a more complex phase behaviour. Taken from [30] as an adaptation of [29]

so that liquid crystal phases appear only for high values of this parameter [29] (Figure 2.3).

2.2.3 Self-assembly in spherical confinement

Self-assembly is the fascinating process in which a great number of particle self-organized in a defined structure. In this thesis, we will actually mainly focus on self-assembly in a geometrically well defined spherical environment. Experimentally, this system could be created by dispersing the colloidal particles in emulsion droplets suspended in a liquid phase [31]. By slowly evaporating the solvent inside the droplets, the surface tension constrains the particles in a smaller volume. The resulting increase of density could actually lead to the self-assembly of the colloidal particles.

It is worth noting that the interactions between particles and the droplet surface are not trivial to predict. However, in the limit of sufficiently big droplets, the influence of the droplet interface interactions could be negligible for the final configuration of the system. This consideration is supported by a work from de Nijs *et al.*, who reproduced by computer simulations the final configuration of supraparticles experimentally obtained by emulsion droplet evaporation [32]. In particular, they demonstrated that, by modelling the particle-interface forces either as attractive, repulsive or non-interactive (hard-spheres interaction), the final configuration was not significantly affected. Remarkably, the work also showed that the spherical confinement dramatically affected the crystallization pattern of

the spherical colloids. As shown in section 2.2.1 a bulk hard spheres system always crystallizes in a face-centred-cubic (FCC) structure. In fact, although already in 1952 Sir Charles Frank suggested that the local most favourable arrangement for hard spheres is in a five-fold icosahedral geometry, this symmetry is not commensurate with long-range scale [33,34]. However, this is not required anymore in a spherical confinement. As the work of de Nijs et al. clearly shows, not only do supraparticles obtained by drying emulsion droplets display a icosahedral structure, but computer simulations studies demonstrate this structure being the thermodynamically most favoured for systems constituted by up to several thousands of hard spheres.

2.3 Dynamic simulations of colloids

Being a collection of a big number of particles, each one interacting with the other and all under the influence of thermal motion, a colloidal system can fairly described as *complex*. Although very chaotic, a system of this kind may however exhibit a group common characteristic, an average emerging property which arises from the specific features and behaviour of each of its single constituents. Despite too complex to be predicted *a priori* analytically, nowadays calculation power could, under certain assumptions, allow us to computer simulate a similar system and to even predict properties a real system may eventually display. In this section, the main ideas behind the Molecular Dynamics simulations will be generally introduced. That will allow to give an overview of the Brownian Dynamics algorithm, which is the simulation method we actually employed in the present work for the study of the confined particles dynamics.

2.3.1 Molecular Dynamics (MD) simulation

Molecular Dynamics simulation is a technique for computing the equilibrium and transport properties of a many-body system. The main feature of the method is the use of the classical mechanics laws for predicting the dynamics of the system, and thus its emerging behaviour. This assumption is a very good approximation for colloidal particles, since quantum effects begin to be important at far lower dimension scales [35]. By taking explicitly into account the dynamics of the system, MD differs from other class of algorithm, like Monte Carlo simulation, in which systems are sampled according to thermodynamical laws. However, as far as simulated dynamics are able to explore all different available configurations to the system, the so-called *ergodic hypothesis* is verified and the average values over time

of physical quantities should be equal to their statistical averages. As a result, Molecular Dynamics algorithms provide the same results as obtained through Monte Carlo simulations via thermodynamics evaluation.

Let's assume of being interested in determining the total energy of a closed system consisting of N particles through a Molecular Dynamics simulation. The operator associated with the total energy is called Hamiltonian (H) and is defined as the sum of the kinetic energy (K), which is the energy associated with the movement, and potential energy (U), which is the energy possessed due to occupying a certain position in the space:

$$H(t) = K(t) + U(t) = \sum_{i=1}^{N} \frac{p_i(t) \cdot p_i(t)}{2m_i} + \sum_{i=1}^{N-1} \sum_{j=i+1}^{N} U_{ij}(r_{ij}(t)) \tag{2.18}$$

where m_i is the mass of each particle, r_i is its position and p_i its momentum. From equation 2.18, given the starting configuration and velocities of the system, we could in general calculate the change in position and momentum of each particle by resolving *Hamilton's equations of motions*:

$$x_i(t) = \frac{p_i(t)}{m_i} = \frac{\partial H(t)}{\partial p_i(t)} \tag{2.19}$$

and

$$dp_i(t) = \nabla U_i(t) = \frac{\partial H(t)}{\partial x_i(t)} \tag{2.20}$$

However, since the potential $U_i(t)$ of each particle depends on its relative position compared to all the other particles of the system, evaluating the potential implies solving a system of N coupled equations. This problem clearly doesn't have a analytic solution, which means the only viable way is to use a numerical approach.

In general, numerical methods look for the approximate solution of a complex problem by translating continuous variables and functions into discrete counterparts. In the case of MD simulations, the temporal variable t is discretized into timesteps Δt which define how good the approximated outcome is. Lower the value of Δt, more accurate is the simulated dynamics but also more computational demanding the simulation will result. Given a certain timestep, there are many available algorithms that can be used for actually solving Hamilton's equation of motions. One of the most common, and also simple, is the Velocity Verlet algorithm. Generally, given a certain set of positions and momenta at time t and a set pair potential between the particles, we can use a likewise Velocity Varlet algorithm to calculate the new positions and orientations at the time $t + \Delta t$. The process can be iterated many

times and therefore longer dynamics of the system can be simulated. The number of steps (N_{steps}) times the timestep will determine the total length of the simulation:

$$t_{sim} = N_{steps}\Delta t \tag{2.21}$$

It is important to underline that, given a certain timestep extension, different algorithm can provide different magnitude of accuracy. The *order of accuracy* is therefore defined as the power law by which the error in the evaluation method is related to the stepsize. For instance, Velocity Verlet algorithm computes the new positions of a system with a fourth order of accuracy, which means that the related error is $\propto \Delta t^4$.

2.3.2 Brownian Dynamics (BD) simulation

The dynamic of a colloidal system is not only determined by the interaction between particles. In fact, molecules of the solvent also play a fundamental role, by inducing a random Brownian motion. A way to take into account the effect of the medium could be to perform a bigger Molecular Dynamics simulation in which we explicitly take into account the molecules of the solvents. In principle, that is possible and we just need to introduce three different kind of pair potential for particle-particle, particle-solvent molecule and solvent molecule-solvent molecule interactions. However, a simulation of this kind would be absolutely too computationally onerous, as aiming to determine the dynamics of the colloidal particles, we would spend a lot of computational afford to simulate also the motion of a huge number of solvent molecules. A much more convenient approach is therefore to consider the solvent as a continuum, and to take into account the Brownian effect into the particle equation of motion [36].

In general, assuming hydrodynamics considerations of the solvent can be neglected, the effect of solvent molecules can be taken into account by using a stochastic differential equation that considers both the frictional effect of the solvent and the random motion. This is known as *Langevin dynamics*:

$$dx = \frac{p}{m}dt, \quad \text{where} \quad dp = -[\nabla U(x) - \gamma p]dt + \sqrt{2\gamma k_B T m}\, dW \tag{2.22}$$

where W indicates a stochastic Wiener process. A simplification of the classic *Langevin dynamics* could be obtained by considering the order of magnitude of the frictional constant γ. A very convenient way to estimate it is by considering the Reynold's number, which quantifies the ratio between inertial forces and viscous forces:

$$Re = \frac{inertial\ forces}{viscous\ forces} = \frac{av\rho}{\eta} \tag{2.23}$$

where η is the liquid dynamic viscosity (measured in $kg/m \cdot s$), ρ its density and a the radius of an object moving at velocity v. In the case of micro-sized colloidal particles, it can be found that $Re \ll 1$. We refer to a very interesting introduction by Purcell on how movement is affected at low Reynold's number [37]. At such low Re, the frictional constant can be considered to go to infinite, and the Langevin Dynamics can be rewritten as:

$$dx = -\frac{\nabla U(x)}{m} + \sqrt{\frac{2k_BT}{m}}dW \tag{2.24}$$

namely the *Brownian Dynamics equation of motion*. A simple and popular method for numerical solution of the above equation is the *Euler-Maruyama method*:

$$x(t+\delta t) = x(t) - \frac{\delta t}{m}\nabla U(t) + \sqrt{\frac{2k_BT\delta t}{m}}R \tag{2.25}$$

where R is a variable with a standard normal (gaussian) distribution of mean 0 and variance 1.

2.3.3 BAOAB limit case

A different algorithm for solving Langevin Dynamics in the limit of high frictional conditions was recently reported by Leimkuhler *et al* [38]. The BAOAB method consists of separating the dynamic evaluation in three different parts, which are solved sequentially. The letters A, B, O in particular refer to the motion part, the potential part and the Ornstein-Uhlenbeck stochastic part.

$$dx = \underbrace{-\frac{p}{m}dt}_{\text{A}} \quad \text{and} \quad dp = \underbrace{-\nabla U(x)dt}_{\text{B}} + \underbrace{-\gamma p dt + \sqrt{2\gamma k_BTm}\,dW}_{\text{O}} \tag{2.26}$$

In the BAOAB method, at each timestep the potential part is solved first, than the motion part, the stochastic one and then again the motion part and the potential part. Leimkuhler et al. showed that in the limit case $\gamma \to \infty$ the BAOAB algorithm reduces to:

$$x(t+\delta t) = x(t) - \frac{\delta t}{m}\nabla U(t) + \sqrt{\frac{k_BT\delta t}{2m}}(R_t + R_{t+\delta t}) \tag{2.27}$$

Although 2.27 closely resembles 2.25, in this work we preferred the BAOAB-limit algorithm as it is shown to approach a second order of accuracy for configurational averages,

while the *Euler-Maruyama method* is known be of the first order [36]. In fact, the accuracy gain in the BAOAB-limit algorithm is obtained with almost no computational expense, since the most computational onerous part, the force evaluation, is still required only once per simulation step.

2.4 Confocal Microscopy

2.4.1 The Point Spread Function (PSF)

In any imaging system, a fraction of the light emitted by a source is collected by the objective and focused at a corresponding point in the image plane. However, if the source reduces to a ideal point source, of infinitely small dimensions, the objective lens do not focus the emitted light to an infinitely small point in the image plane, but a spreader image is obtain. The obtained image and the point source are so linked by a function called the point spread function (PSF). By applying the Linear Systems Theory, any object can be approximate as the sum of a large number of point sources, each producing a point spread function in the three dimensions $PSF(x, y, z)$. It follows that the image collected with a microscope is therefore always a convolution of the imaged object function $f_{object}(x, y, z)$ and the PSF, with the addition of random noise ζ:

$$f_{image}(x, y, z) = f_{object}(x, y, z) \circledast PSF(x, y, z) + \zeta$$

where $\circledast$ indicates the convolution function, ie:

$$f_{object}(x, y, z) \circledast PSF(x, y, z) = \int_{-\infty}^{\infty} \int_{-\infty}^{\infty} \int_{-\infty}^{\infty} f_{object}(x, y, z) PSF(x + x', y + y', z + z') dx' dy' dz' \tag{2.28}$$

The operation of convolving the PSF function with the object function can be easily interpreted as the sum of the point spread functions generated by all the ideal point sources constituting the imaged object. In other words, the operation consist in summing PSFs "weighted" on the function representing the object itself.

2.4.2 Confocal laser scanning microscope (CLSM)

Confocal laser scanning microscope (CLSM) is a imaging technique characterized by two main features, the point-by-point illumination of the sample and the rejection of the out-

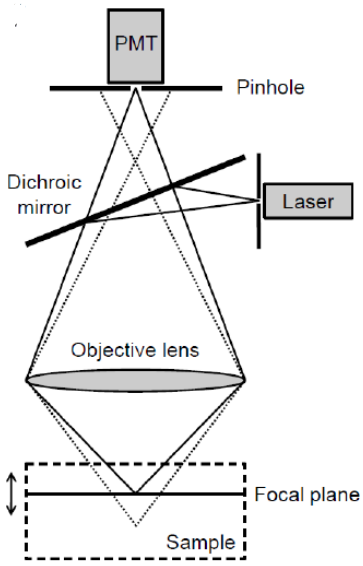

Figure 2.4: Scheme of a confocal laser scanning microscope (CLSM). Note that the presence of a pinhole in front of the detector increases the rejection of out-of-focus emission. Taken from [39].

of-focus light [40]) (Figure 2.4). Point illumination is achieved by a pinhole that is placed in front of the excitation laser combined with a high aperture objective lens, which serves as both the objective and condenser lens. When the fluorescent sample is excited, emitted light passes through the dichroic mirror and reaches the detector, while out-of-focus emission light is rejected by a pinhole placed in the conjugate focal plane of the sample. The point illumination combined with rejection of out-of-focus light results in a higher resolution, as the PSF of the confocal is the convolution of the illuminating PSF and the detection PSF. In theory, the combination of this two effects reduces its dimension by a factor $\sqrt{2}$ as compared to conventional light microscopy.

$$PSF_{conf}(x, y, z) = PSF_{ill}(x, y, z) \circledast PSF_{det}(x, y, z) \tag{2.29}$$

The PSF can be both calculated analytically or determined experimentally so to deconvolve the obtained image and partially reconstruct the original object function. It is anyway worth noting that the PSF function is more spread in the axial plane than in the lateral one, so that the resolution in the z-direction is generally lower than in xy-plane.

The resolution of the image is finally dramatically affected by refractive mismatch in the microscope setup, for instance between the lens immersion liquid and the sample or between

the sample itself and its surrounding environment (eg the solvent). In the case two medium possess different refractive index, in fact, light does not transmit linearly from one to the other, but its direction deviate. This effect in turn leads to the blurring of the image, with reduced resolution and image aberration.

Imaging of different sources in a index-matched solvent through confocal microscopy is generally possible only if the relative signals are well-separated. In fact, the point spread function net effect mainly consists in expanding the emitted signals, thus leading emissions of nearby sources to overlap. In order to image single particles constituting a concentrated colloidal systems, fluorescent-labelled cores were separated by growth of several surrounding non-fluorescent silica shells. In principle, imaging a dense phase on a single particle level is potentially achievable only if the particle fluorescent core is surrounded by a non-fluorescent coating which is thicker than the PSF dimension.

2.5 Synthesis

In last decades, a lot of effort has been put in identifying procedures to produce particles of different aspects, materials and dimensions. Nowadays, methods of variable difficulty have been developed for an incredibly wide range of shapes, ranging from spheres to cubes, from polyhedral to dumbbells to rhomboidal [41, 42]. Silica in particular is arguably a very versatile material both for the production of particles and their functionalization. Silica rods, dumbbells, spheres, cubes and cones synthesis, among others, are now available in literature [43–46]. In this section, we will focus on two specific synthetic mechanisms for the production of silica spheres and rods of micro-sized dimensions.

2.5.1 Synthesis of spheres

Monodisperse colloidal silica spheres can be prepared by a simple procedure from tetraethyloxysilane (TEOS) in ethanol. This procedure, known as Stöber method, consists of two reactions, namely hydrolysis and condensation [47] (Scheme 2.1). Both reactions are catalysed by the presence of ammonia (NH_3), which also plays a role in stabilizing the colloidal system by the creation of a basic environment, which in turn provides the particles with a negative screening surface charge.

The mechanism for the synthesis of the colloidal particles have been extensively studied, first by Helden *et al.* and subsequently by Bogush *et al.* [48, 49]. Finally, Van Blaaderen *et al.* demonstrated that the rate limiting step is the hydrolysis and that the actual formation

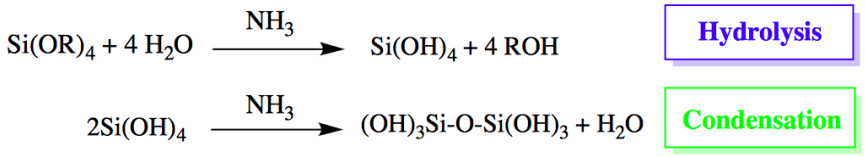

Scheme 2.1: Reaction scheme of amorphous silica synthesis via Stöber method

of the particles happens in two steps [50]. First, hydrolysis and condensation create small particles of few nm in size which are not yet stable in the solution and aggregate forming bigger particles. Then, as soon as these formed particles reach the colloidal stability due to the charges at the surface, condensation happens mainly at the surface of the formed nuclei and particles grow in dimensions. Interestingly, the starting amount of ammonia and water was found important for the final size of the colloidal particles. In fact, by decreasing the initial concentration of both species, double layer forces tend to be stronger, stabilizing the particles more. This in turn makes the aggregation step to stop early, so that a larger number of particles grows to a smaller final size.

2.5.2 Synthesis of Rods

The rod synthesis was performed according to a procedure recently reported by Kuijk *et al.* [51]. The method is based on the hydrolysis and condensation of tetraethyloxysilane (TEOS) in a system consisting of a water in 1-penthanol emulsion stabilized by polyvinylpyrrolidone (PVP) polymer and citrate (Figure 2.5). As the condensation of the alkoxysilane requires the presence of water, a silica nucleus first form at the surface of the water droplet. Successively, TEOS molecules anisotropically supplied from the water droplet itself condensate on the surface of the formed nucleus, so that the particle predominately grows from one side only. The final particles have a bullet shape, with the round side which formed first.

Importantly, the synthetic method allows the reaction conditions tp be tuned in order to obtain higher values of aspect ratio (total length over diameter of the final rod). For instance, decreasing initial water and ammonia content or increasing ethanol was shown to lead lo longer rods. However, the downside of obtaining particles of high aspect ratios consist in the eventual formation of curly rather than straight rods. Finally, note that additional silica shells can be successively grown on the surface of the bullet-shaped rods, resulting in particles which closer resemble a spherocylindrical shape.

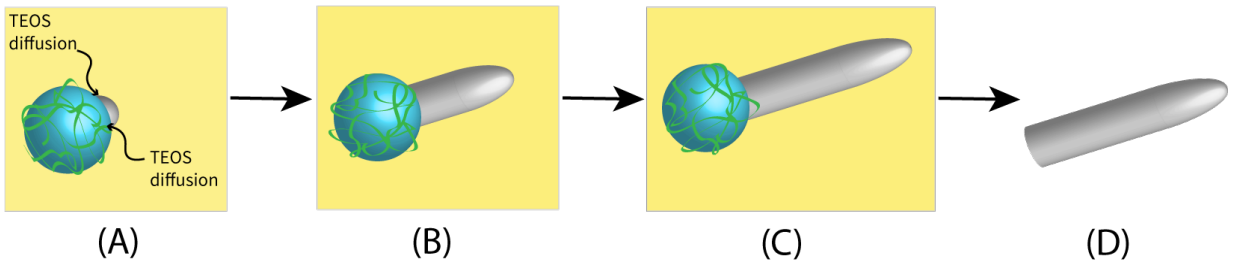

Figure 2.5: Schematic mechanism of the formation of silica rods. An emulsion of water droplet in 1-penthanol is stabilized by addition of polyvinylpyrrolidone (PVP) polymer, which is represented here as a green random coil at the water-penthanol interface. (**A**) A first nucleus of amorphous silica forms due to condensation of TEOS on the water droplet surface. (**B**), (**C**) The silica rod growth is determined due to the anysotropical supplement of hydrolysed TEOS molecules from the water phase. (**D**) The synthetic mechanism results is a bullet-shaped particle, which can be eventually isolated from the reaction mixture through successive washes.

Chapter 3

Self-assembly of Colloidal Spheres

3.1 Methods

3.1.1 Brownian Dynamics (BD) Simulations

Self-assembly of spheres in a shrinking spherical confinement was studied employing Brownian Dynamics (BD) simulations, using a code developed in the Soft Condensed Matter (SCM) group, University of Utrecht, by Robin van Damme. The dynamic of the system was evaluated at each timestep by employing the BAOAB-limit integration scheme as reported in Section 2.3.3. Spheres of diameter σ interacted through a Weeks-Chandler-Andersen (WCA) potential, which consists in a Leonard-Jones (LJ) potential truncated at the minimum potential energy of $r_{ij} = 2^{1/6}\sigma$ and shifted upward by an amount ϵ on the energy scale:

$$U(r_{ij}) = \begin{cases} 4\epsilon\left[\left(\frac{\sigma}{r_{ij}}\right)^{12} - \left(\frac{\sigma}{r_{ij}}\right)^{6}\right] + \epsilon, & \text{for } r_{ij} \leq 2^{1/6} \\ 0, & \text{for } r_{ij} > 2^{1/6} \end{cases} \tag{3.1}$$

where r_{ij} indicates the distance between particle i and j. The WCA potential was chosen as a steep repulsive potential which is computationally cheap to evaluate. The interacting potential between spheres and the confining wall was modelled using a WCA potential ten times more repulsive compared to the particle-particle potential. In order to improve the stability of the simulation, evaluated forces corresponding to a particle moving more than 1/10th of its diameter in one timestep were softened to the highest accepted value. However, the time step was kept small enough so that this truncation was hardly never necessary. All simulations were performed evolving the dynamics by linearly shrinking the spherical cavity radius and starting from a initial packing fraction $\phi_{initial} = 0.20$ to $\phi_{final} = 0.70$,

where ϕ is defined as the ratio between the total volume of the particles and the volume of the confining cavity. The shrinking rate of the cavity was therefore fully determined by the values of timestep Δt and number of steps n_t set for the specific simulation. Finally, it is worth noting that depending on the input parameters employed, simulations could become unstable for high values of ϕ. In these particular circumstances, forces might frequently exceed the threshold value and visual inspection of simulation snapshots might show particles overlapping strongly. Whenever that was the case, outcomes outside the stability region were not taken into account.

3.1.2 Identifying crystalline domains

In order to identify the crystalline domains, we identified solid-like particles using a local bond orientational order parameter based on spherical harmonics $Y_{l,m}$ [52, 53]. In particular, for each particle i we evaluated,

$$q_{l,m} = \frac{1}{N_b^i} \sum_{j=1}^{N_b^i} Y_{l,m}(r_{ij}) \tag{3.2}$$

where N_b^i is the number of neighbour particles with center of mass at distance $r_{ij} < 1.4\sigma$. We set $l = 6$ and quantified the correlation between two particles i and j by:

$$C_6(i,j) = \frac{\sum_{m=-6}^{+6} q_{6,m}(i) q_{6,m}^*(j)}{\left(\sum_{m=-6}^{6} |q_{6,m}(i)|^2 \right)^{1/2} \left(\sum_{m=-6}^{6} |q_{6,m}(j)|^2 \right)^{1/2}} \tag{3.3}$$

Finally, we considered a particle to be crystalline if it retains at least 7 solid-like connections, whereas a connection between two particles was considered solid-like if $C_6(i,j) > 0.6$. This in turn allowed us to calculate the crystalline fraction of the system, defined as the ratio between the crystalline particles and the total number of particles involved in the simulation.

In addition to evaluating the crystalline fraction of the system, different crystalline domains were identified by considering that the local environment of two neighbours solid-like particles should display more similarities if they belong to the same domains. A crystalline particle j was therefore added to the crystalline domain of particle i if $C_6(i,j) > 0.9$.

3.1.3 Synthesis of fluorescent labelled silica spheres

Core Synthesis Fluorescent silica spheres were synthesized according to a procedure reported by Van Blaaderen *et al.* [54]. First, fluorescent label precursor was prepared by adding 61.3 mg of Rhodamine isothiocyanate(RITC, mixed isomers, Sigma Aldrich) and 90 μL of the coupling agent (3-aminopropyl)triethoxysilane (APS, $\geq$ 98%, Sigma Aldrich) to 20 mL of absolute ethanol (Baker) and leaving the obtained mixture react under stirring overnight. The following day, 31.8 mL of ammonia solution in water (Sigma Aldrich, 25% wt.) and the dye precursor were added to 360 mL of absolute ethanol. After 30 min of stirring, 15 mL of tetraethyloxysilane (TEOS, Sigma Aldrich, 98%) were injected at once under strong stirring to prevent multiple nucleation events. The reaction was then left under stirring overnight.

Silica-shell growth Non-fluorescent silica shells were successively grown in the reaction mixture by successive dropwise addition of a total amount of 33.4 ml of TEOS (at a rate of 4 ml per hour) and water. Water was added so to maintain the molar ratio water:TEOS at least 10:1. The slow addition of the reagent is required so to avoid a secondary nucleation process to take place, which would eventually lead to the formation of new spherical particles of smaller size. Obtained particles were then extensively washed by centrifugation in ethanol (500g, 80min, where g is 9.81 ms^{-2}).

In order to obtain spheres of the final desired dimension and to be able to resolve single particle images through confocal microscopy, further non-fluorescent silica shells were grown by dispersing the obtained particles in 400 mL of ethanol by dropwise addition of a total of 78 ml of TEOS and 38 ml of water in presence of 32 mL of ammonia (26 v%). Obtained particles were then washed 3 times in ethanol.

After a purification procedure aimed to improve monodispersity (see Section 3.2.2 for details) 85 mg of the purified particles were dispersed in 90 mL of ethanol, 7.2 mL of ammonia (26 v%) and 4 mL of deionized water. A total amount of 360 μL of TEOS were added dropwise. Obtained particles were then washed in ethanol and redispersed in this solvent.

The particles were imaged with transmission electron microscopy (TEM, FEI Tecnai 10) after synthesis and each shell coating step to determine their sizes. At least 100 particle diameters were measured to provide reliable average dimensions and polydispersity values.

3.1.4 Self-assembly in Spherical Confinement

Self-assembly in spherical confinement can be experimentally reproduced by addition of colloidal particles into the dispersed phase of an emulsion and by its slow evaporation. In a

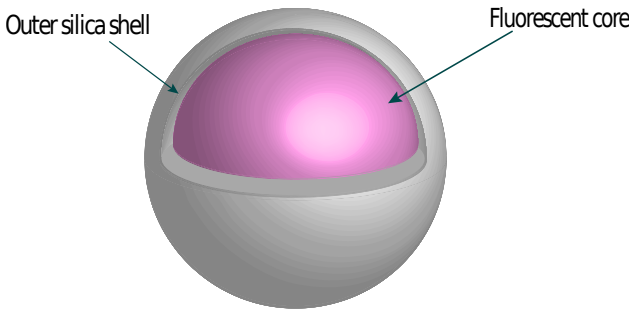

Figure 3.1: Scheme of silica spheres as synthesized in the present thesis. A rhodamine-labelled fluorescent core (*pink*) is surrounded by additional non-fluorescent silica coatings (*grey*). Synthesis of the outer silica shell is mainly aimed to separate signals emitted by adjacent particles, thus allowing imaging at single-particle level via confocal microscopy.

similar system the confinement is consequently represented by the interface tension between the two phases composing the emulsion. An obvious requirement for the procedure is the use of a moderately volatile solvent as droplet phase for the particle dispersion. In particular, as silica spheres display a considerable degree of polarity due to the dissociation of silanol groups at the surface, deionised water was selected as a harmless, inexpensive polar solvent for the colloidal particles. Hexadecane was chosen as continuum phase for the emulsion due to its high boiling point of 287°C, while SPAN80 surfactant was selected for stabilizing the water-in-oil emulsion. It is worth noting however that the selected system may in principle be completely reversed, so that a oil-in-water emulsion might be preferred after previously switching the particle polarity by coating them with an appropriate apolar polymer.

Experimentally, the considered water-in-oil emulsion was prepared in a 20-ml glass vial by addition of 100 μl of particle suspension in deionised water (8 mg/ml, 4 v% ca.) in 5 ml of hexadecane ($C_{16}H_{34}$, $\geq$ 98%, EMD Millipore, ρ = 0.773 - 0.774 g/mL) containing 1 wt% of SPAN80 surfactant (Sorbitan monooleate, Sigma Aldricht) and by subsequent shaking by hand. A shrinking spherical confinement is then obtained by slowly evaporating the water phase. This task was achieved by exploring different procedures to partially seal the vial in order to slow down the evaporation of water. The procedures generally involved the use of Teflon tape, Parafilm or a porous septa and are better discussed in Section 4.2.4. As the water phase is not density-matched with the oil phase, the system was constantly kept under mixing using a controlled shaker (IKA KS 269 basics). A mixing speed of 250 or 300 rpm was generally used. In fact, by leaving the sample undisturbed, water droplets would sediment at the bottom of the containing vial, so that the droplet shape would result

distorted thus not reproducing anymore a well-defined spherical confinement. The dryness of the sample was eventually determined by visual inspection, as the strongly scattering emulsion was observed to turn clear after water had evaporated. After evaporation of the water phase, the vial was removed from the controlled shaker and left undisturbed to allow sedimentation of the colloidal particles. After removing the oil supernatant, particles were washed once with around 5 ml of hexane and concentrated again by sedimentation. Samples for the scanning electron microscope (SEM) analysis were prepared by casting few drops of the concentrated solution in hexane on a silica mirror and drying it overnight in the oven at 65°C so to remove hexadecane impurities. SEM images were taken with Phenom ProX microscope.

3.1.5 Confocal microscopy

Selection of the solvent Colloidal particles were generally imaged in a refractive index-matched solution so to maximize the photon detection and to reduce blurring. In particular, two different solvent mixtures composed by dimethylsulfoxide (DMSO)/water (93wt%) and glycerol/water (85wt%) were employed to (nearly) index-match amorphous silica, which have a refractive index of $\nu_D^{25} = 1.45$ [55] (Table 3.1). The glycerol/water mixture was used principally for its high viscosity, which slows down the Brownian motion of the particles allowing better imaging. It is worth noting that in these polar solvents the ionic strength is generally controlled by traces of the ions present as small impurities. As shown in Section 2.1.2, the ionic strength influences the Debye screening length of the colloidal particles. In order to ensure reproducibility especially in the case of the sedimentation experiments, lithium chloride salt (LiCl) was added to the index-matched mixtures to the final concentration of 6.5 x 10^{-4}M of this salt. It has been estimated experimentally in the group that for a concentration of 5.5 x 10^{-4}M LiCl in glycerol/water (85:15 wt.) the Debye length is approximatively 10.3 nm [56]. Due to its use in a slightly higher concentration, we expect in our case the Debye length to be shorter than that value.

Preparation of the imaging cell for supraparticles Confocal microscopy samples of supraparticles obtained through spherical confinement self-assembly were prepared as follows. After washing the supraparticles with hexane, the concentrated dispersion in hexane was dropped on a microscope coverglass. After solvent evaporation, a bi-adhesive tape was cut in the central part to display a squared hole at the center. The tape was then stuck on the coverglass leaving the hole in correspondence with the cast particles. A droplet of a

Solvent	ρ (g/ml) ($25°C$)	n_D	η (cP)
DMSO	1.096 [57]	1.477 ($25°C$) [57]	1.99 ($25°C$) [57]
glycerol	1.258 [58]	1.474 ($20°C$) [58]	1410 ($20°C$) [58]
93 w% DMSO/water	1.096 [57]	1.472 ($20°C$) [39]	2.6 ($22°C$) [39]
85 w% glycerol/water	1.219 [58]	1.452 ($20°C$) [39]	92 ($22°C$) [39]

Table 3.1: Properties of solvents and solvent mixtures used in the present thesis. ρ indicates the density, n_D the refractive index and η the absolute viscosity.

index-matched glycerol/water mixture was then added to the sample and finally a second coverglass was stuck on the top of the former one, so that the solvent mixture containing the particles was segregated between the two coverglasses in the width of the tape.

Confocal imaging Confocal microscopy images were recorded with a Leica SP8 microscope. Either a 100×/1.4 (oil) or a 93×/1.35 (glycerol) (Leica) immersion lenses was used. In particular, the 93×/1.35 (glycerol) lent combined with a glycerol/water (85:15 wt.) mixture as immersion liquid was preferred in the case of sedimentation experiments. As we aimed to image deep into the sample a small index mismatched between the immersion medium and the sample itself would in fact result in considerably blurred images. This undesired effect was therefore minimized in most cases by using the same mixture both as solvent for the colloidal system and immersion liquid for the microscopy. Both the 100×/1.4 (oil) and the 93×/1.35 (glycerol) lenses were coupled with a 170 μm thick (#1.5) coverglass. As we aimed to deconvolve the acquired images, voxel dimensions were set to 50x50x100 nm, so to approximate the dimensions of the PSF for this microscope. Deconvolution was carried out with Huygens Professional commercial software using the Classic Maximum Likelihood Estimation algorithm [59]. Generally, the deconvolution was found a crucial step for dramatically increase the resolution of the obtained images.

Since the colloidal spheres were labelled with rhodamine dye, laser pulse set at the excitation frequency of 552 nm was employed coupled with a hybrid detector set to detect photons in emission spectrum between 540 nm and 700 nm.

As described in Section 2.4, confocal microscope main feature consist in rejecting out-of-focus light using a pinhole placed in the conjugated focal plane of the sample. In particular, the pinhole size may be tuned depending on sample under investigation. The diameter of the pinhole of the Leica SP8 microscope can be modified from 1.0 Airy units AU to around 0.25 (AU). Smaller is the pinhole, more out-of-focus light is rejected but also lower is the

detected signal-to-noise ratio. In the case of silica spheres of size around 0.5 μm, the pinhole diameter was set at values between 0.35 and 0.50 AU.

Exciting laser intensity can in turn be increased in order to generate more signal in the detection region. However, as the particles were labelled with an organic dye, overexposure to the excitation light leads to fast degradation of the dye and bleaching of the particles. In order to control this effect, the speed of the image acquisition may be tuned so to collect images of adequate quality but avoiding extensive bleaching of the sample.

3.2 Results and discussion

3.2.1 Brownian Dynamics simulations on spherical particles

Since the main focus of the present thesis consisted in studying the self-assembly of colloidal particles through spherical confinement, we first moved to simulate the dynamics of colloidal spheres in a shrinking spherical cavity. As reported in Section 2.2.3, a similar study involving both experiments and simulations had already been realized within the group by De Nijs *et al.* [32].

Their work had remarkably suggested that the final crystalline geometry of the system was dramatically affected by the presence of the confinement, since it preferentially displayed an anti-Mackay geometry rather than the most common face-centred-cubic (FCC) structure of bulk systems. However, while the referred work was completed using Event Driven Molecular Dynamics (EDMD) algorithm, we preferred employing Brownian Dynamic (BD) simulations as easier to extend to anisotropic particles.

Inspired by De Nijs *et al.*, we modelled interaction between particles and the confining wall by using a WCA potential, being it a steep repulsive potential (see Section 3.1.1). In fact, the referred study already demonstrated that spherical particles spontaneously assemble in anti-Mackay geometry both in a hard and in a soft repulsive spherical confinement. Finally, WCA potential was used also for modelling an (almost) hard-particle interaction between colloidal spheres.

A first series of simulations were exploited in order to identify a reliable value of timestep Δt for later studies. The timestep represents a crucial parameter in dynamic simulations, since it determines their actual quality in describing a real system. By underestimating its value, the system cannot sufficiently evolve in the given simulation number of steps with the result that the simulated time is too short to be significant. On the other hand, by overestimating it we over-discretize the continuum time variable, so that the outcomes do

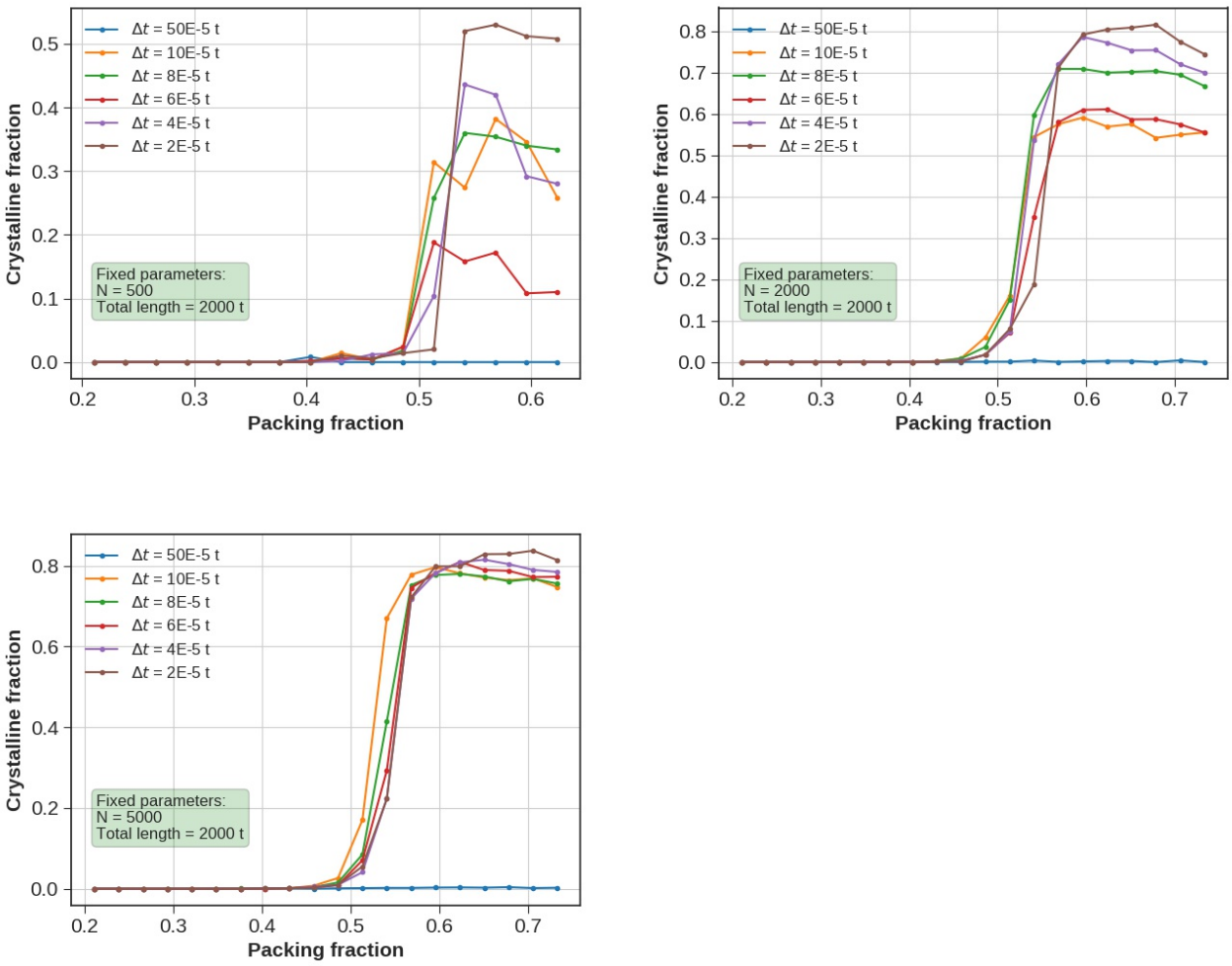

Figure 3.2: Fraction of crystalline particles as a function of packing fraction ϕ for different values of timestep Δt as indicated in the legend. For each diagram, common parameters for the set of simulations are reported in the green box.

not have any real physical significance. A range of timesteps was therefore considered for different sets of particle numbers. The number of timesteps were adjusted in order to simulate the same overall time of 2000 t for all cases. The outcomes were then quantitatively analysed by plotting the crystalline fraction of spheres (as described in Section 3.1.2) on the linearly increased packing fraction ϕ (Figure 3.2). Note that since the packing fraction increases with the time, an increase in packing fraction can also be considered as moving forward in time.

Our analysis revealed that when the timestep was short enough a large part of the confined spherical particles crystallized. In particular, a steep increase of the crystalline fraction suggests that a first-order phase transition takes place between $\phi = 0.48$ and $\phi = 0.54$.

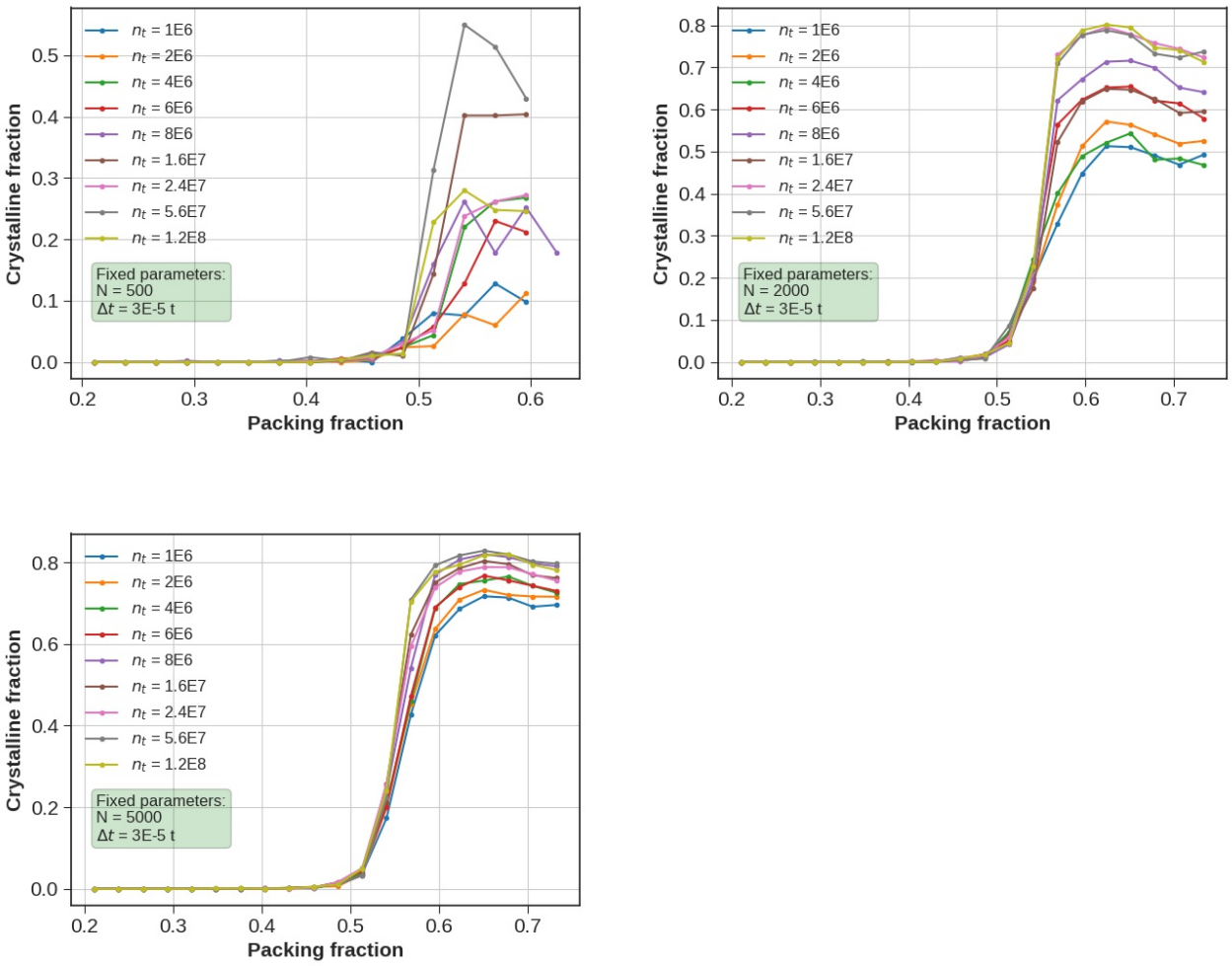

Figure 3.3: Fraction of crystalline particles as a function of packing fraction ϕ for different number of timesteps n_t as indicated in the legend. For each diagram, common parameters for the set of simulations are reported in the green box.

Moreover, the final amount of crystalline particles increases for smaller timestep, although this effect appears more severe when a smaller number of particles is involved. In fact, we observed that the constraining influence of the confinement is more significant for smaller systems. This conclusion is also supported by the fact that simulations for $N = 500$ revealed instabilities already at values of ϕ down to 0.65. This outcome clearly results from considering spheres as incommensurate to the spherical cavity, thus that they leave some empty spaces when self assemble. If the system is small, the optimal configuration for filling the available space is reached at lower values of ϕ, so that if particles are forced in an even narrower region they cannot but overlap, thus generating strong repulsive forces which ultimately

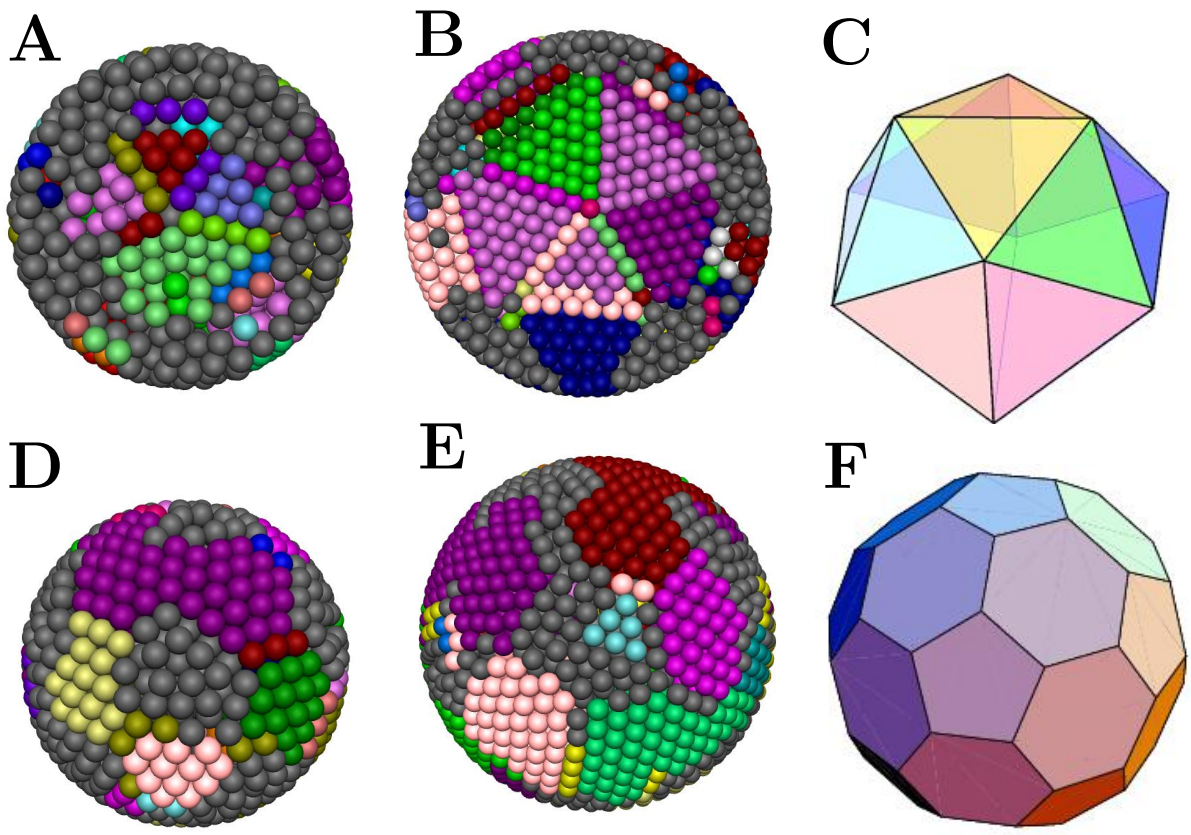

Figure 3.4: **A** Internal arrangement of $N = 2000$ spherical particles in a shrinking confining cavity. Different crystalline domains are identified with different colours. The typical five-fold symmetry of a icosahedral configuration is visible. **B** Internal arrangement of $N = 5000$ spheres. Icosahedral structuring for the system is easily detectable. **C** Reproduction of a convex regular icosahedron solid. **D** External arrangement of a system composed by $N = 2000$ and **E** $N = 5000$ spherical particles. Note that the crystalline domains seemingly constitute a truncated icosahedral structure as shown in **F**.

lead to instabilities in the simulation. Finally, it is worth noting that in case of the small system of 500 particles the evaluation of the crystalline fraction resulted in a more noisy trend, although it anyway displays the same general feature as other bigger systems.

By estimating the quality of the simulation on the final degree of crystallinity reached by particles, we evaluated simulations run for $\Delta t = 2E-5$ and $\Delta t = 4E-5$ as comparable, since only a slight difference in crystalline fraction was observable for big system, while their deviation for $N = 500$ was considered acceptable given the noisy of the parameter for small systems. The intermediate value of $\Delta t = 3E-5$ was therefore selected for later simulations. New computer experiments were therefore performed in order to explore how the crystalline

fraction of the final configuration was influenced by the compression speed of the spherical confinement. This is in fact a remarkable feature to evaluate since the shrinking rate of the confinement may in principle be tuned also in real experimental methods, generally by adjusting the evaporating rate of the emulsion droplets containing the particles. In Brownian Dynamics simulations, the shrinking speed of the confining cavity was tuned by fixing the starting and ending value of ϕ and changing the overall number of timesteps n_t (Figure 3.3).

Our results confirmed that the compression rate strongly affects the final degree of crystallization, as more crystalline particles were generally detected in the case of slower shrinking rates. This outcome can be interpreted by considering that when the confinement shrinks rapidly, particles have less time available for finding a stable configuration and assemble in a more disordered structure. This conclusion is consistent to what reported by de Nijs *et al.*, who had previously showed that the the fraction of crystalline particles was not affected by the shrinking rate as far as this was slower than a certain value. In the present studies, crystalline fraction of systems with $N = 2000$, 5000 apparently saturates for number of timestep n_t bigger or equal to 2.4E7. Otherwise, a comparable relation between n_t and crystalline fraction value was not observed in the case of N =500. This behaviour may be explained by speculating a smaller system can more easily get stuck in multiple less-ordered configurations which prevent its evolution toward a more ordered arrangement. The hypothesis may also explain the generally noisy trend of the evaluated crystalline fraction.

The simulated structure were then further analysed by considering the size and geometries of the resulting crystalline clusters (Figure 3.4). While in the case of $N = 500$ only very small clusters were found, by increasing the number of particles to 2000, bigger domains composed from tens to one hundred of particles were already clearly visible, whereas their shapes became even more defined in the case the number of particles was further increased. In particular, both the major simulated systems the final configuration strongly resemble the icosahedral structure already observed by de Nijs et al, which consists in 20 FCC ordered tetrahedral domains that share a particle at the centre. Additionally, the surface of the supraparticles also appeared to exhibit a well-defined arrangement closely resembling the truncated icosahedron geometry, consisting of 12 pentagonal faces and 20 hexagonal faces. We believe that the presence of this arrangement on the surface of the supraparticles is the natural resolution of the internal icosahedral structure, which is eventually reshaped at the surface in order to fit the spherical confining cavity.

We finally directed our attention to the crystallization process itself. By inspecting different simulations we clearly noticed that the crystallization process started from the

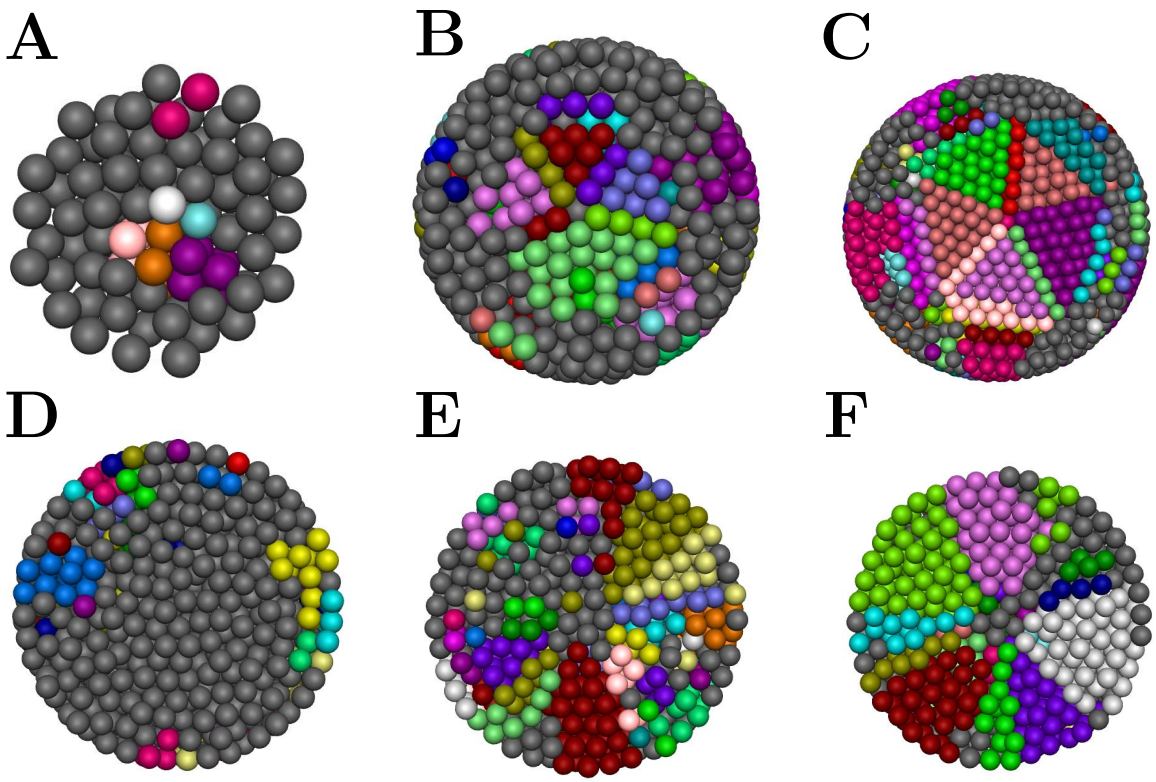

Figure 3.5: *Top* Internal arrangements for increasing number of spheres at low compression rates are shown. Moving from $N = 500$ (**A**) to $N = 2000$ (**B**) and $N = 5000$ (**C**) the ico-like structure becomes more and more defined. *Bottom* The effect of decreasing the shrinking rate of the confinement over a system of $N = 2000$ spheres is reported. In particular, shrinking rate value was fully determined by the total number of simulated timesteps n_t. For $n_t = 1E6$ (**D**), only a small fraction of the particles is observed to crystallize close to the confinement. By increasing n_t to 8E6 (**E**), crystalline domain formation appears to direct also toward the core of the supraparticle. A further increase of n_t to 12E8 (**F**) determines the formation of extended crystalline domains in the whole volume of the spherical cavity.

confining interface and then extended to the core of the supraparticle by further compression. Interestingly, a similar trend was also observed by comparing simulations run for a different number of timestep (see Figure 3.5, *Bottom*)). In particular, by increasing the total length of the simulation, we accordingly decreased the compression rate of the systems and observed that larger crystalline domains subsequently formed. Differently, by increased compression rates we observed that cluster of crystalline particles progressively small and restricted to the edges of the supraparticles. Our observations are in strong agreement with de Nijs et al., who studied the nucleation of the crystalline ordering for similar system. With the present

work we therefore successfully confirmed that the confinement plays a remarkable role in heterogeneously promoting the nucleation of the crystal, even in the case of significantly fast compression rates. We concluded that this latter ability is a further and fundamental function of the spherical confinement, which is in addition to its role in both inducing the crystallization itself by compressing the system and in stabilizing its peculiar anti-Mackay final configuration.

3.2.2 Synthesis of fluorescent labelled silica spheres

Synthesis of fluorescent labelled spherical cores In order to attempt to experimentally reproduce the promising results obtained through Brownian Dynamics simulations, a first batch of silica spheres (DS01) was synthesized according to the procedure reported in Section 3.1.3 Transmission electron microscope (TEM) images of the obtained fluorescently labelled cores are shown in Figure 3.6, *Top*. Note that the reaction clearly resulted in spherical particles of two different distribution of sizes, with respective size around 100 nm, and 160 nm. The reason of this undesired outcome was subsequently uncovered by reviewing the adopted synthetic method. In fact, as TEOS precursor was added in two closely subsequent times during the synthesis of the cores, we presumed two different nucleation episodes occurred during the reaction. Since nuclei formed at the first stage had more time for growing by consumption of hydrolized TEOS, they likely resulted in larger spheres compared to particles which formed afterwards.

Aimed by collecting more monodispersed silica particles, the synthetic method was revisited, by bewaring of adding all the required amount of TEOS simultaneously and under vigorous stirring. TEM images of the resulted fluorescent silica cores are shown in Figure 3.6, *Bottom*. The diameters of the spheres were determined to be 203 nm of mean (μ) and polydispersity (δ) = 0.12, where polydispersity is defined as the standard deviation divided by the mean. It should be noticed that DS02 particle dimensions are consistently bigger compared to those obtained in the previous batch. However, this result can be qualitatively interpreted by considering that the two different nucleation episodes emerged in DS01 synthesis generated a higher number of silica nuclei, which therefore grew up to smaller final diameters by the consumption of the same amount of TEOS reactant.

Silica shells growth It is known that high degree of polydispersity could negatively effect the self-assembly process of colloidal particles. Pusey *et al.* for instance showed that the crystallization of a colloidal suspension in suppressed if the ratio between standard deviation

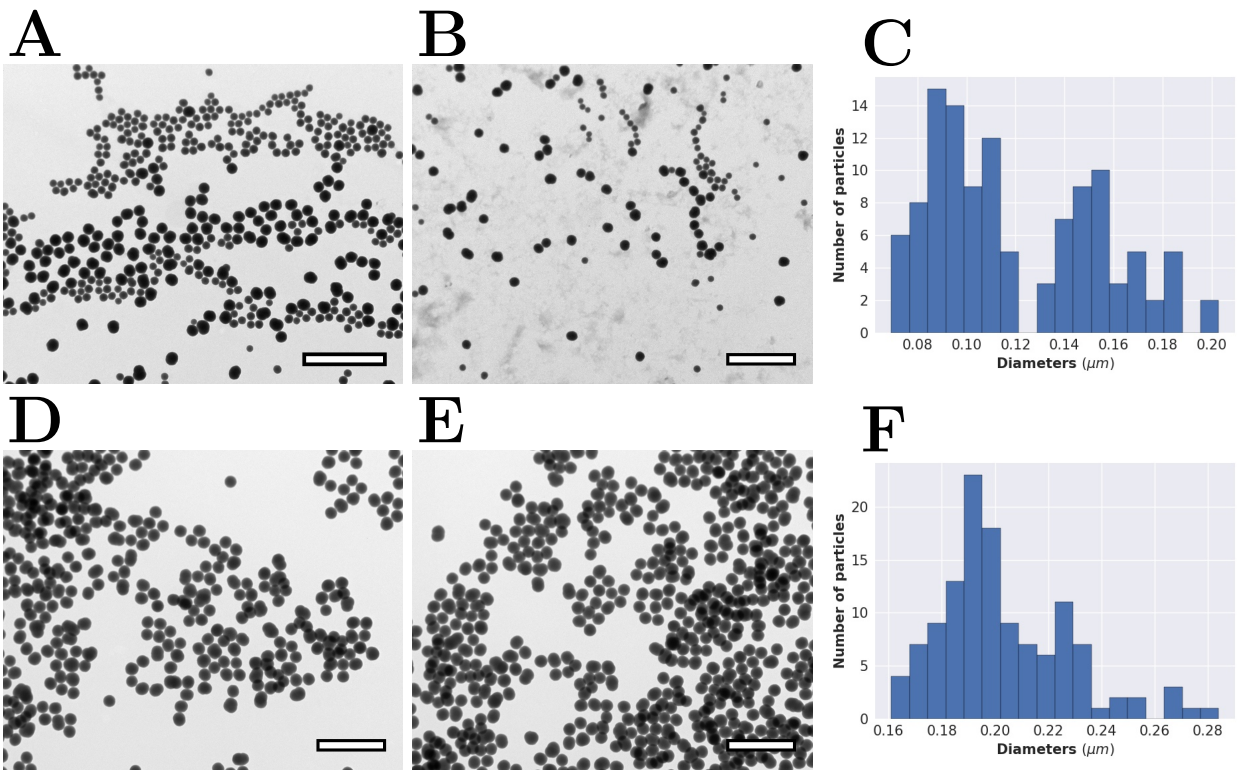

Figure 3.6: (**A-B**) TEM images of DS01 spherical cores and (**C**) histogram of size distribution of the obtained sphere. (**D-E**) TEM images of the DS02 fluorescent-labelled cores and (**F**) relative histogram of size distribution (Mean value $\mu = 203$ nm, polydispersity $\delta = 0.12$.). All scale bars refer to 1 μm

and the mean lies in the range 6 to 12% [22]. In our case, polydispersity of silica particles can be appropriately decreased by growing non-fluorescent silica shells around the fluorescent cores. In principle, as the shell grows approximatively the same thickness on all spherical cores, the mean value subsequently increases while the the overall standard deviation should not be influenced. Furthermore, growing a non-fluorescent silica shell around fluorescent labelled silica cores appears particularly convenient as we aimed to image colloidal particles through confocal microscopy. In fact, as illustrated in Section 2.4, the selected technique allows to effectively image dense systems with single particle resolution only if the fluorescent signals belonging to different particles are separated by a non-fluorescent medium.

After several silica coatings, particles DS02-G3 were eventually obtained (Figure 3.7). In particular, by comparing DS02-G3 to DS02 measurements, we clearly observed that by nearly doubling the diameter of the silica spheres, polydispersity approximatively halved. This trend is in strict agreement with predictions. However, note that at this stage polydispersity was still large enough for negatively affecting the formation of colloidal crystals. In fact,in bulk conditions the segregation of particles of similar sizes can locally decrease

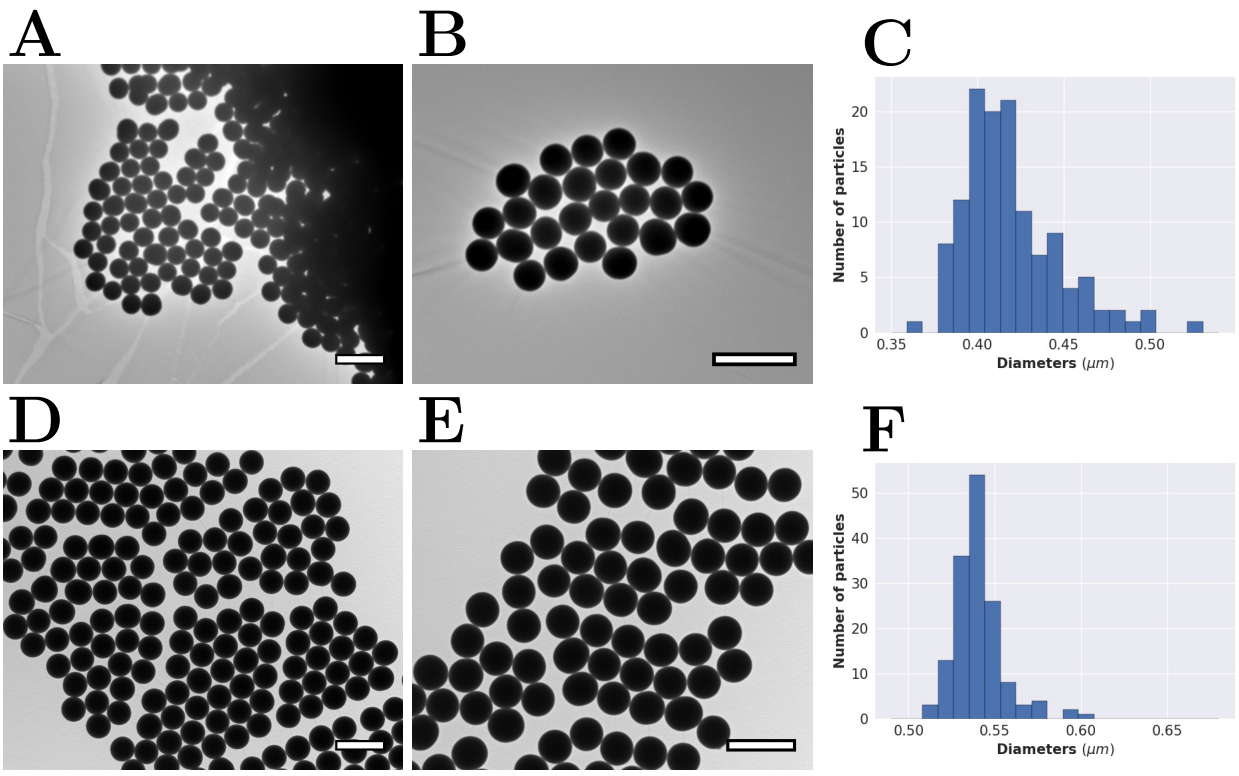

Figure 3.7: (**A-B**) TEM images of DS02-G3 and (**C**) histogram of their size distribution (mean value $\mu = 419$ nm, polydispersity $\delta = 0.07$). (**D-E**) TEM images of the DS02-P2 and (**F**) histogram of their size distribution (Mean value $\mu = 541$ nm, polydispersity $\delta = 0.03$). All scale bars refer to 1 μm

the polydispersity value, thus facilitating the formation of crystalline structures in relatively more polydisperse colloidal systems. In contrast, spherical confinement conditions prevent same-size segregation due to the small volume of the cavity, so that lower values of polydispersity are generally required for the formation of a crystalline organization.

Moreover, the presence of few bigger particles, some of which resemble a dumbbell shape, was clearly noted by close inspection of DS02 outcome (Figures 3.6, *Bottom* and 3.7, *Top*). The origin of these irregularities were partially ascribed to the use of an old bottle of TEOS during the core synthesis. In fact, atmospheric water impurities may hydrolyze TEOS while stored in a not-perfectly sealed bottle, so that when the reagent is added to the reaction mixture unstable small silica particles from the storage bottle may adhere to the just nucleated silica nuclei, thus leading to the formation of a certain fraction of bigger particles. Additionally, it should be considered that the specific reaction conditions may have not completely stabilized silica nuclei during the synthesis, so that some of them may have form aggregates during the growing step thus resulting in dumbbell-shaped particles.

In order to remove bigger particles and improve the monodispersity of silica spheres,

we explored the employment of a similar procedure as described in Section 4.1.3 for the purification of rods. In particular, from the diagram reported in Figure 3.7, *Top*, it was noted that the diameter distribution deviates from the expected Gaussian distribution for bigger values than approximatively 450 nm. As the volume of a sphere (and hence the gravitational force) increases with the cubic of the radius, it could be estimated that the undesired particle are in general 1.5 times heavier than particles at around 400 nm of diameter.

The following procedure was therefore performed: diluted samples of DS02-G3 particles was left sedimenting for several hours, so that a sedimentation gradient, composed by a thick sediment at the bottom, a turbid supernatant in the middle and a clear supernatant at the top, was clearly visible by eye. The clear supernatant was removed and approximately 1/3 of same volume of turbid supernatant was collected from the top. The procedure was repeated several times. The particles obtained (DS02-P1) with this procedure were measured be 0.424 on average, with $\delta = 0.04$, thus confirming that our purification procedure successfully increased the monodispersity of the spherical particles.

DS02-P1 particles were subsequently further coated with non-fluorescent silica, and DS02-P2 spheres were finally obtained (see Figure 3.7, *Bottom*). Dimensions and polydispersity values of the spherical particles at different synthetic steps are summerized in Table 3.2.

Sample name	Diameter (nm)	Polydispersity	NF-Shell (nm)
DS02	203	0.12	0
DS02-G3	419	0.07	108
DS02-P1	424	0.04	108
DS02-P2	541	0.03	166

Table 3.2: Dimensions of the particles after selected synthetic steps. NF refers to the non-fluorescent silica shell thickness.

3.2.3 Self-assembly of Spheres in Spherical Confinement

As described in Section 3.1.4, a spherical confining environment was achieved using a water-in-oil emulsion with particles inside the polar droplets. However, a central aspect to consider in regard of the outlined general method is how to prevent too fast evaporation of the dispersed phase. In fact, it was observed that when a 5-ml sample is prepared in a glass vial so that the vial is left completely open to the atmosphere, the water content evaporated approximatively in one hour. From previous experience in the group, this time was considered

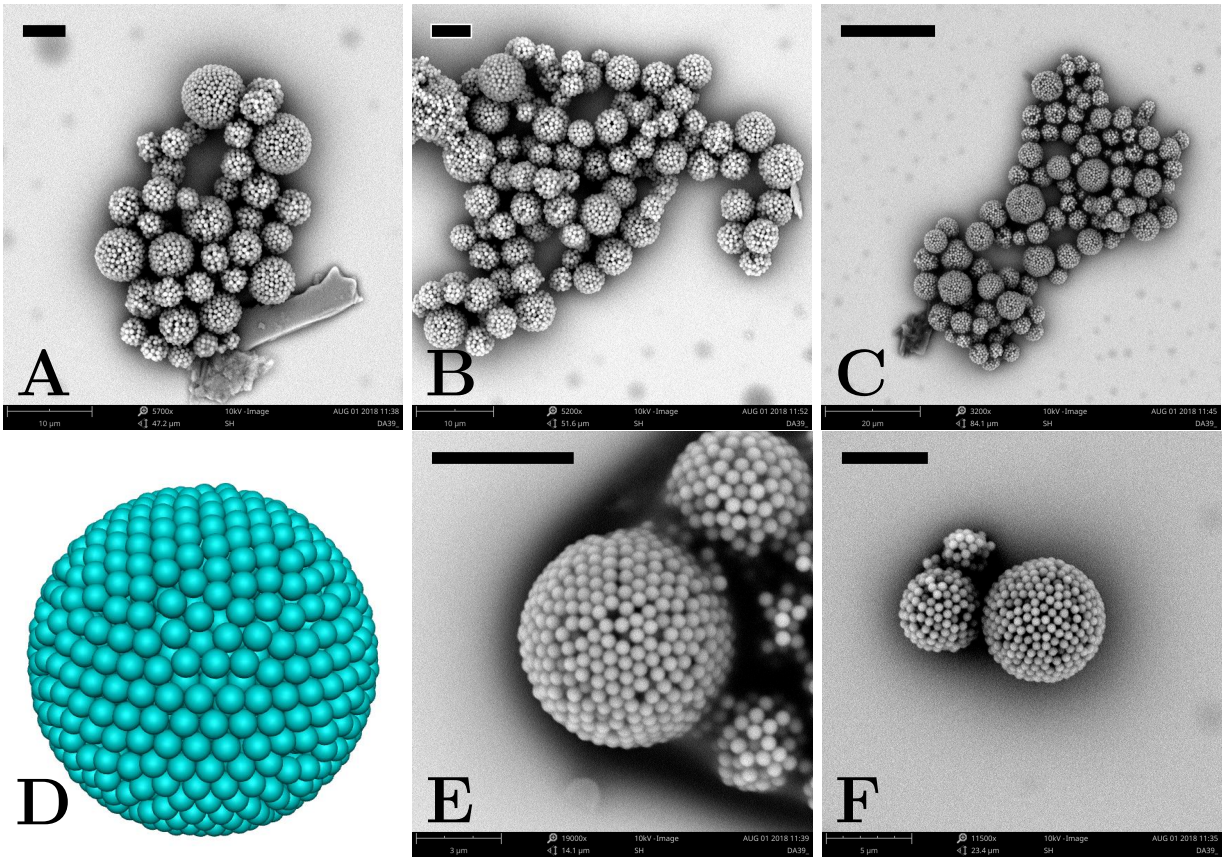

)

Figure 3.8: **A-C** Scanning electron microscopy (SEM) images of aggregates of several supraparticles constituted by silica spheres. **D** The external configuration of a Brownian Dynamics simulated system of spherical particles ($N = 2000$, packing fraction $\phi = 0.65$, crystalline fraction = 0.80) is qualitatively compared to SEM images of supraparticles collected through experimental procedure (**E-F**). All scale bars refer to 5 μm.

too short for allowing micron-sized particles to assemble in ordered structures similar to the ones observed through computer simulations.

Several different setup were therefore explored in order to keep the system under stirring while allowing slow water evaporation from the sample. A general trend showed that in the case the former requirement was not adequately satisfied, for instance due to slow or not continuous shaking, big particle aggregates of undefined shape formed. This outcome was ascribed to the sedimentation and merging of water droplet at the bottom of the vial. The use a controlled shaker, as anticipated in Section 3.1.4, was therefore identified as the best option for later studies. In regard of the latter requirement, in the case water evaporation was too fast, scanning electron microscope (SEM) revealed colloidal spheres likely formed

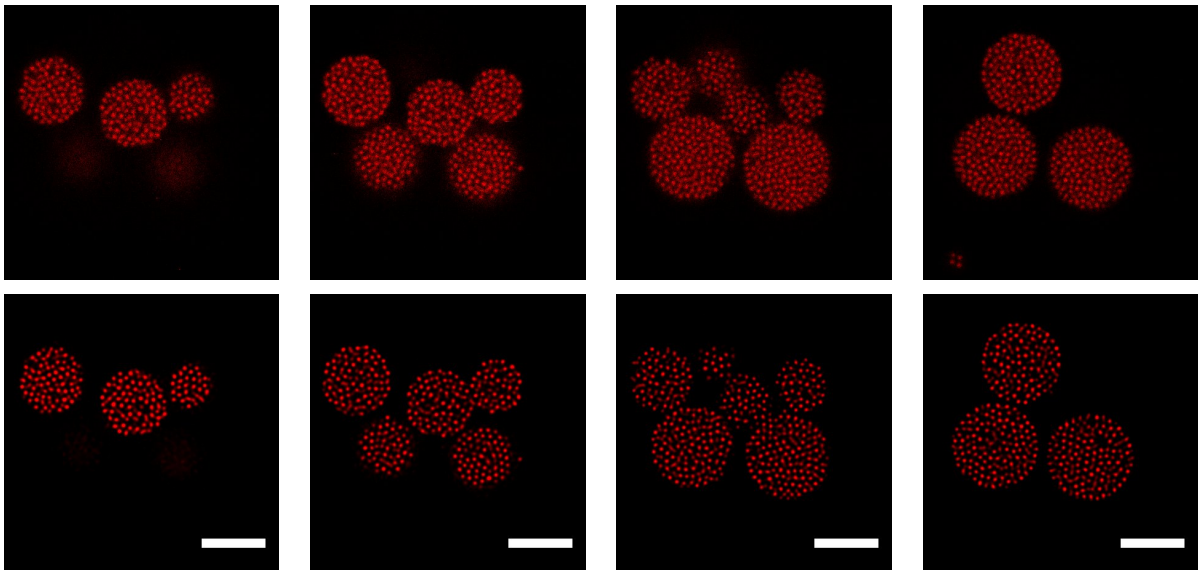

Figure 3.9: Laser scanning confocal microscopy (LSCM) images of an aggregate of supraparticles consisting of colloidal spheres. Images on the right represent closer sections to the coverglass. Clearness of the original confocal images (*Top*) consistently improves after deconvolution process (*Bottom*). Scale bars refer to 5 μm.

supraparticles of disordered configurations. In fact, we extensively employed SEM as a simple, fast technique for collective overview over the quality of the obtained supraparticles. On the other hand, in the case water evaporation completed in approximatively one day, rather satisfying outcomes were obtained.

In here we only report a representative sample prepared in a 20-ml vial so that the vial aperture was sealed by using several layers of Teflon tape. Although no holes were drilled in the Teflon cover, water was observed evaporate overnight by migrating through the tape itself. After wash of the vial content with hexane, obtained supraparticles were imaged with SEM (Figure 3.8). Note that our method successfully provided supraparticles of generally well defined spherical shape. Supraparticles themselves, whose dimensions approximatively range between 2 μm and 8 μm, are in turn constituted by silica spheres, which are supposedly stuck together due to Van der Waals attractive interactions. By considering a final packing fraction of around 0.65, we could estimate supraparticles being composed by a number of spheres between 30 to 2000.

Detecting the order of the configuration from the outside aspect is not a trivial task. Moreover, simulations for $N = 2000$ had already revealed that the icosahedral structure

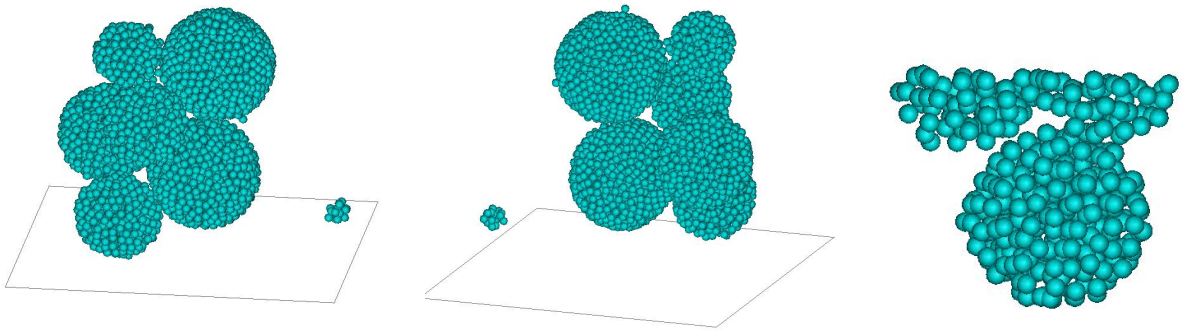

Figure 3.10: Reconstructed supraparticle configurations as obtained from confocal microscopy data. *Left* and *centre* images refers to the aggregate shown in Figure 3.9.

is more clearly evident only when outer layers of particles were not considered. For these reasons, the examination of the external part of the supraparticle is not to be considered a conclusive analysis on the structure of the supraparticle. However, we qualitatively scrutinized SEM images and observed the order was likely not homogeneously distributed within the system, as some more distorted supraparticles were revealed together with much more well-defined spherical shaped ones. Similarly to simulations results, a 5-fold symmetry compatible with a icosahedral ordering was sometimes noticed for latter supraparticles.

In order to quantitatively compare experimental and simulated outcomes, we revealed the internal structure of supraparticles by using confocal scanner laser microscopy (CLSM). In particular, 3D confocal imaging was possible since the constituting colloidal spheres were fluorescent labelled during the synthetic procedure. Images taken of an agglomerate of supraparticles are shown in Figure 3.9. Note that the deconvolution of the obtained images dramatically improved the resolution and decreased the background noise. By taking a stack of several images at different depth into the sample, the full configuration of the supraparticle can be reconstructed. We subsequently derived the positions of single spherical colloidal particles using a algorithm by Crocker and Grier so to reproduce and further analyse the entire configuration [60]. We report two examples of obtained structures (Figure 3.10). The first one is an agglomerate of six supraparticles constituted by a total of around 4500 particles. In the second case, a particle composed of around 500 particles is shown. Having obtained the position coordinates of single constituent particles, we were also able to quantitatively analyse the configuration using the same bond order parameter algorithm as employed for the simulation data. Unfortunately, our analysis showed that only little order was present, since a values of crystalline fractions around 0.07 and 0.03 was respectively determined, while no crystalline clusters were identified. Since Brownian Dynamics simulations had already

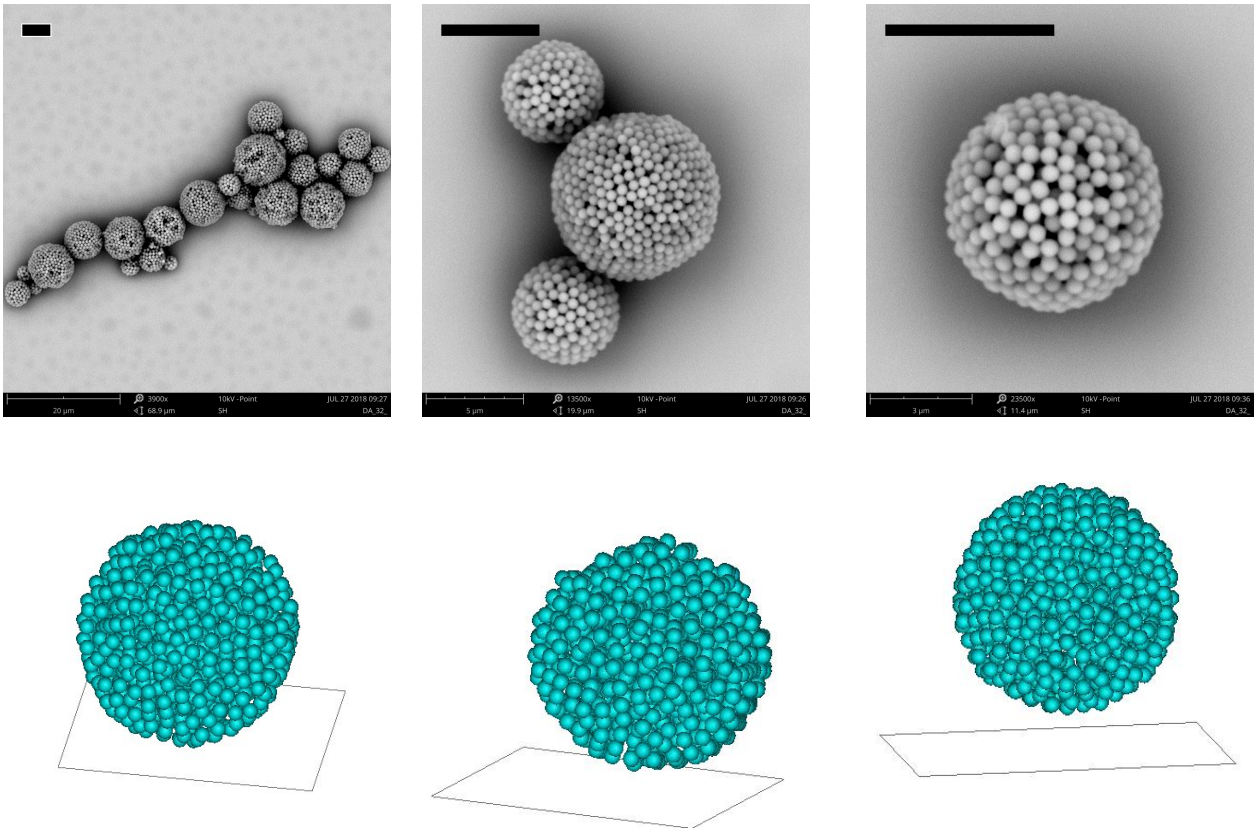

Figure 3.11: *Top:* SEM images of supraparticles obtained from silica spheres by lowering water evaporation rate. Scale bars refer to 5 μm. *Bottom* Reconstructed configurations from confocal microscopy data.

revealed that bigger supraparticles are generally more ordered, we believe that this argument may also apply in this case to explain the slight difference in crystalline fraction between the two systems.

As low value of order were attributed to fast evaporation rate of water from the system, further experiments aimed to decrease the evaporation rate of water were performed. At this stage, the vials were covered by using a few layers of parafilm in addition to Teflon tape. In particular, Teflon tape was observed be essential to prevent the dissolution of parafilm caused by hexadecane, while parafilm itself was found be able to completely prevent evaporation of water. The covering layers were therefore holed three times using a 0.9 mm needle so to allow slow water evaporation, which completed in around two or three days. SEM microscopy showed that the new method successfully provided well-shaped supraparticles of diameter between 3 μm to 9 μm (Figure 3.11). Samples were subsequently imaged using confocal

microscopy, and the internal structures were reconstructed. However, quantitative analysis on the reproduced configuration demonstrated only little order has been obtained, with values of crystalline fraction oscillated between 0.03 and 0.06. Finally, the quantitative analysis allowed to estimated the packing fraction reached in the supraparticles, which was calculated between 0.60 and 0.70.

It is worth underlying that for all examined samples we desisted from an extensive analysis over the internal structure of a big number of particles. Since certain degree of heterogeneity within the samples had already been revealed by SEM microscopy, we thus recognize the few reconstructed structures cannot be regarded as fully representative of the examined samples. It is therefore possible that ordered supraparticles were eventually present in the sample but were not taken into consideration. However, we presume fast water evaporation rate from the system should be regarded as the main reason behind the failure in producing structurally ordered supraparticles. This supposition may be further supported by our computer simulations studies, which clearly show that for fast compression rates particles cannot arrange into crystalline domains and a glass is eventually obtained.

3.3 Conclusions

In conclusion to this section, simulation and experiments were extensively used in order to study the self-assembly of colloidal spheres in spherical confinement. Brownian Dynamics simulations successfully reproduced results previously obtained by De Nejs/Dussi *et al.*, thus confirming the value of our simulation technique. In particular, simulated spherical particles arranged into ordered structures resembling icosahedral geometry. A similar arrangement would be infeasible within bulk conditions. Notably, we additionally reported that our simulated final configurations displayed a particular external arrangement resembling the truncated-icosahedral structure. The formation of a similar pattern can be explained by the requirement for the system to fit an icosahedral geometry within a spherical confinement.

In order to experimentally produce structurally ordered supraparticles, fluorescent labelled silica spheres were successfully synthesized with a polydispersity value of around 3%. Our attempts confirmed that the use of a fresh bottle of TEOS and its addition at once under strong stirring in the reaction mixture may play a fundamental role in the production of well-shaped monodisperse spherical particles. An experimental procedure consisting of evaporating water from a water-in-oil emulsion was subsequently employed for reproducing the self-assembly of spherical colloids in a spherical confining environment. By scanning elec-

tron microscopy (SEM) technique we observed that our procedure successfully resulted in generally well-shaped spherical supraparticles constituting of hundreds to a few thousands of colloidal spheres. Inspection of the internal structure of the supraparticles was then possible by confocal laser scanning microscopy (CLSM). However, in this case we did not observe a high degree of crystallinity inside the system. The present outcome was mainly ascribed to the high evaporation rate of water, which likely prevented particles from self-organize into more ordered structures.

Chapter 4

Self-assembly of Colloidal Rods

4.1 Methods

4.1.1 Brownian Dynamics (BD) simulations

Brownian Dynamics simulations were performed according to the same general features as described in Section 3.1.1. However, additional considerations were required to respect of the difference in shape of spherocylinders compared to spherical particles. In fact, in the case of spheres, particles can be reduced to points so that the force vector can be determined by simply considering the distance of the centers of mass. Differently, spherocylinders were modeled as line segments and the repulsive forces between two particles were calculated depending on the shortest distance between the representative segments. Shortest distance between rods was therefore evaluated by using a specific algorithm, which is similar to the one reported by Vega and Lago [61]. Generally, interaction between two spherocylinders would also generate a torque which induces a rotation in the interacting particles. The torque was simply calculated as T = F x l, where the lever arm l is the vector connecting the center of mass on the rods to the point on the line segment where the force F is applied. Similarly to the case of spheres, a WCA potential was used to model repulsive potential between simulated particles.

4.1.2 Order parameters and identification of Smectic demains

Global and local order parameters can be generally employed to distinguish between isotropic and various liquid crystalline phases. In particular, global order parameters are usually involved for quantify a long-ranged ordered configuration, while local order parameters are

better suitable for determining the degree of order in the local environment of a given particle. The global nematic order parameter can be obtained by diagonalizing the nematic order parameter tensor:

$$\mathbf{Q}_{\alpha\beta} = \frac{1}{N}\sum_{i=1}^{N}\left[\frac{3}{2}\mathbf{u}_{i\alpha}\mathbf{u}_{i\beta} - \frac{\delta_{\alpha\beta}}{2}\right] \tag{4.1}$$

where $\mathbf{u}_{i\alpha}$ is the α-th component of the unit vector describing the orientation of the long axis of the rod i, N is the number of particles and $\delta_{\alpha\beta}$ is the Kronecker delta, which is equal to 1 if $i = j$ and 0 otherwise. The global order parameter S is defined as the largest eigenvalue of $\mathbf{Q}_{\alpha\beta}$ and ranges from -0.5 to 1. However, as in the present work we aimed to extensively study the ordering induced by a spherical shaped confinement, we also required the evaluation of a local nematic order parameter. In fact, while the overall simulated system may not be preferentially directed towards one single direction, particle orientations may anyway display some preferential direction locally. We therefore defined the local order parameter S_i of particle i as reported in [62] as:

$$S_i = \frac{1}{n_i}\sum_{j=1}^{n_i}\left[\frac{3}{2}\mathbf{u}_i \cdot \mathbf{u}_j - \frac{1}{2}\right] \tag{4.2}$$

where n_i is the number of neighbours of particle i, defined as the particles with center of mass closer than $(L + D)/2$, where L refers to the particle length and D to its diameter. S_i also ranges from -0.5 to 1.

The global tendency of the system to form smectic order can be evaluated by employing the global smectic order parameter, which is defined in [63] as:

$$\tau = \max_{l}\left|\sum_{j=1}^{N} e^{2\pi i \mathbf{r}_j \cdot \mathbf{n}/l}\right|, \tag{4.3}$$

where $\mathbf{r}_j$ is the position of particle j and l is a real number. In this case. the number of l which maximizes the above expression is the layer spacing.

However, it was noted that a global order parameter as defined above is rather noisy and not suitable for capturing the order of small system or when the smectic layers are higly fluctuating. We therefore introduced a novel local smectic order parameter which has a similar form of the one already reported by Dussi [52]. We first calculated:

$$\Delta_i = 1 - \frac{1}{n_i}\sum_{j=1}^{n_i}\left|\frac{\mathbf{r}_{ij} \cdot \mathbf{u}_i}{|\mathbf{r}_{ij}|}\right|, \tag{4.4}$$

where $\mathbf{r}_{ij}$ is the distance vector between the centers of mass of particle i and neighbour particle j. $\Delta_i = 1$ corresponds to the ortogonality condition between $\mathbf{r}_{ij}$ and the direction of the rod $\mathbf{u}_i$. Compared to the form used by Dussi, the use of the additional external absolute value ensures that misalignments of the positions of neighbour particles is always take into account, since dot products of opposite sign cannot cancel out. Moreover, by normalizing by the absolute value of the distance vector we established that all neighbour particles are equally taken into account. In order to discriminate between the case rods are transverse one to the other, Δ_i is multiplied by the local nematic order parameter S_i. We therefore define

$$\tau_i = S_i \Delta_i \tag{4.5}$$

as the local smectic order parameter, so that a particle i was considered smectic ordered if $\tau_i > 0.35$.

In addition to defining local order parameters, we aimed to identify different smectic demains for a more effective visualization of the obtained structures. We therefore considered two neighbours rods i and j as belonging to the same smectic domain if both particle were identified as smectic ordered and they were aligned on the other. The latter requirement was satisfied in the case their dot product $\mathbf{u_i} \cdot \mathbf{u_j}$ was determined as > 0.90.

4.1.3 Synthesis of fluorescent labeled silica rods

Cores Synthesis Non-fluorescent silica rods were synthesized according to Kuijk et al. procedure [51]. In a 1L bottle, 80g of polyvinylpyrrolidone (PVP, Sigma Aldrich, avg. mol. wt. 40000 g) were dissolved in 1-pentanol (Sigma Aldrich, $\geq 99\%$) by shaking and sonication. After thermal equilibration at a given temperature (see Section 4.2.2 for details), 80 mL of ethanol (absolute, Baker), 19 mL of milliQ water (Millipore System) and 8 mL of 0.18 M sodium citrate (tribasic dihydrate, Sigma Aldrich, $\geq 99\%$) were added to the solution, which was then shaken vigorously in order to create the water-in-oil emulsion. After addition of 17 mL of ammonia (Sigma Aldrich, 26% wt.) and 8.5 mL of TEOS (Sigma Aldrich, 98%), the solution was shaken once more and left undisturbed for several days at fixed temperature. The obtained particle cores were separated from the reaction mixture by centrifugation (1500 g/110 minutes) followed by washing once with ethanol (100%, Interchema), once with deionized water and then again twice with ethanol. Finally, particles were dispersed in ethanol.

In order to improve monodispersity of the resulting rods, large and small particles were discarded. In the former case, particles were centrifugated at 700g for 15 min and the turbid

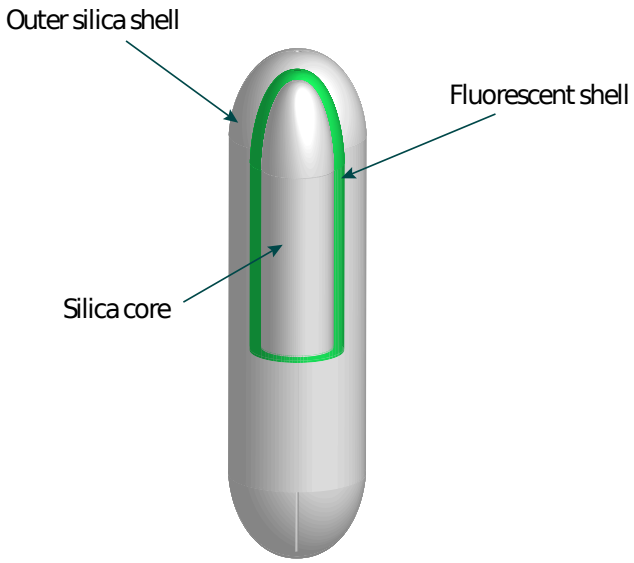

Figure 4.1: Scheme of rod-shaped silica particles as synthesized in the present thesis. A fluorescein-labelled fluorescent shell (*green*) is formed around a non-fluorescent silica core. Additional non-fluorescent silica coatings cover the outside of the rod. Synthesis of the outer silica shell is aimed to separate signals emitted by adjacent particles, thus allowing imaging at single-particle level via confocal microscopy.

supernatant was removed. The procedure was repeated several times until the supernatant appeared clear. In order to remove large particles, the dispersion was diluted into several 20-ml vials and left to sediment. After several hours, a sedimentation gradient was clearly visible by eye, as a sediment was forming at the bottom, a turbid supernatant in the middle and a clear supernatant at the top. The clear supernatant was removed and approximately the same volume of turbid supernatant was collected for further use. The procedure was repeated several times until a consistent amount of particles were collected.

Silica-shell growth A uniform fluorescent shell around the core was grown according to the procedure reported in [55]. 5 mg of the fluorescent dye fluorescein isothiocyanate (FITC, isomer I, 90%, Sigma-Aldrich) were added to 7 μl of the coupling agent (3-aminopropyl)triethoxysilane (APS, $\geq$98%, Sigma Aldrich) in 1 ml of absolute ethanol and left react overnight under stirring. The day after, approximatively 90 mg of silica rods cores were dispersed in 90 ml of absolute ethanol, followed by the addition of 5.5 ml of deionized water, 6.5 ml of ammonia (26% wt.) and the FITC-APS solution. After stirring, 18 μl of TEOS were added six times every 20 min. After additional 4 hours under stirring, the reaction mixture was centrifuged (700g, 20 min) and washed 3 times with ethanol. The resulting particles were then dispersed

in ethanol.

In order to be able to resolve single particle position with confocal microscope, several non-fluorescent silica shells were additionally grown on the fluorescent rod according to the method reported in the same article [55]. The procedure is similar to the fluorescent coating describe above, but without involving the fluorescent dye and the coupling agent. As the fluorescent shell growth method can lead to some irreversible particle aggregation, after the first non-fluorescent shell coating heavier particles were removed according to the procedure reported in the previous paragraph.

The particles were imaged with transmission electron microscopy (TEM, FEI Tecnai 10) after synthesis and each shell coating to determine their dimensions. In all cases at least 100 particle lengths and diameters were measured to provide reliable average dimensions and polydispersity values.

A schematic representation the final structure of fluorescent-labelled silica rods is reported in Figure 4.1.

4.1.4 Sedimentation experiments

Sedimentation-induced self-assembly experiments were performed by preparing a diluted suspension of particles ($\sim$ 10% v/v) and by leaving it to sediment in a home-made cell (Figure 4.2). The cell was prepared by cutting the back of a glass Pasteur Pipette (WU Mainz, short size, cross sectional area 22.1 mm^2), polishing the edges with glass paper and gluing it to a microscope cover-glass. A hole wide enough for inserting the cell is then drilled in a glass slide and both the glass slide and the microscope cover-glass are glued together so that the obtained system can be held in a conventional microscope stage. In this thesis, we involved two different index-matched solvents for the sedimentation experiment, either consisting in a water/glycerol or in a water/DMSO mixture. In the former case, a UV curing glue was used in the preparation of the cell. Differently, since it is known that DMSO is not compatible with the UV curing glue, candle wax was preferred in the latter case [64]. The cell was then filled with the colloidal suspension, sealed with Teflon tape and left undisturbed for several days.

4.1.5 Self-assembly in Spherical Confinement

Spherical confining conditions were reproduced according to the same general method employed for spheres and reported in Section 3.1.4.

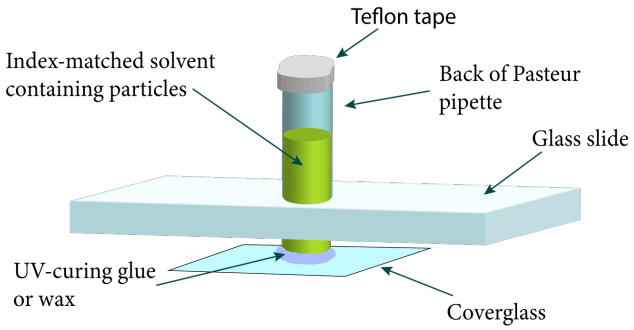

Figure 4.2: Scheme of a sedimentation cell.

4.1.6 Glassware coating with OTMOS

In some cases, self-assembly experiments were prepared in glass vials which had previously been coated by using Octadecyl Trimethoxy Silane (OTMOS). This additional step was introduced in order to prevent silica particles to stick to the vial walls by making the glass hydrophobic due to its functionalization with C18 alkane chains. The employed coating methods closely resembles the Stober reaction: the methoxy-groups first undergo hydrolysis catalyzed by ammonia, and then condense with the silanol groups on the glass surface. In particular, a coating solution was prepared by addition of 7.78 ml of 10v% OTMOS solution in chloroform to 7.78 mL of ethanol and 5.44 ml of ammonia (26v%). A 20-mL vial was then coated by filling it with the prepared solution and leaving it under slow swirling for at least 2 hours. After that time, the coated vial was extensively washed with ethanol and sonicated with chloroform in order to remove particles eventually formed during the procedure.

4.1.7 Rod tracking

Positions and orientation of rod-shaped particles were extracted from confocal images using an algorithm developed by Besseling *et al.* [65]. After blurring of the images by a Gaussian function and removing of the background noise, the algorithm identifies particles backbones by examining voxels brighter than a certain threshold value and looking for collinearity by fitting a straight line to the voxels. Once backbone voxels are identified and grouped into clusters of neighbours voxels, the algorithm further analyzes the intensity of surrounding regions and determines the rod ends by evaluating where the intensity is lower than a certain threshold which has been set manually. Finally, the fitting is refined by eliminating overlapping rods together with those which have little intensity or are too short. The outcome of the fitting procedure can be then visually checked by overlaying the found particle over the

image. In particular, input threshold values were found essential for the correct detection of the particles and manually tuned until most of the rods have been correctly identified. The fitting procedure result in a complete set of position and orientation coordinates per each rod, which allows to reproduce the particle configuration and quantitatively analyzed the order of the system.

4.2 Results and discussion

4.2.1 Brownian Dynamics simulations on rods in spherical confinement

Previous results described in Section 3.2.1 demonstrated our simulation technique successfully reproduced similar configurations as obtained by de Nijs *et al.* both experimentally and through computer simulation [32]. Although we failed to fully replicate the reported experimental structures, we anyway concluded the employed Brownian Dynamics simulation scheme was reasonably representing the main feature of a spherical confinement process lead for sufficiently low compression rates. On this basis, we decided to extend our investigation to the self-assembly of rod particles. At the best of our knowledge, we report one of the first studies considering the dynamic behaviour and final geometries arising from the self-assembly of rods in spherical confinement.

Similarly to what previously accomplished in the case of spherical particles, our first simulations were aimed to establish a dependable value of timestep δt to employ in later studies. In particular, the quality of the computer experiments for different values of δt was determined by both inspection of the reproduced dynamics and by quantitative analysis of the local nematic and local smectic order parameters during the simulations. Note that we simulated particles with an aspect ratio L/D = 5.0 for allowing better comparison between simulated systems and real experimental results (see Sections 4.2.2 on synthesis of rod-shaped colloidal particles). Remarkably, high degrees of order in our preliminary examinations revealed that spherical confinement was able to induce not only nematic ordering but also smectic layering in the simulated systems. We further observed that, as expected, the order increased for shorter timesteps until the limit value of $\delta t = 6E - 5$ was reached, so that by further decreasing the value of δt the degree of order did not change significantly. The found limit value is therefore to be considered the optimal for obtaining reliable dynamics of the system at limited computational expense according to our code. We anyway ran later

simulations with the conservative value of $\delta t = 3E - 5$ so to be wholly confident about the reliability of the outcomes. Note that this value was the same as the one employed in the case of spherical particles studies.

We subsequently pointed our attention on determining to which extend the observed order in the final configurations depends on the compression rate (Figure 4.3). Again, the compression rate was adjusted by fixing the initial and final packing fraction and by tuning the total number of simulated timesteps n_t. By quantitative analyzing the results, we clearly showed that in all cases spherical confinement induced an increases in the local nematic and smectic order parameters, thus indicating the system spontaneously organize into smectic layers. On the other hand, considering global nematic order parameter generally leads to detection of small global order in the system. The outcome therefore revealed that for the relatively small systems we took into consideration the spherical environment generally prevents the formation of a single ordered domain, so that local order parameters are generally required for capturing the ordering of the system. Furthermore, the final arrangements evidently showed to depend on the compression rate, since more ordered structures were obtained for increasing total number of timesteps. By comparing the trend to the one obtained in Section 3.2.1 for spheres, we additionally observed that the increase in order is less steep compared to the crystallization process of spheres. This tendency is reasonable since both nematic and smectic ordering are weakly first-order phase transitions, and thus smoother transformations compared to the crystallization of hard-spheres.

Aiming to study the smectic layering in the simulated supraparticles, different smectic domains were determining by using the method describe in Section 4.1.2 (Figure 4.4). In the case of $N = 100$, the systems showed a tendency in forming a single big smectic domain at the centre of the supraparticles, while other two smectic layers preferentially formed at opposite sides of the main smectic domain and oriented orthogonally to the central domain and one to the other. The formation of these latter smaller layers is apparently due to the necessity to "cap" the main layer allowing particles to fill the all the spherical cavity. Note that moderately high values of the global nematic order for the present case already indicated most particles were aligned according to one preferential direction.

By increasing the number of simulated particles to 400, the systems seemingly displays a tendency in forming a major smectic layer at the center of the supraparticle. However, a careful inspection revealed the supposed major smectic layer doesn't completely fill the entire central portion of the sphere, and that a total of 3 domains of similar dimensions mainly constituted the structure of the supraparticle. In particular, each of these layers

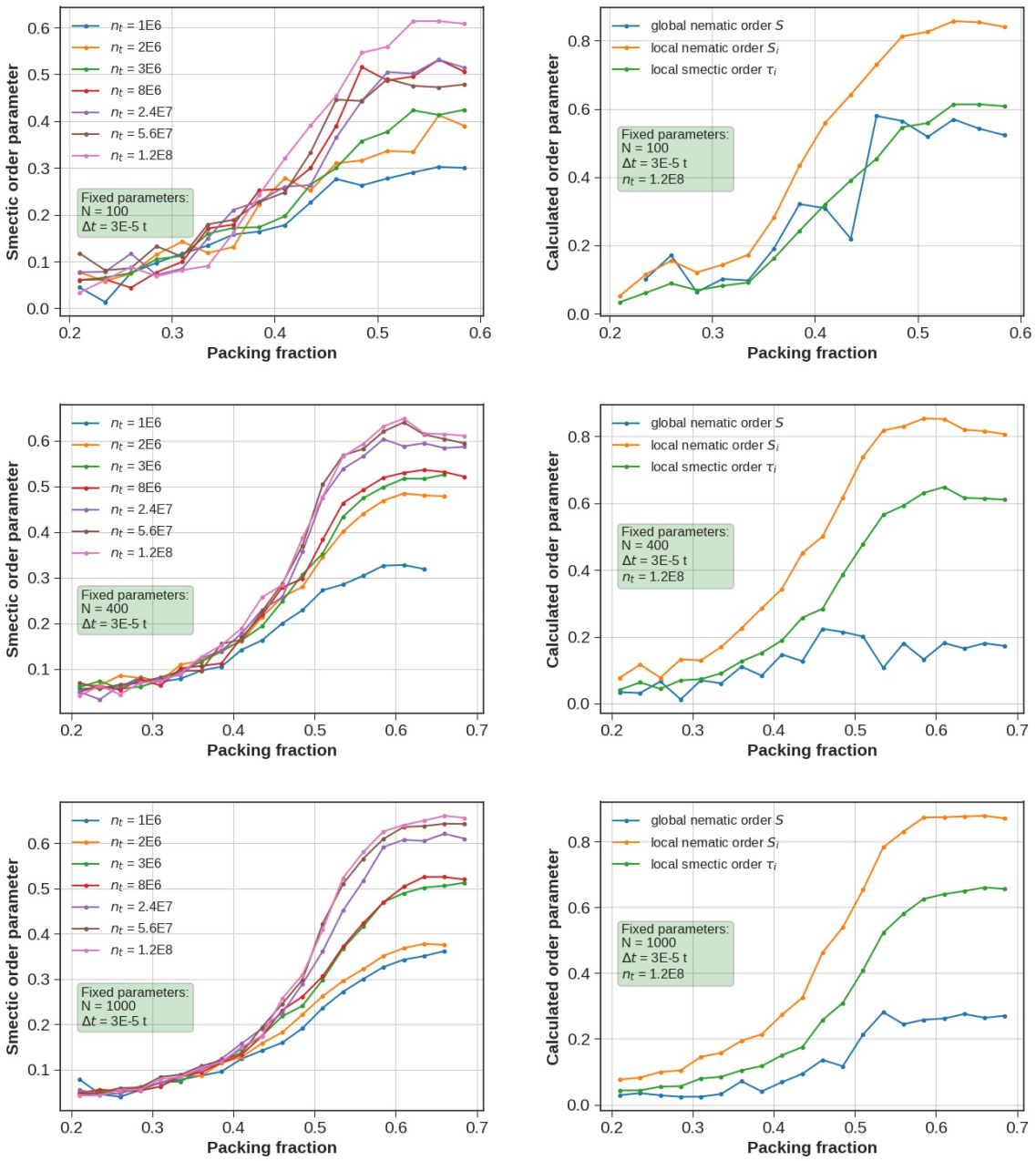

Figure 4.3: *Left:* Smectic order parameter value as a function of packing fraction ϕ for different numbers of timestep n_t as indicated in the legend. By decreasing the compression rate, the order within the system correspondingly increases. *Right:* Comparison between considered order parameters for different systems. While a local tendency in forming nematic and smectic order is detected for all cases, global nematic order parameter evaluation reveals simulated rods generally fail in directing toward a single preferential direction. In fact, high values of global nematic order are observed only in the case of the small system constituted by $N = 100$ particles.

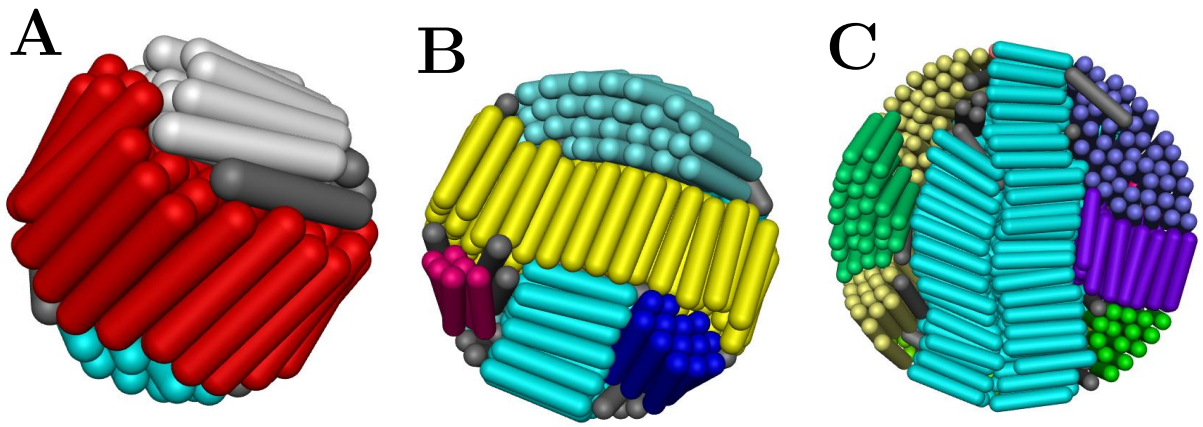

Figure 4.4: Final configurations of simulated rods in spherical confinement. Different smectic domains are identified with different colours. By comparing systems of increasing dimensions, an apparent tendency in exhibiting a single major smectic domain at the core is displayed. Additional separate smectic domains are observed to form perpendicularly to it. From left to right, systems consisting of $N = 100$ (**A**), $N = 2000$ (**B**) and $N = 5000$ (**C**) are shown.

assumed a C-shaped structure, so that the almost entire organization of the supraparticle arise from the com-penetration of complementary smectic domains. We called this pattern as "baseball" fashion arrangement, since all the structure was outlined by the com-penetration of C-shaped layers interrupting one the other (Figure 4.5, textitTop). Apparently, this configuration fallows from the one already observed for $N = 100$. By increasing the number of particles and thus the dimensions of the final supraparticle, minor layers already observed in the former case gradually expand also in the central part of the structure and hamper the formation of a major domain at the center.

We subsequently directed our attention to the simulation for $N = 1000$. In this case, the supraparticle is large enough to accommodate two smectic layers in its central part forming one single domain. However, it was observed that the present layers do not remain parallel one the other, but they conversely cross in order to more effectively filling the centre of the supraparticle.

An insight in the formation of this particular structure can be obtained by observing how the internal organization of the supraparticle changes during the simulation time (see Figure 4.5, *Bottom*). After the nucleation of small smectic domains starting from the region close to the confinement, smectic domains extend until they form a major single smectic domain spread in all the size of the supraparticle. However, by further increasing the packing fraction, the spherical constrain forces single smectic layers to misalign one the other for filling the

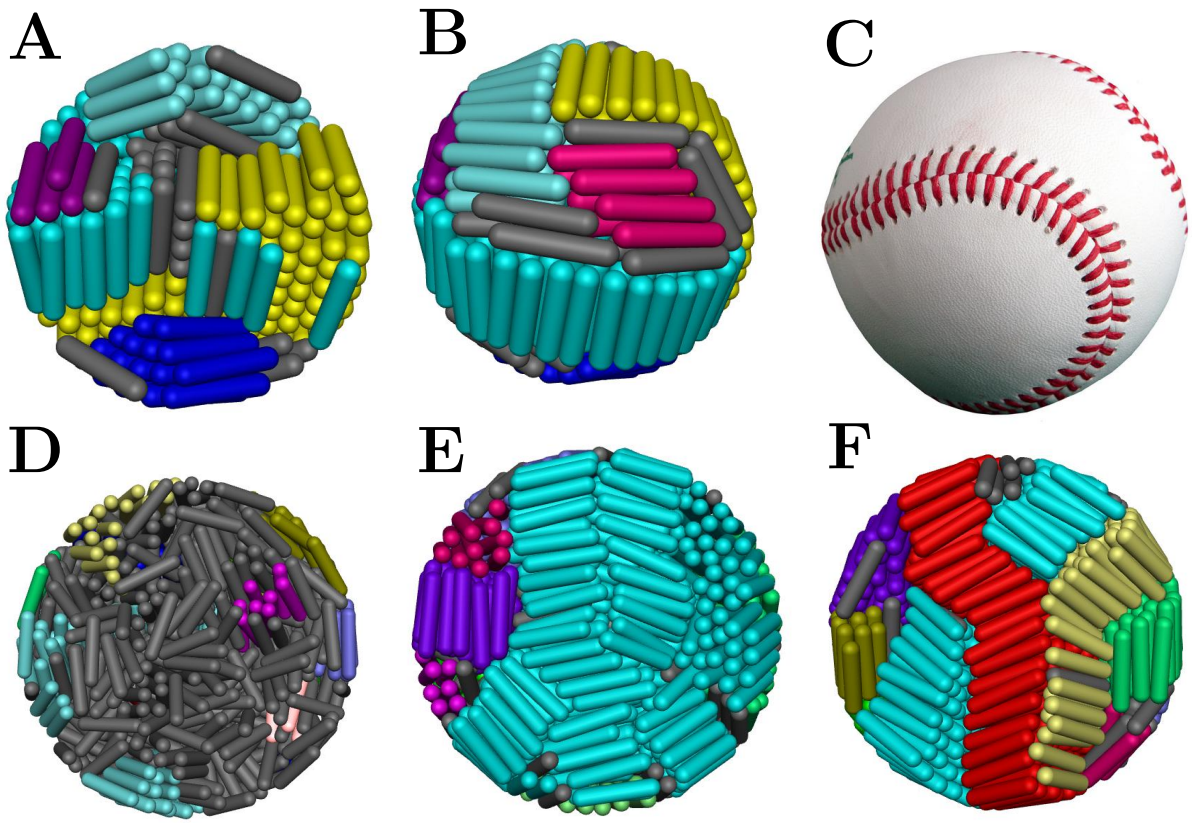

Figure 4.5: *Top:* Internal (**A**) and external (**B**) configuration of a system of $N = 400$ spherocylindrical particles in a shrinking confining cavity (packing fraction $\phi = 0.70$). Different smectic domains are identified with different colours. The whole volume of the spherical cavity is occupied by complementary C-shaped smectic domains which form a peculiar fashion resembling a baseball (**C**). *Bottom:* A system constituted by $N = 1000$ as appears at values of ϕ. Smectic layers show to nucleate close to the confinement (**D**, $\phi = 0.46$) before smectic ordering spreads in all the cavity volume by forming a single main smectic domain (**E**, $\phi = 0.58$). By further increasing the packing fractio, the presence of the confinement forces the major domain to separate into smaller ones which are not aligned one the other (**F**, $\phi = 0.68$).

spherical cavity, so that the major domain is split into smaller ones. A similar pattern was also visible in the case of $N = 400$. Note that in the final configuration each of the two crossing layers constituting the major domain also bend with respect to the other, so that they may also be recognized as different domains in the identification of single smectic regions. In this case as well, the outside aspect of the supraparticle seemingly reproduces the "baseball" fashion already observed in the previous example.

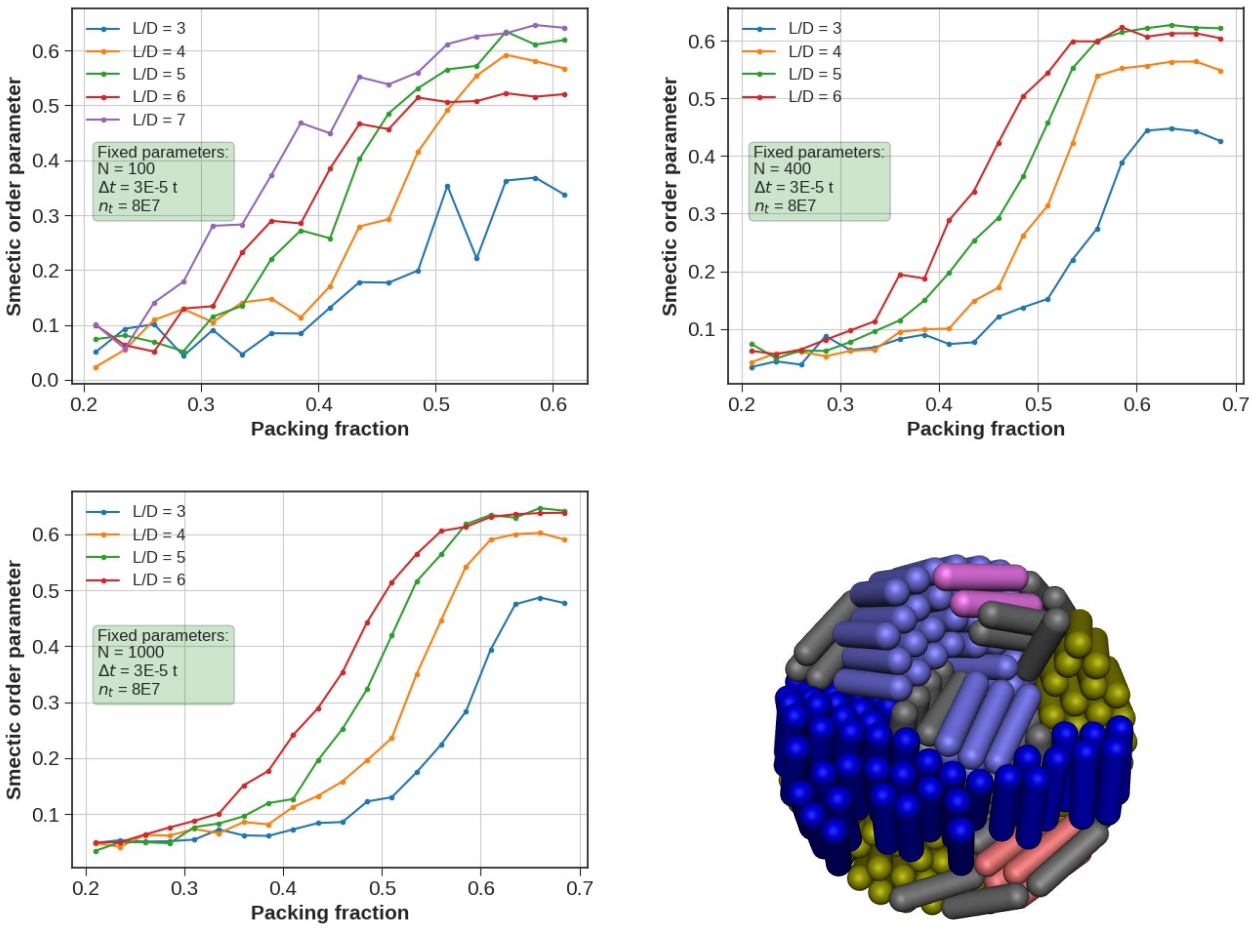

Figure 4.6: Smectic order parameter value as a function of packing fraction ϕ for different aspect ratios L/D as indicated in the legend. By decreasing aspect ratio of simulated particles, the order within the supraparticle correspondingly decreases. Notice that for $L/D = 7.0$, dynamics of bigger systems were not taken into account since related simulations displayed some instabilities. The internal structure of a representative system consisted of $N = 400$ particles with $L/D = 4.0$ is shown.

Aiming to qualitatively investigate how the simulated structures were affected by the compression rate, we observed that shorter simulations generally conducted to the formation of smaller smectic domains. By increasing the compression rates even further, we noticed that some smectic ordering was recognized only in the region close to the boundary. The observation once more confirmed the spherical confinement plays a fundamental role, not only in providing the spherical shape to the final structure but also in acting as an heterogeneous initiator of the smectic ordering.

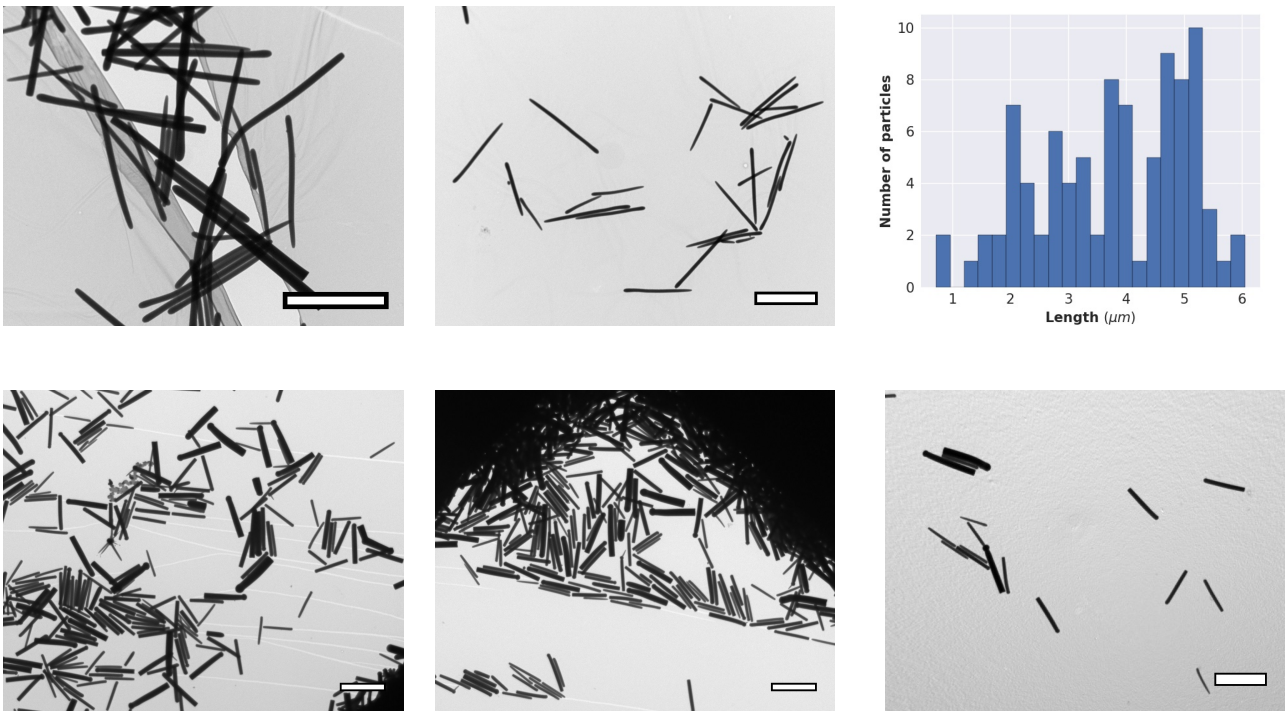

Figure 4.7: *Top:* TEM images of DR01 (left, center) and histogram of the distribution of the length(right). Scalebars indicate 3 μm. *Bottom:* TEM images of DR02 after removing smaller particles. Scale bars refer to 5 μm

A final investigation was subsequently outlined by similarly simulating the self-assembly of rods of different aspect ratios L/D (Figure 4.6). We thus verified that the ordering of the system clearly depends on the variation of this parameter, since generally higher values of order were reached for higher anisotropy in the particle shapes. Interestingly, we observe the formation of smectic layer also in the case of $L/D = 3.0$, although smectic domains appeared much smaller compared to other cases. By inspection of the obtained structures, we finally proved that a similar patter as described above was generally present, since layers preferentially arranged into complementary C-shaped domains typical of what we defined as the "baseball" fashion.

4.2.2 Synthesis of fluorescent silica rods

In order to experimentally study the self-assembly behaviour of spherocylinders, we proceeded in the synthesis of rod-shaped colloidal particles. It is well known that hard spherocylinders exhibit a wider range of phases, such as liquid crystal phases, only if their aspect

ratio is higher than a certain threshold [29]. For an analogous synthetic method to the one we employed, Kuijk noted that longer and thinner rods are obtained at increased temperature [55] . Since we were interested in synthesizing particles capable to dispose into smectic layers, a first batch of silica rods cores (DR01) was therefore prepared according to the procedure described in Section 4.1.3 by leaving the reaction undisturbed for 3 days at 30 °C. Note that this temperature is slightly higher than room temperature usually employed for the synthesis. TEM images on the obtained particles are shown in Figure 4.7, *Top*). The method noticeably provided long and thin rods, with the mean length of 3.77 μm ($\delta_L = 0.33$) and diameters of 0.17 μm ($\delta_D = 0.23$, aspect ratio $L/D = 22.1$). However, we additionally observed that the resulting high values of aspect ratio were reached at the expense of the straightness of particles, so that many bent rods were also detected.

Since separation of bent from straight rods would not be possible with the simple centrifugation procedure described in Section 4.1.3, a new batch was rather prepared by setting the temperature to 25 °C and leaving the reaction undisturbed for 3 days (DR02, Figure 4.7, *Bottom*). Noticeably, the outcome confirmed that temperature plays a major role in determining the final aspect of the particles, since a slight decrease in temperature resulted in generally straighter and shorter particles. However, we noted that many of the obtained rods also exhibited a sphere at one end. This interesting feature was already observed in the group, and may be ascribed to the use of an old bottle of TEOS [46]. Exposed to the atmospheric water part of the TEOS can pre-hydrolize in the storage bottle due to water impurities. As hydrolized TEOS can react really fast, once added to the reaction mixture it can condense in the oil phase, forming silica spheres, or migrate from the oil medium and quickly condensate to the water-oil interface, forming a silica shell outside the water-droplet. By then, when silica rods anisotropically grows from the water-in-oil droplet, it ends with a sphere merged in one of its extremity.

As clearly DR02 particles do not completely resemble the spherocylindrical particles we aimed to produce, a new batch (DR03-core) was prepared bewaring to use a new bottle of TEOS. The reaction was performed at 25 °C and left undisturbed at constant temperature for 5 days (Figure 4.8, **A-C**). The new batch resulted in straight particles of a wide range of length and aspect ratio. Particles were therefore purified according to the procedure reported in Section 4.1.3, which successfully reduced the polydispersity of the rods (DR03-GB, Figure 4.8, **D-F**). The sample was than coated with a fluorescent labeled silica shell and further non-fluorescent silica coatings were performed before a new purification step. The latter procedure was required as the growth of the fluorescent silica shell resulted in many

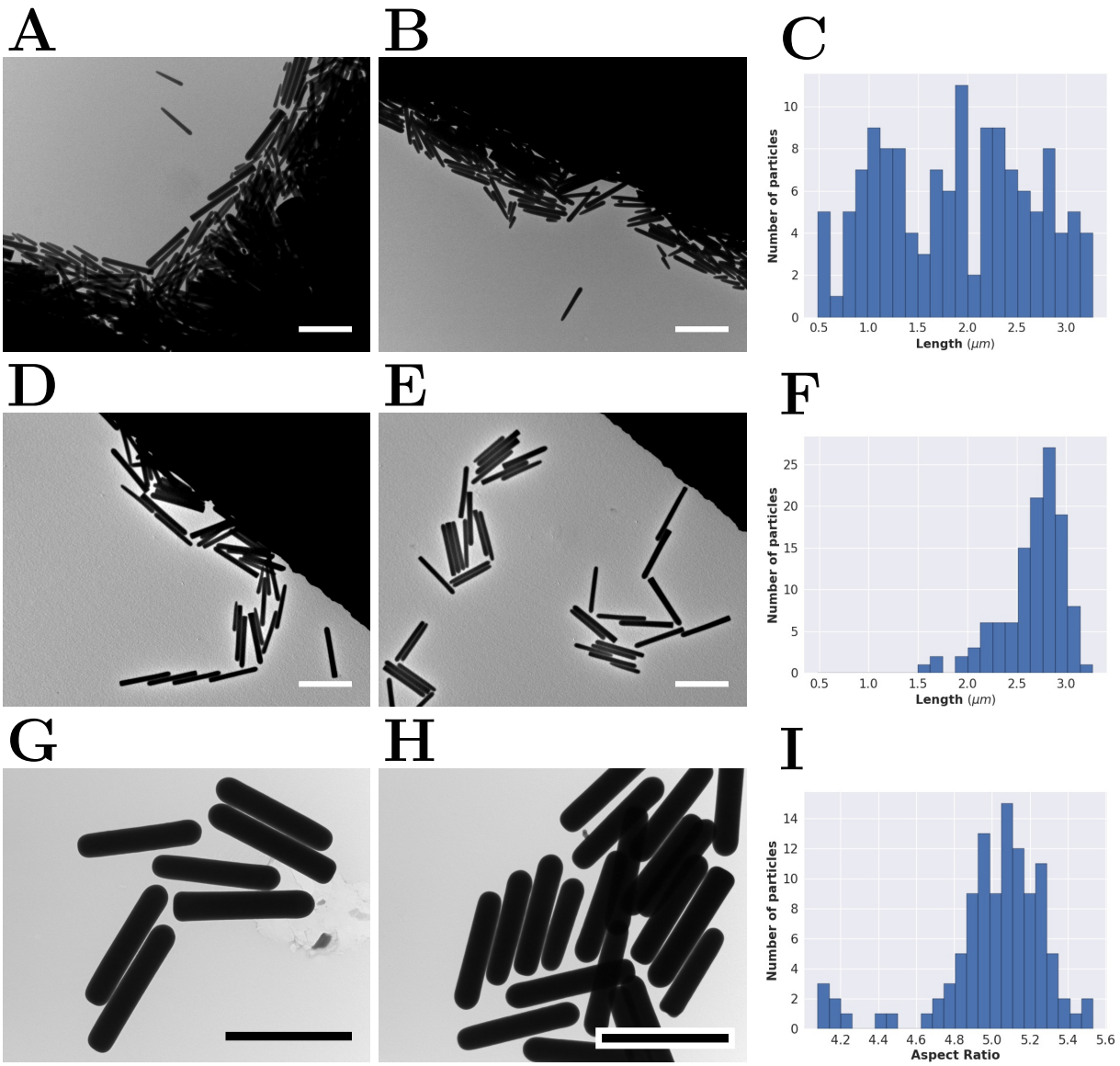

Figure 4.8: (**A-B**) TEM images of DR03 cores and (**C**) histogram of the distribution of the length(*right*). Mean length L = 1.89 μm, Mean diameter D = 220 nm. (**D-E**) TEM images of the DR03 cores and (**F**) relative distribution of the length after the purification procedure (DR03-GB, L = 2.68 μm, D = 245 nm). (**G-H**) TEM images of final rod-shaped particles DR03-B2 (L = 3.00 μm, D = 598 nm). A histogram of the distribution of the aspect ratios is additionally reported (**I**). All scale bars refer to 3 μm

particles irreversibly aggregated. This is thought to be due to the presence of the silane coupling agent, APS, which destabilize the surface of rods by incorporating positive charges on the surface [56]. After the purification, several silica coatings were grown so to obtained a non-fluorescent silica shell of the desired thickness (DR03-B2, Figure 4.8, **G-I**) to allow single particle optical microscopy. Dimensions of rods at selected synthetic steps are shown

in Table 4.1.

Sample name	L (μm)	δL	D (nm)	δD	L/D	NF-Shell (nm)
DR03-core	1.89	0.39	220	0.20	8.4	//
DR03-GB	2.68	0.12	245	0.16	11.1	//
DR03-B2	3.00	0.09	598	0.05	5.0	134

Table 4.1: Dimensions of the particles after selected synthetic steps. NF refers to the non-fluorescent silica shell thickness

4.2.3 Sedimentation experiment on Rods

Computer simulation studies discussed in Section 4.2.1 clearly showed that the modelled spherical confining conditions may induce spherocylindrical particles to self-assemble by forming smectic layers. Our first experimental investigations were therefore aimed to demonstrate the synthesized rods were generally capable to form a smectic liquid crystal phase in a bulk system. It must be stressed that, differently from the simplified system used in the simulation studies, a real system always presents additional elements, such as Van der Waals interaction, polydispersity values and not perfectly spherocylindrical shape, which in principle can affect the phase behaviour of the particles. Polydispersity in particular has been shown to dramatically affect the self-assembly process, so that ordered phases may become more problematic to form or even disappear for high values of polydispersity in sizes [66]. In order to study the phase behaviour of the system, a thick sediment was prepared according to the procedure reported in Section 4.1.4 by using a index-matched solvent solution either constituted by DMSO/water or glycerol/water. As micro-sized colloidal particles are strongly affected by the gravitational field, rods at the bottom of a thick sediment experience a significant pressure due to the weight of overlaying particles. The applied compression can in turn induce their self-assembly in a ordered structure. In principle, a thick sediment may be employed to study all the phase behaviour of the particles, since various values of pressure are realized at different depth in the sediment.

By preparing the sedimentation cell using a DMSO/water solution as a solvent, we took advantage of its low viscosity, which allows the system to reach the equilibrium configuration in less time compared to the use of glycerol/water solution. In particular, we observed that in the case of DMSO/water solvent, rods already formed small smectic layers at the bottom of the sediment few days after the preparation of the sedimentation cell. The extension of

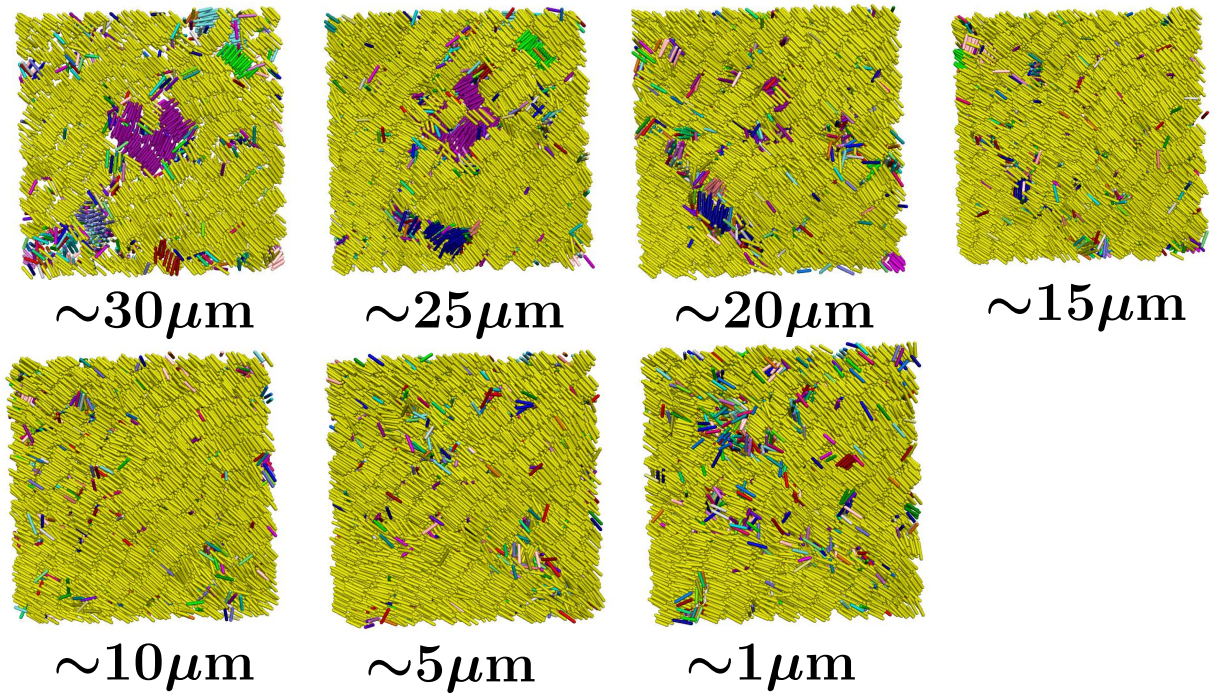

Figure 4.9: Reconstructed configuration of a thick sediment constituted of more than 17,000 silica rods immersed in a index-matched glycerol/water solution. Displayed measures refer to approximate distances from the coverglass while images are shown as looking upwards from the bottom of the sediment. Various colours were used for representing different smectic domains.

the smectic layers was then recognized to increase further until 7-10 days has passed from the preparation of the cell. At this time, we assumed that the sediment had finally reached its final configuration since no appreciable alterations in the structure were observed by leaving the system equilibrating for longer times.

The overall experiment qualitatively allowed to verify that the obtained particles were able to form liquid crystalline smectic layers. However, due to the low viscosity of the employed solvent, computation of the particle positions and orientations was not completely possible. In fact, since the solvent cannot sufficiently slow down random Brownian motion of the rods, particle displacements during the microscopy analysis result in more noisy and less resolute images, which therefore are more difficult to process. In order to reconstruct quantitatively the sediment configuration, a similar experiment was repeated by using the glycerol/water solvent. Due to the high viscosity of the solution, particles motion is strongly reduced and the system requires considerably more time for equilibrating. By imaging the sediment after 108 days from its preparation, we observed that the reached configuration

still exhibited significant inhomogeneities since regions at similar depth were observed to consist of either large smectic layers or more disordered phases. The remark clearly pointed out the system in its totality hadn't reached the equilibrium configuration yet. We anyway proceeded in further examining one of the region of the sediment which mostly displayed smectic ordering. In fact, by reconstructing the configuration of that region of the sediment, we eventually aimed to test the reliability of the designed order parameters also for a real experimental system. The reconstruction was performed by using the method reported in Section 4.1.7 (see Figure 4.9).

Notice that the images represent a sediment of 24 μm of thickness as they appear by looking upward from the coverglass and that in each image the prospect is moved forward closer to the bottom of the sediment itself. We clearly denoted the considered region as mainly dominated by one single domain. By using the same domain identification algorithm as described in Section 4.1.2, smaller smectic domains and defects are evidently visible. In particular, at the top of the sediment smectic layers which are not aligned with the main director are present. Notably, most of the smectic domains lay perpendicular to the gravitational field. This behaviour is thought to arise adue to rods at the bottom preferentially align parallel to the coverglass and thus acting as heterogeneous initiators of the smectic ordering. However, note that at the top of the sediment a smectic domain pointing perpendicularly to the gravitational field is shown. This particular case may reveal a homogeneous nucleation of the order may in our experiment. However, it should be stressed that not-aligned domains probably arises from the out-of-equilibrium conditions of the system and are likely to disappear by leaving the sediment to equilibrate for longer times.

By moving deeper in the sediment, misaligned domains increasingly disappear until the reconstructed section only consists of a single, extensive smectic domain. By observing further deeper in the sediment, small defects emerge again. Their presence is believed to depend on the Van der Waals attraction between the particles and the coverglass, which may induce some rods to stick to the glass preventing them from aligning to the surrounding particles within the smectic layers. Moreover, it has been shown that since bigger rods are more affected by the gravitational field, they tend to accumulate at the bottom of the sediment thus increasing the polydispersity locally and reducing the degree of order [39]. However, we expect this effect to be of limited impact in our case due to the low values of overall polydispersity and the absence of rods of considerable bigger sizes compared to the average dimensions. Finally, we stress that a number of the misaligned single rods may also arise because of a not correct identification of the particles by the employed rod tracking

algorithm.

Global and local order parameters for the reproduced system were eventually evaluated. The summarized results are reported in Table 4.2. The overall analysis showed that the defined order parameters were suitable for the description of the experimental results, since high values in th order parameters correctly reflected the significant degree of order qualitatively observed by eye inspection. Note that the estimated local smectic order qualitatively confirmed a threshold of $\tau_i = 0.35$ was a reasonable value for distinguish between a smectic ordered particle from a disordered one in the single domain identification algorithm.

Order parameter	Value
Global nematic S	0.82
Local Nematic S_i	0.88
Local Smectic τ_i	0.56

Table 4.2: Order parameter values calculated from the reconstructed configuration of a thick sediment of rod-shaped particles. Details over the order parameter evaluation are reported in Section 4.1.2.

4.2.4 Self-assembly of Rods in Spherical Confinement

Preliminary Attempts

Self-assembly of rods in spherical confinement was experimentally reproduced by using the same method as described in Section 3.1.4 and earlier employed in the case of spherical particles. As in the case of colloidal spheres, significant attention should be given to the particular setup used for preventing fast evaporation of water from the sample. In fact, by slowing down the evaporation rate of water we simultaneously reduce the compression speed of the confinement. On the other hand, simulation studies had already shown that slow compression rate may be crucial for the formation of ordered phases inside the supraparticle.

First spherical confinement-induced self-assembly attempts were experimentally exploited by preparing the usual water-in-oil emulsion containing particles in a 20-ml vial. The vial opening was then closed with some layers of Teflon tape, which were then holed by using a 0.6 mm needle. Finally, the prepared sample was kept in a controlled shakers at a speed ranging from 250 to 300 rpm and the water content appeared to dry overnight. Scanning electron microscopy (SEM) images of the procedure outcome are shown in Figure 4.10. By

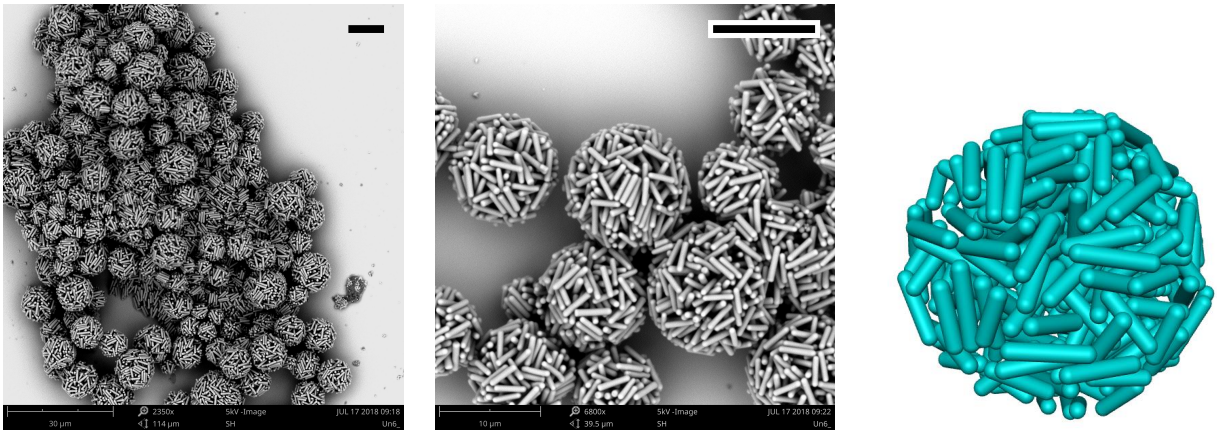

Figure 4.10: Supraparticles constituted by silica rods in a disordered configuration as obtained in preliminary experimental attempts. SEM images (*left, center*) and a reconstructed configuration (*right*) are reported. Scale bars refer to 5 μm.

the microscopy technique we confirmed that the method successfully provided well-shaped spherical supraparticles of diameter between 5 to 12 μm. Each supraparticle in turn was constituted by rod-shaped particles which adhered one the other in a stable configuration due to Van der Waals forces. However, the inspection of the outside of the supraparticles Through SEM microscopy already suggested that the rods had failed to organize in a liquid crystalline phase. The outcome clearly disagreed with what observed through Brownian Dynamics simulations, as we expected rods to spontaneously self-assemble in smectic layers due to the compression of the confinement.

Since the colloidal particles were fluorescent labelled, we further revealed and reconstructed, the internal structures of the supraparticles by using confocal laser scanning microscopy (CLSM) and the tracking algorithm as described in Section 4.1.7. Althought the analysis qualitatively confirmed an overall disordered configuration was present also at the inside of the supraparticles, quantitative analysis of the local order parameters interestingly determined values respectively of $0.16 < S_i < 0.20$ for the local nematic and $0.08 < \tau_i < 0.10$ for the local smectic order. Note that the inspected supraparticles were composed by between 100 and 250 rod-shaped particles and the final packing fraction was estimated between 0.42 and 0.52.

Effect of decrease of water evaporation rate

The above outcomes remarkably revealed that despite the overall disorder of the structure, the system displayed a modest but measurable tendency to align rods locally toward the

formation of crystalline phases. We therefore considered to decrease the evaporation rate of water from the sample in order to allow rods more time to equilibrate in a more stable configuration. This task was pursued by covering the vial aperture with several layers of Teflon tape but avoiding to make a hole through them. Water drying was therefore reduced as water molecules had to migrate through the Teflon cover in order to evaporate. In particular, the samples appeared to dry at this stage in around 20 hours. SEM images of the vial content after washing with hexane are reported in Figure 4.11, *Top*. In this case, the supraparticles were estimated be between 5 and 15 μm. Interestingly, although the supraparticles still generally resulted not ordered, they anyway displayed a well-defined single smectic layer on the external part. This feature appeared particularly evident and was observed on a considerable number of supraparticles. On the other hand, small supraparticles apparently displayed some degree of order in their outer organization.

By reconstructing the internal structures through confocal microscopy, we eventually successfully determined the associated order parameters values. For bigger supraparticles composed by between 400 to 930 rods, local nematic order parameter was measured be $0.14 < S_i < 0.28$, while local smectic parameter $0.08 < \tau_i < 0.14$. According to our predictions, a comparison between these values and the ones previously reported confirmed that the order inside the supraparticles increased by decrease of the water evaporation rate. In Figure 4.11 (*Bottom*) we further show an example of reconstructed supraparticle which exhibited a similar smectic layer at the surface as observed through SEM. Other smectic layers were also identified on other sides of the supraparticle, even though of comparatively smaller dimensions. Although the origin of this interesting feature cannot be completely clarified, we propose that the observed smectic layers actually represent the first nucleation of the smectic ordering of the system. This assumption can be supported by an increase of the order parameters values compared to the disordered configurations detected in previous attempts. Moreover, computer simulations studies tend to suggest the smectic ordering first arises from the confinement before spreading to the internal volume of the supraparticles. In a real system, alignment of rods at the interface may be additionally favoured by complex attractive interactions between particles and the interface itself. We therefore suggest the evaporation rate of water was slow enough for allowing the nucleation of few smectic layers at the water-oil interface. However, too fast compression likely prevented the internal volume of the supraparticle to self organize, so that Van der Waals forces froze recovered configurations before rods had enough time to fully dispose into smectic layers.

Finally, we successfully reconstructed the internal configuration of smaller supraparticles,

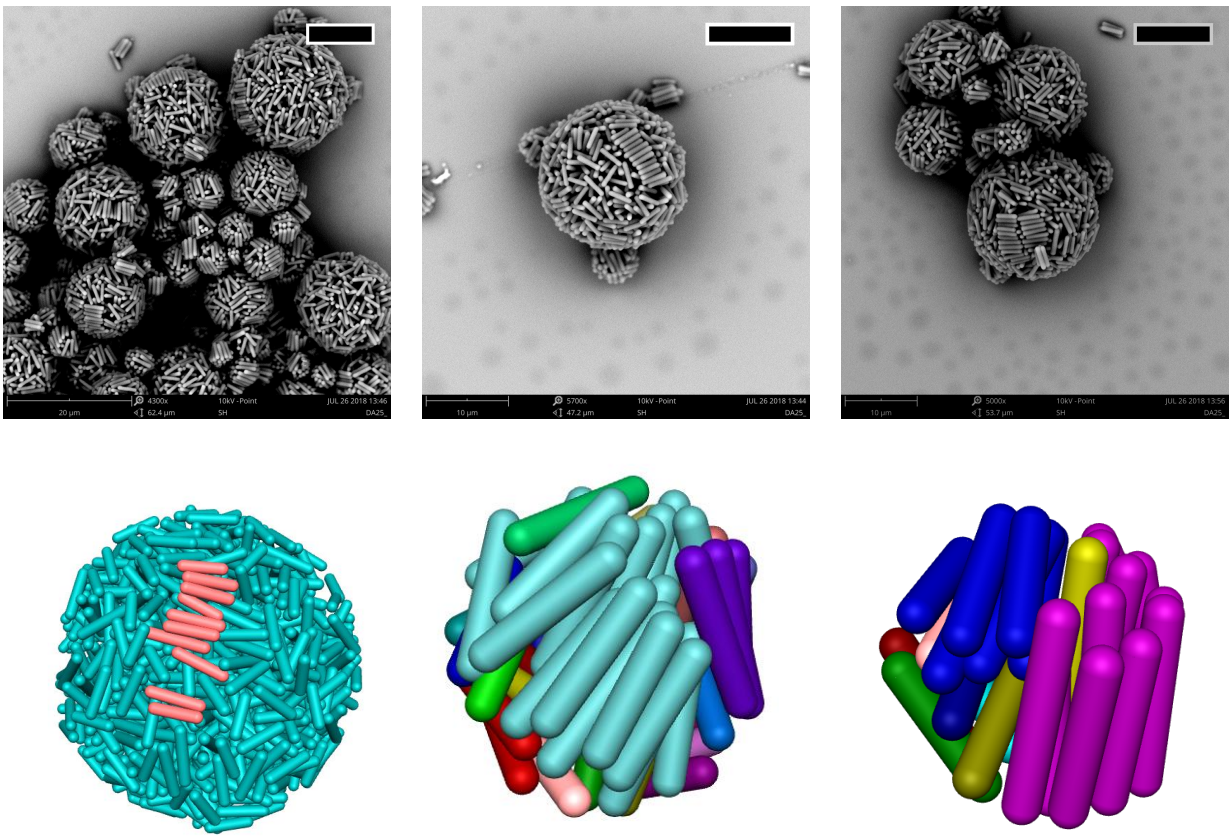

Figure 4.11: *Top:* SEM images of supraparticles constituted by silica rods as obtained by lowering the water evaporation rate from the emulsion. Smectic layers of rods are clearly visible on the surface of most of the supraparticles. Scale bars refer to 5 μm. *Bottom*: reconstructed configuration of supraparticles of various size. In the case of the bigger supraparticle (*left*), our reconstruction process successfully reproduced the smectic layer of rods at the surface as observed form SEM images.

composed by around 30 to 50 rods (see Figure 4.11, *Bottom*). The structures displayed larger degree of local nematic and local smectic order, which were quantified be respectively $0.54 < S_i < 0.66$ and $0.32 < \tau_i < 0.43$. The comparably high degree of order also allowed identification of different smectic domains. In particular, we revealed that higher order parameters values were calculated when considering smaller supraparticles. This trend was reproduced also in the case of large supraparticles and is reversed to what observed via computer simulations.

The origin of this discrepancy may be associated to complex interactions between rods and the water-oil interface which may partially reslut in rods migrating toward the interface and align. Evidences supporting a similar behaviour will be further presented in the fallowing

sections. In the case of sufficiently small emulsion droplets, the particle/boundary interaction is accordingly believed to become increasingly relevant, thus favouring the rod alignment at the surface. On the other hand, since we simply modelled the particle/interface interaction by a WCA potential, a similar behaviour would be impossible to observe through our computer simulations.

Determination of emulsion dimensions during slow drying

In previous efforts, higher degree of local nematic and smectic order were measured by decreasing water evaporation rate from the sample. However, even in latter attempts rods failed to fully organize in a liquid crystalline structure. We therefore proceeded in slowing down the evaporation rate of water even more. To this extend, a slightly different set up was explored; in this case 5 ml of the water-in-oil emulsion were still prepared in a 20-ml vial, but the vial opening was closed by using a porous septum (Figure 4.12, **A**). The septum was subsequently skewered with a variable number of needles and the vial was kept on a controlled shaker at the usual speed. Notice that for a similar system water evaporation should result substantially hindered since water molecule need to diffuse for all the way through the needle length in order to evade the sample.

In line with our predictions, the new method successfully appeared to slow down the evaporation rate of water, since samples were observed not to have dried even after several days from their preparation. However, before proceeding with the addition of colloidal particles to the water phase so to induce their self-assembly, we preferred first to study how the realized set up influenced the emulsion dimensions during the drying process. In fact, while the controlled shaker has been extensively employed for preventing water droplet sedimentation, we still ignored whether the fast shaking affected the formed emulsion. A fresh experiment was therefore prepared as described above by using a single needle of 0.2 mm of diameter. Since the vial content cannot be directly observed *in situ*, aliquots of the emulsion were subsequently collected and observed through optical microscope (Leica DM IL LED inverted microscope equipped with a Phantom Miro eX4 camera, magnification = 20x, Figure 4.12, **D**). Obtained images were then analysed in order to compute the dimensions of the water-in-oil droplets. To this end, we employed python library cv2.HoughCircles based on the use of Hough Transform function. Details on the method can be found in [67].

It must be noted that in the general procedure as described above, water removal process from the sample can be assumed as composed by two subsequent steps: first water evaporates from the water-in-oil system to the gaseous phase inside the vial, then water vapour diffuses

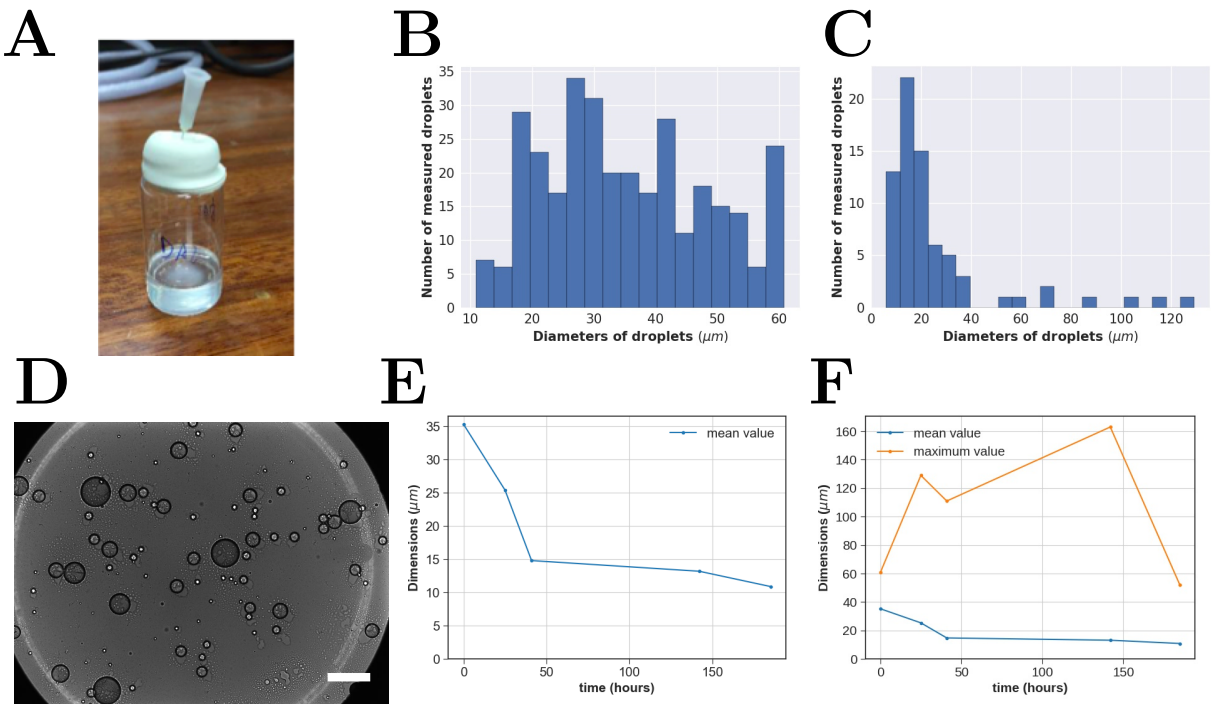

Figure 4.12: (**A**) A 20-mL vial as prepared for preventing fast water evaporation. Size distributions of the water droplets is shown as obtained both immediately after preparation of the water-in-oil emulsion (**B**) and after 25h (**C**) is reported. Droplet sizes were measured from optical microscopy images like (**D**). The scale bar refers to 50 μm. Note that in the considered time droplets of diameter >40 μm apparently coagulate to form consistently bigger ones. (**E**) Mean value of droplet diameter sizes was plotted as a function of the drying time in a separate diagram for a more clear representation of its trend. (**F**) Mean and maximum values of measured diameter as a function of drying time. While the mean value constantly decreases in the considered time, big droplets were observed to form after preparation of the emulsion and dried only at long time.

through all the length of the needle to the outer atmosphere. Since in the present case water evaporation was observed to involve several days, as compared to several hours of previous experiments, it was clear that for the considered system the rate determining step of the overall process is the water diffusion from inside to the surrounding environment through the needle. It follows that the gaseous phase inside the vial can be assumed as always saturated of water vapour.

In the quantitative study of the emulsion dimensions as outlined above, examined sample aliquots were each time collected by temporarily removing the porous septa from the vial. In those occasions, saturated vapour from inside the vial could easily diffuse to the atmosphere and the evaporation process cannot be assumed as simply lead by the diffusion through the

needle. Nonetheless, although the illustrated results should not be considered a meaningful quantitative analysis over the typical drying procedure, we believed they could anyway give us some qualitative evidence over the general effect of the controlled shaker on the emulsion droplet dimensions.

Water-in-oil emulsion prepared by hand-shake was observed to consist of considerably polydispersed water droplets, of diameters between 10 to 60 μm (see Figure 4.12, **B**). After just few hours from the preparation, a micro-sized emulsion appeared in all the oil medium in addition to the major emulsion. This behaviour, which was observed also when the sample was left undisturbed after preparation, is believed to result from the slight solubility of the water in hexadecane. Due to the presence of surfactant in the oil phase, supersaturation of water in hexadecane may therefore provide the formation of small stable water droplets.

By plotting the mean of the water droplet sizes over the time, a seemingly exponential decay in size can be observed (Figure 4.12, **E**). However, by considering the distribution of the diameter dimensions, we noted that in addition to an overall decrease in the diameters sizes, bigger water droplets formed, of size up to few hundreds of μm (Figure 4.12, **C** and **F**). Finally, for longer times, both small and big water droplet appeared to progressively dry. From the reported observations, we deduced that the controlled shaker was able to suspend water droplets of diameter at least up to 35 μm. This consideration may also be supported by considering that the supraparticles usually reached maximum diameters of around 15 μm. By assuming, in fact, that the colloidal particles are concentrated around $(35/15)^3 = 12.6$ times, the starting packing fraction of 0.04 v/v is predicted become around 0.50 v/v. Note that this value agrees with the estimated packing fractions reported in previous sections for reconstructed final structures.

Additionally, our analysis revealed that bigger droplets than a certain diameter size combine to form major ones. This behaviour is presumably due to the fact that the controlled shaker cannot suspend massive droplets, so they sediment at the bottom of the vial where they merge one the other. This consideration also explains the formation of huge aggregates of rods which were occasionally observed in the purified sample through SEM microscopy and which we didn't discuss above as not interesting to the extend of our studies.

Self-assembly of Rods at slow compression rates

Since we demonstrated our new setup was successful in decreasing the evaporation rate of water by at least one order of magnitude, we repeated the self-assembly experiment by using the same method as described above, bewaring to skewer the porous septa with several

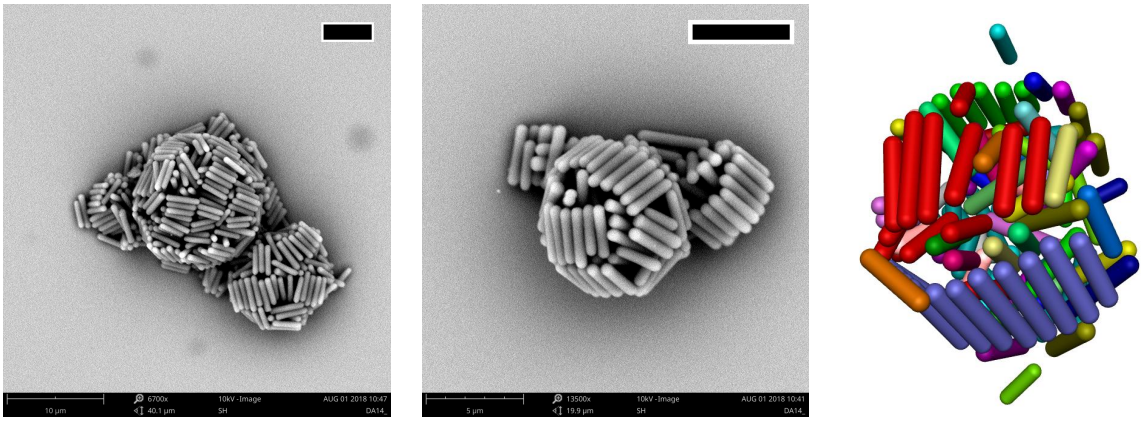

Figure 4.13: Supraparticles constituted by silica rods as experimentally obtained for slow compression rates. SEM images (*left, center*) and a reconstructed configuration from confocal microscopy data (*right*) are reported. As well-defined smectic layers were clearly exhibited on the outside of the supraparticle, inspection of the internal arrangement surprisingly revealed a hollow structure had been obtained. Scale bars refer to 5 μm.

needles of 1.2 mm of section in order to prevent evaporation becoming too slow. Note that in this case employed glassware was previously coated with OTMOS by using the procedure described in Section 4.1.6. In fact, it was noted that for long times hydrophilic silica particles tended to stick to the walls and bottom of the vial. By substituting the terminating hydroxyl groups with long C18 aliphatic chains we therefore ensured hydrophobic properties for the glass, thus preventing attractive interaction with silica particles.

The so prepared samples appeared to dry in 21 days. SEM images remarkably revealed supraparticles exhibited well defined smectic layers on the outside (Figure 4.13). However, when we employed confocal microscopy to detect the inner structure, we interestingly observed that rods were present mostly in the outer part of the supraparticles, while the inside displayed only few disordered particles or no particles at all. Supraparticles constituted by around 100 rods were subsequently reconstructed and local nematic and local smectic order parameters were respectively determined be $0.53 < S_i < 0.66$ and $0.35 < \tau_i < 0.39$. Clearly, the high values of local order reflected the substantial smectic organization of the outer part of the supraparticles.

In order to self organize on the water-oil interface, colloidal particles presumably exhibited some kind of attractive interaction to the interface. To test this assumption, a water-in-oil emulsion containing colloidal particles was prepared as usual and subsequently inspected by confocal microscopy (Figure 4.14). It can be noted from the collected images that rods

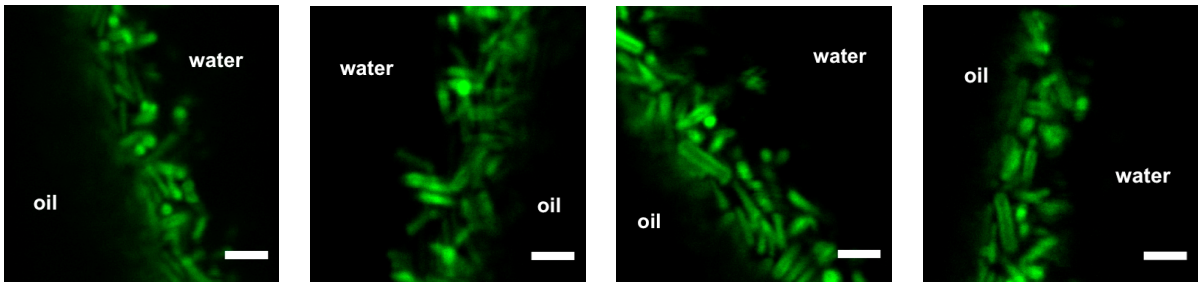

Figure 4.14: Laser scanning confocal microscopy (LSCM) images of a water-in-oil emulsion containing rod-shaped colloidal particles. Colloids spontaneously migrate toward the water-oil interface. Scale bars refer to 3 μm.

evidently displayed a strong tendency in moving toward the interface. The outcome was therefore explained by considering both the attractive rod-interface interaction and the slow evaporation rate of water. In fact, previous experiments determined a constant change in the interface size due to fast water evaporation and thus prevented rods to organize at the water-oil region. However, at the present case evaporation rate was low enough to consider the interface be quasi-static. As far as the water-oil surface is too extended compared to the rods dimensions, the local packing fraction is too low for inducing self organization into smectic layers. On the contrary, as soon as the surface reaches a sufficiently small extension, rods at the surface may 2D self-assemble into the observed smectic order. Finally, Van der Waals may affect the particles, forcing them to stick one the other and thus halting the final structure.

Among others, Loudet et al. studied the interaction between anisotropic particles at the interface [68]. By considering a water-oil system not far from the one employed in the present work, he noted that ellipsoidal colloidal particles have the tendency to migrate to the interface and disposing parallel to it. Moreover, he observed that in the case of silica-coated particles, ellipsoids preferentially aligned side-to-side due to capillary forces. Although in the present case particles resemble more a spherocylindrical shape than ellipsoidal, we estimate capillary interactions may play an important role in the formation of the observed 2D self-assembly.

Self-assembly of Rods by drying on the rotating stage

A final self-assembly procedure was tested using a completely different setup. In this experiment, a rectangular capillary of section 0.3 x 3.0 mm was filled with the usual water-in-oil emulsion containing colloidal rods. The capillary was then put to dry on a rotating stage,

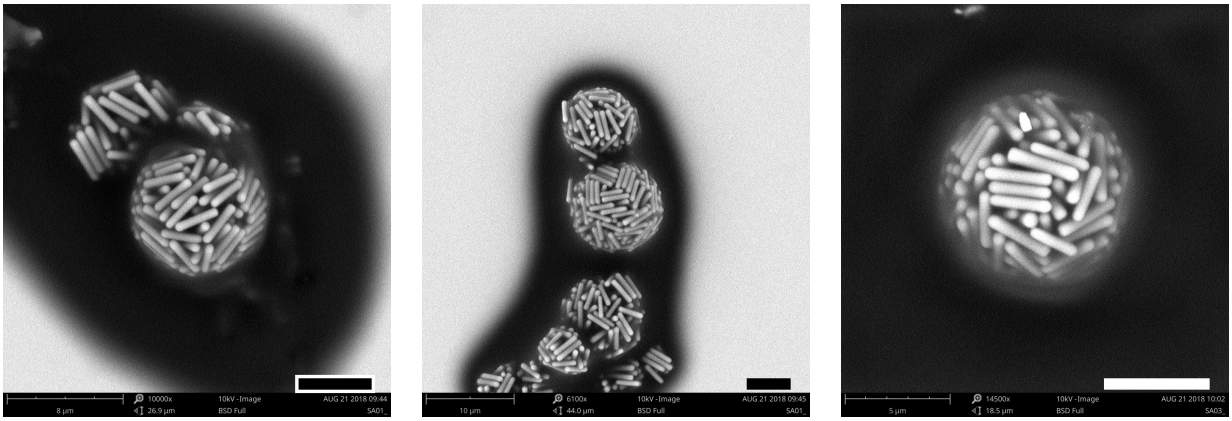

Figure 4.15: SEM images of supraparticles of rods as obtained by slow evaporation of the water-in-oil emulsion on the rotating stage. Scale bars refer to 5 μm.

which consists of a sample holder, made from a silicone elastomer, in which several slots were created to accommodate microscope glass slides. The sample holder results in turn attached to an electric motor which rotates it around a horizontal axis. A detailed description over the manufacture of the employed device is reported in [69]. The reportedly net effect of the rotating stage on the sample is to average the gravitational field, thus simulating microgravity and preventing colloidal particles from sedimenting.

After 40 days from the preparation of the emulsion, the sample was observed being dried and thus imaged with SEM microscopy after washing with hexane. Images are shown in Figure 4.15. Note that the dark spots around the supraparticles probably arise due to the presence of SPAN80. In fact, the collection of small amounts of particles through the described method prevents their extensive washes due to the chance of removing also an important fraction of particles. The microscopy technique qualitatively revealed obtained supraparticles exhibited moderate degree of smectic order at the outside. Although the low water evaporation rate from the capillary extremities, particles constituting the supraparticles didn't appear to have preferentially migrated toward the interface to form hollow supraparticles as observed in the previous paragraph. The reason of this interesting discrepancy is not completely clear. Unfortunately, determination of the internal structure via confocal microscopy was not possible because of the time limit imposed to the present project. A quantitative evaluation of the order parameters was therefore not achieved.

4.2.5 Conclusions

Self-assembly of rods in spherical confinement was extensively investigated by using both computer simulation technique and experimental approaches. In particular, Brownian Dynamics simulation of spherocylindrical colloids in a shrinking confining cavity was first employed in order to study the effect of the confinement on the final configuration of the system. Interestingly, we demonstrated that particles interacting via repulsive potential spontaneously self-organize into smectic layers. Differently from a bulk system, the presence of the confinement remarkably prevented the formation of a single smectic domain. In particular, smectic ordering appeared to nucleate at the confining boundary before spreading in all the supraparticle volume. However, by increasing the compression even further, the confinement clearly affected the organization by splitting the single domain into different ones. Although the final configuration apparently displayed a tendency in creating a single smectic domain at the core of the supraparticles - while smaller smectic layers at the supraparticle edges tend to organize perpendicularly to the mentioned main domain - for increasingly number of rods few com-penetrating smectic layers of comparable extension occur. This behaviour, which we defined as "baseball"-like, clearly arises from the necessity of accommodating particles in the available spherical volume. The quantitative evaluation of the local smectic order by using a correspondent order parameter clearly revealed the organization of the particles into smectic layers was encouraged by the slow shrinking rate of the confining cavity.

In order to experimentally reproduce self-assembly of spherocylinders in spherical confining conditions, we successfully synthesized fluorescent-labelled rod-shaped silica particles of moderate polydispersity in size. Remarkably, the synthetic method confirmed to be extremely sensitive to the reaction parameters, in particular with respect to the selected temperature and the use of fresh TEOS, as the employment of incorrect conditions prevented the formation of particles of the desired shape. By the use of a sedimentation cell, we further demonstrated that the obtained silica rods were able to self-organize into smectic layers in a bulk system. A shrinking spherical confinement was reproduced by dispersing colloidal particles in water and drying the subsequently formed water-in-oil emulsion. Although scanning electron microscopy (SEM) technique first unveiled the formation of well-defined spherical supraparticles from emulsion droplets, the reconstruction of the internal structures from confocal images revealed a generally disordered configuration also inside the supraparticles. By reducing the evaporation rate of water, a moderate increase in the smectic ordering of the system was observed. Remarkably, the formation of single smectic layers on the sur-

face of the supraparticles possibly revealed the nucleation of smectic organization from the water-oil interface. However, by decreasing the water evaporation rate even further, hollow supraparticles exhibiting smectic ordering only on the surface were collected. This interesting behaviour was interpreted as a 2D self-assembly at the interface which may form in the case of slow shrinking rates and in the presence of attractive interaction between colloidal particles and the water-oil interface. The existence of the latter condition in the present case was demonstrated by observation of a water-in-oil emulsion containing the considered particles with confocal microscopy.

Finally, we eventually investigate the employment of a different setup involving the use of a rotating stage for slowly evaporating the water content from the sample. Interestingly, the new setup qualitatively appeared to mostly provide more ordered supraparticles compared to the previous method, failing to exhibit any evidence for the colloidal particles to stick one another while preferentially migrating toward the interface. The origin of different outcomes from the two employed methods is still not clear. Unfortunately, because of time limits determination of the internal structure via confocal microscopy and quantitative evaluation of the order parameter for this case were not possible.

Chapter 5

Self-assembly of Colloidal Rods and Spheres

5.1 Introduction

Most of the smart materials commonly in use are mixtures of several components. In fact, more than one constituent is generally required to determine the essential material properties for a given application. Although binary mixtures of hard spheres have been largely studied in last decades, phase behaviour of mixtures of hard spheres and spherocylinders represent a somehow new subject for colloidal science research.

Koda *et al.* first reported a theoretical study involving free energy calculations in order to determine a nematic-smectic A phase transition in a system constituted of hard spheres and parallel hard spherocylinders [70]. Remarkably, by evaluating the obtained density waves for spherocylinder and spheres in the smectic A structure, their work revealed a microphase separation occurs, so that spheres preferentially dispose between layers of aligned spherocylinders. The same configuration was also obtained by computer simulation using a Monte Carlo technique in a NPT ensemble.

After addition of spheres of a polystyrene (PS) polymer in a suspension of filamentous bacteriophage fd virus, Adams *et al.* observed a wide range of phases which depends on the concentration of the two components. In particular, when the concentration of spheres is increased, demixing of the two components occurs and the spheres are observed dispose into columns perpendicular to the nematic director of rods [71]. By further increasing the sphere concentration, lamellae of spheres spacing between layers of fd virus eventually form. However, it should be observed that charge, chirality and flexibility of the fd-viruses may

play an important role in determining their phase behaviour. An experimental study involving rigid and achiral rods has been recently outlined and reported by the group [72]. By leaving sedimenting a system of silica spheres and rods, a binary smectic liquid crystalline organization was clearly observed, in which smectic layers of rods alternate with layers of spheres. In addition to real-data analysis, Monte Carlo simulations confirmed the observed organization can be stabilized by entropy alone. Notably, the latter study also revealed that for high molar fractios of spheres and at high pressure, the binary smectic phase tended to become unstable and single layers of rods in coexistence with a sphere-rich isotropic phase was observed.

Other than a scientific interest, the self-assembly of spheres and rods may be regarded with great attraction for future applications which may take advantage of the combination of different length scales and different materials. For instance, it has been suggested that for the described binary smectic system the use of gold nanorods and spherical semiconductor may display prominent plasmonic properties [72]. In fact, spherical semiconductor particles at the gold nanorod tips are likely to experience strong plasmon enhanced electromagnetic fields, which in turn may result in intensifying the luminescence of the semiconductor particles. In addition to creating bulk systems, we largely discussed an experimental method for assemble colloidal particles in a shrinking spherical confinement. A similar technique would allow the formation of stable, spherical supraparticles which may easily be collected and isolated thus incrementing the range of conditions allowing the application of the technology.

Since currently our investigations have failed in experimentally providing well-defined, liquid crystalline configuration in the final supraparticles - and also because of time limits imposed to the project - results reported in the present chapter have been mainly obtained via computer simulation approach. The current results should therefore be considered as an exploratory study, which could eventually pave the way for future experimental investigations.

5.2 Methods

5.2.1 Sedimentation experiment

Sedimentation experiments involving both silica rods and spheres were conducted following the general method described in Section 4.1.4. Since particles of different shapes were labelled by using two distinct fluorescent dyes, confocal microscopy can be used to image them

separately. In particular, rods were labelled with fluorescein dye, which can be excited at 488 nm and mainly emits between 490 and 600 nm, while we employed rhodamine dye for spheres, whom absorbance maximum is located at 552 nm while the emission lays in the range 540-700 nm. As a result, lasers set at different wavelengths can be used to excite either of the two particle species, while detecting windows of separate detectors can be adjusted to discriminate the emission of either rods or spheres.

5.2.2 Brownian Dynamics (BD) simulations

Brownian Dynamics simulations of mixture of rods and spheres in spherical confinement were performed according to the same method as described in Section 3.1.1. In the case of spherocylindrical particles, additional considerations as reported in Section 4.1.1 still apply. Note that the use of both rods and spheres introduces in a new degree of freedom in the system. In reported simulations we therefore introduced a supplementary parameter X which represent the molar fraction of spheres over all the simulated particles.

5.2.3 Order parameters

In order to quantitatively evaluate the formation of binary smectic in our computer simulations, we introduced a novel local order parameter. In preceding work, it was observed that the main feature of the supposed configuration is the microphase separation between rods and spheres, which leads to the formation of layers of rods and spheres. The layering of the spherical particles was therefore quantified using a global order parameter which is in fully analogy with the one for rod reported in Section 4.1.2.

$$\tau_{sph} = \max l \left| \sum_{j=1}^{N} e^{2\pi i \mathbf{r}_j \cdot \mathbf{n}/l} \right|, \tag{5.1}$$

where $\mathbf{r}_j$ is the position of particle j and l is a real number. The number of l which maximize the above expression coincide with the layer spacing.

However, similarly to what already stated in the case of rods, the defined global order parameter is not suitable for evaluating the order of small systems or fluctuating layers because too noisy. The introduction of a novel local order parameter is therefore required for correctly evaluating the degree of order in the system. In our case, we observed that layers of spheres in the considered configuration preferentially form planes which are orthogonal to the smectic layer director of rod (Figure 5.1, *left*). In general, the orthogonality of two vector $\mathbf{a}$, $\mathbf{b}$ forming an angle θ can be evaluate by considering the function:

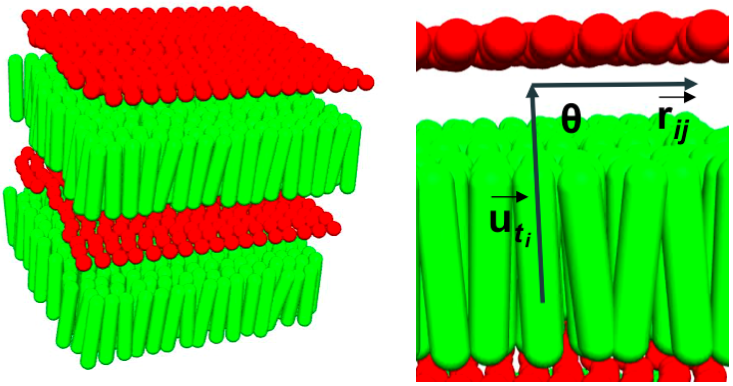

Figure 5.1: Graphic representation of the considered binary smectic order. Orthogonality condition between vectors $\mathbf{u}_{t_i}$ and $\mathbf{r}_{ij}$ was considered for evaluating the formation of alternating layers of rods and spheres.

$$f(\theta) = 1 - 3cos^2(\theta) = 1 - 3(\mathbf{a} \cdot \mathbf{b}), \tag{5.2}$$

$f(\theta)$ clearly ranges between -2 and 1 and has the advantage to be equal to 1 in the case of perfectly orthogonal vectors and to 0 for a random distribution of angles θ. Estimating expression 5.2 as a good candidate for our novel local order parameter, for each sphere i we first determined the rod t_i with the closest tip to i. We then evaluated:

$$\Theta_i = \frac{1}{n_b} \sum_{j=1}^{n_b} \left[1 - 3 \left(\frac{\mathbf{r}_{ij}}{|\mathbf{r}_{ij}|} \cdot \mathbf{u}_{t_i} \right)^2 \right] \tag{5.3}$$

where $\mathbf{u}_{t_i}$ represent the direction of rod t_i and n_b is the number of neighbour spheres j, defined as spherical particles which satisfy the condition $\mathbf{r}_{ij} < 1.4\text{D}$ (Figure 5.1, *right*). In this case $\mathbf{r}_{ij}$ is the distance vector between the centres of mass of particle while D is the particle diameter.

In order to include in our evaluation also the local tendency in forming smectic layers of rods, the *local binary smectic order parameter* $\tau_{sph,i}$ was eventually defined as:

$$\tau_{sph,i} = \Theta_i \tau_{t_i} \tag{5.4}$$

where τ_{t_i} is the local smectic order parameter for rod t_i as defined in section 4.1.2. Spherical particle i was considered ordered in the case $\tau_{sph,i} > 0.20$. Note that seemingly low selected value is justified by the cutoff of 0.35 employed in the definition of smectic ordered rods.

By considering both the smectic layering of rods and the orthogonality between layers of rods and spheres, we believe our novel order parameter successfully takes into account all the main feature of the binary smectic configuration.

5.3 Results and Discussion

5.3.1 Sedimentation experiment

A thick sediment consisting of silica rods and spheres was prepared as described in Section 4.1.4 by dispersing particles in either a DMSO/water or a glycerol/water index-matched solvent solution. In fact, the experiment mainly aimed both to test the aptitude for the present system in displaying a binary smectic configuration and to reproduce results reported in [72]. After 70 days from preparation, confocal microscopy was therefore employed to observe the sample prepared in glycerol/water. Our inspection revealed the tendency of rods in disposing into smectic layers, although the formation of extensive ordered domains was not observed. Again, the present result can be explained with the high viscosity of the dispersing solution, which prevented the system from reaching an equilibrium configuration in the given time by slowing down the particle motion.

A similar investigation was subsequently lead over a sedimentation cell prepared by using the DMSO/water solution. Due to the relatively low viscosity of the dispersing agent, equilibration of the system was noticed already after several days from the preparation of the sample (Figure 5.2). In particular, at the top of the about 100 μm thick sediment we observed a fluid phase only constituted by spherical particles. By moving deeper into the sediment, the fluid phase becomes increasingly more dense until silica spheres eventually crystallize into a face-centred cubic (FCC) fashion. Further deep into the sample, rod-shaped particles appear into small smectic domains which progressively extend in dimensions and align with each other. It is worth noting that the additional presence of micro-phases of spheres to smectic layers of rods persist until the bottom of the sediment is reached. In the bottom section of the sediment the presence of alternating layers of spheres and rods revealed the supposed formation of the binary smectic configuration. Remarkably, except for the top section of the sediment, spheres are always observed organized into FCC-crystalline organization. This behaviour, which in here is observed for the first time, was already supposed in [72] and was likely achieved due to the low polydispersity in size of our particles compared to the ones reportedly employed. The detection of the binary smectic configuration also deep into the sediment confirmed it represents an actual characteristic phase for a mixture of rods and

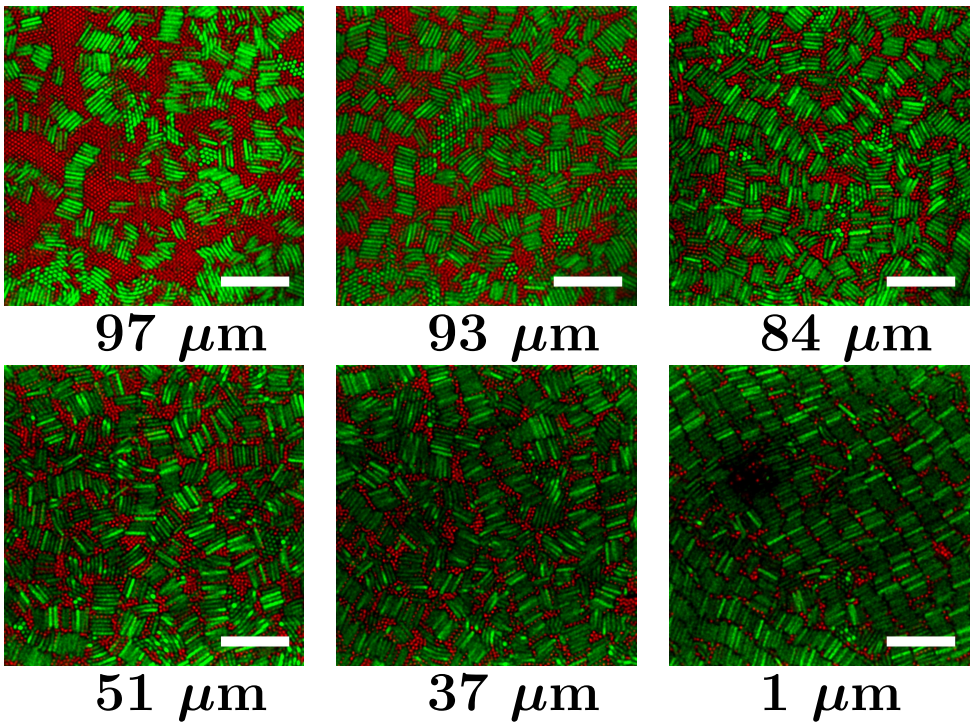

Figure 5.2: Representative scanning laser confocal microscopy (LSCM) images of a thick sediment of fluorescent spheres (*red*) and rods (*red*). Reported measures refer to their relative distance from the coverglass. Scale bars indicate 10 μm.

spheres acting as quasi-hard particle system.

5.3.2 Brownian Dynamics simulations of mixture of rods and spheres

Self-assembly in spherical confinement of mixtures of rods and spheres was investigated by using Brownian Dynamics simulations. In particular, two representative systems were considered, consisting of a total number of particles N of 500 and 1000. The relative composition of the system was varied by tuning the molar fraction of spheres x between 0.1 and 0.9.

Similarly to what accomplished in Sections 3.2.1 and 4.2.1, a consistent timestep value δt was first determined by performing several experiments for different δt at fixed $x = 0.50$. The effect of the time-discretization procedure was subsequently evaluated by both qualitative scrutiny of the reproduceed dynamics and quantitative analysis of the local nematic and rod smectic order parameters.

In general, our investigation revealed a consistent tendency for particles constituting the system to separate according to their shape (see Figure 5.3). At $X = 0.10$, a microphase separation consistent with the formation of a binary mixture configuration is observed.

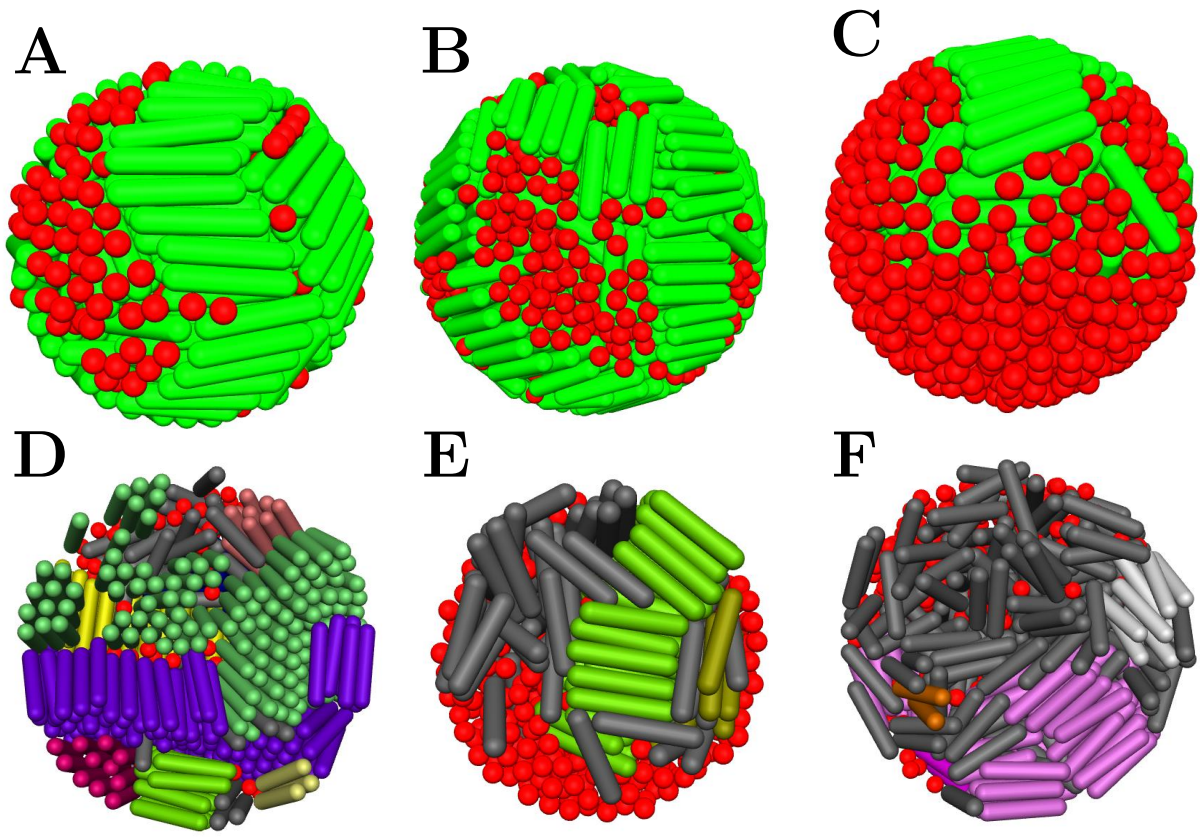

Figure 5.3: Simulated final configurations of mixtures of rods and spheres in spherical confinement. *Top:* external appearance of obtained supraparticles is shown. Different colours have been employed to distinguish rods (*green*) from spheres (*red*). **A** total number of particles $N = 500$, fraction of spheres $X = 0.3$. **B** $N = 1000$, $X = 0.3$. **C** $N = 1000$, $X = 0.8$. Note that by increasing the fraction of spheres segregation of spherical particles becomes increasingly evident. *Bottom:* representative examples of internal configurations for different conditions. Equally coloured spherocylindrical particles belong to the same smectic domain. **D** Internal final structure of a system constituted by $N = 1000$, $X = 0.2$. The presence of spheres (*red*) between smectic layered rods attests the presence of the considered binary smectic order. **E** $N = 1000$, $X = 0.8$. Despite the presence of only a small fraction of rods compared to spheres, former particles are yet observed to form some degree of smectic layering. **F** Internal configuration of a system of $N = 1000$, $X = 0.5$ as observed at intermediate packing fraction $\phi = 0.46$. Note that in the meanwhile spheres segregate toward one side of the spherical cavity, smectic ordering of rods is observed to nucleate close to the confinement and opposite to spheres preferential direction.

However, at $X = 0.20$ some degrees of segregation of spheres from a rod-rich phase appears. By increasing the molar fraction of spheres, segregation of spherical particles at one pole of the supraparticle becomes more and more evident. Note that the presence of spheres appeared not to disrupt the liquid-crystallinity of rods, as well-defined smectic layers were observed to form in all cases. Moreover, a modest number of spheres laying between layers of smectic rods were observed in most of the configurations, revealing a modest but not negligible tendency in creating a binary smectic configuration.

An insight into the segregation dynamics can be obtained by inspecting how the configuration changes at increased compressions. At low packing fractions, rods and spheres are spread in all the volume of the confining cavity and a fully disordered homogeneous phase is formed. However, for increasing packing fractions spheres progressively segregate toward one pole of the spherical cavity. Meanwhile, smectic layers of rods is shown to nucleate on the opposite pole of the supraparticle. Note that the nucleation of order in the region close to the interface was already observed in previous simulations involving rods or spheres alone. It is however interesting to observe that in the case of binary mixture smectic ordering for rods originate exactly in the region where concentration of spheres is lower.

Quantitative analysis of the simulated dynamics was outlined according to the method reported in Section 5.2.3 (Figure 5.4, *Top, Centre*). In particular, rod local smectic order τ evaluation correctly detected the observed propensity for rods in organizing into smectic layers. On the other hand, calculated values of local smectic order parameter for spheres τ_{sph} appeared to decrease at increasing values of X, thus reflecting a modest local tendency in forming a binary smectic configuration which decreased for increasing fractions of spheres. Note that in some cases values of τ_{sph} resulted in a rather noisy trend and occasionally in negative values of order. This behaviour, which is more evident for $N = 500$, can be illustrated by considering that small systems of poorly ordered particles are examined. Since τ_{sph} ranges from -2 and 1, small fluctuations around the 0-value can also lead to evaluation of negative values.

In order to obtain a more effective representation of the actual tendency in forming a binary smectic configuration, the fraction of smectic ordered spheres was evaluated (Figure 5.4, *bottom*). In particular, a particle was considered to have smectic order if the relative value of τ_{sph} was higher than 0.20. By using the proposed method for low fractions of spheres, up to around half of spherical particles were identified as belonging to a binary smectic configuration, while at increased values of x the relative amount of ordered particles decreased. The observation suggests the existence of a saturation concentration for spheres

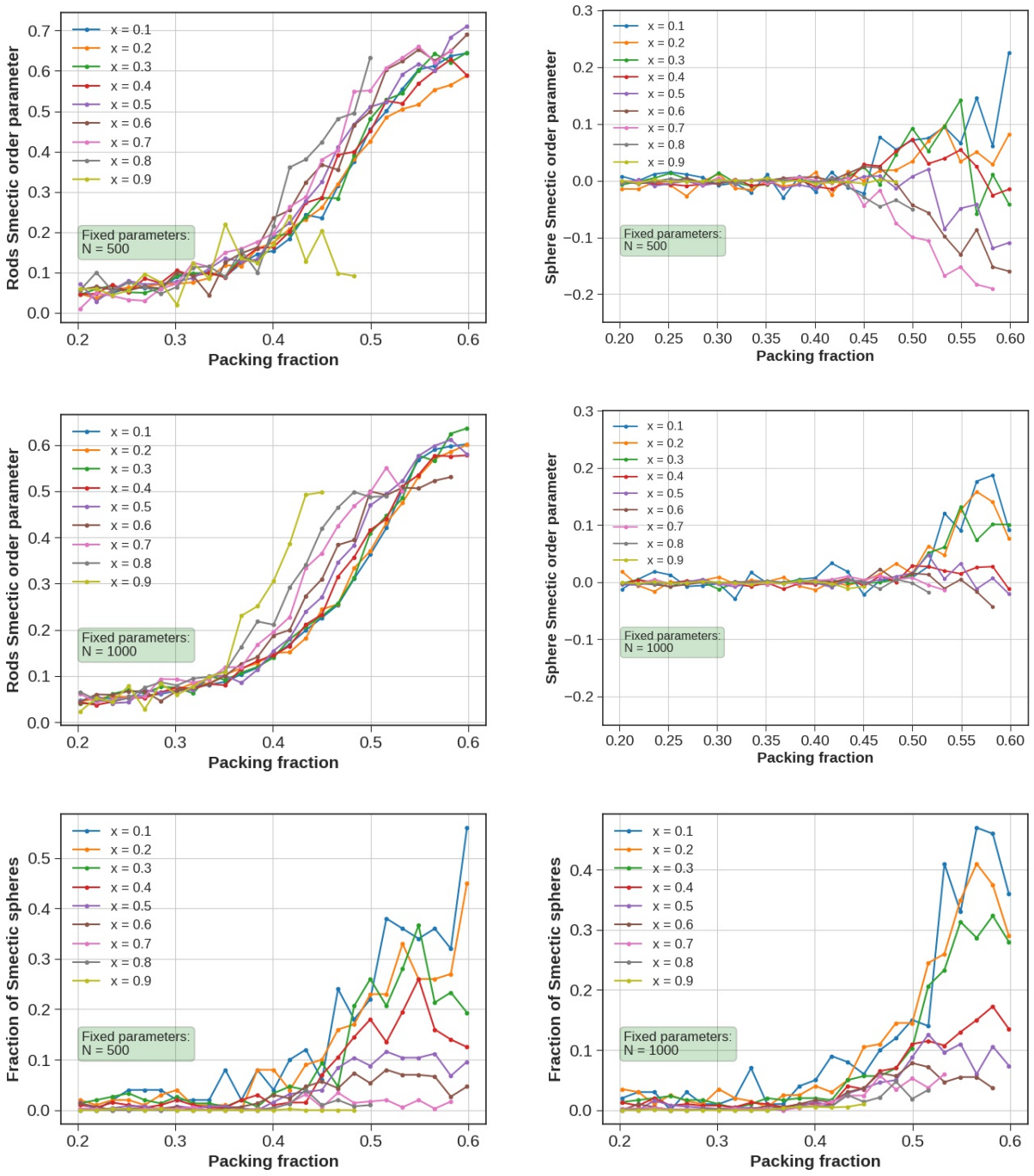

Figure 5.4: *Top, Center*: local smectic order parameters for rods and spheres as a function of the packing fraction as calculated for different fractions of spheres X. *Bottom*: fraction of smectic spheres as a function of the packing fraction. Spherical particles were considered ordered if their relative order parameter τ_{sph} satisfies the condition $\tau_{sph} > 0.20$.

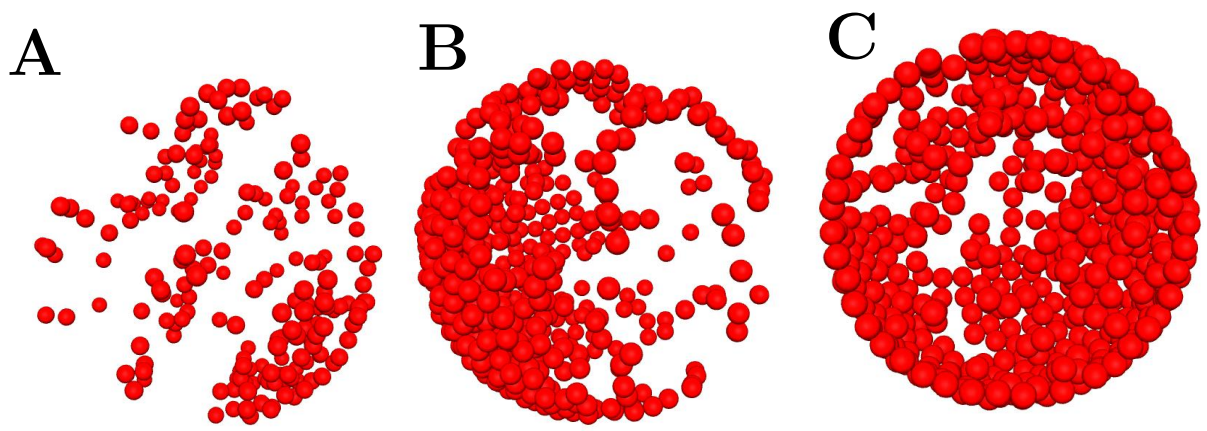

Figure 5.5: Final configuration of simulated binary mixtures consisting of $N = 1000$ particles in spherical confinement as obtained by removing spherocylindrical particles. While at $X = 0.20$ (**A**) the organisation of spheres into layers suggests the formation of a binary smectic configuration, by increasing the value of X, phase separation of spheres is evident. At $X = 0.50$ (**B**) spherical particles concentrated at on pole of the cavity and close to the confinement. However, note that some spheres are still arranged into layers, thus revealing binary smectic order formation still occurs to some extend. At $X = 0.80$ (**C**) spheres ultimately migrate toward the boundary region. In this case, no qualitative evidence of binary smectic ordering is detectable.

into the rod-rich phase, so that if a larger number of spheres per rod is added in the system, spherical particles spontaneously segregate in a separate phase.

By eventually removing all spherocylindrical particles from final simulated configurations, a simplified qualitative identification of the organization within the system is obtained (see Figure 5.5). At low values of X, the preferential disposition of spheres in layers clearly revealed the formation of the binary smectic configuration. By increasing the faction of spheres, segregation of spherical particles toward one pole of the supraparticle become more and more pronounced. Moreover, the inspection reveals that in addition to an overall propensity in separating from spherocylinders, spheres also tend to dispose close to the interface. This result can be explained by considering the larger ability for smaller spherical particles in efficiently filling the space close to a curved surface. On the other hand, segregation of particles of similar shapes can be explained by using the concept of depletion. Depletion forces are entropic forces which lead bigger colloidal particles to aggregate by exclusion of smaller ones. Moving from experimental results, Adams already proposed that in a rod-sphere mixture there is an effective rod-sphere attraction and an effective sphere-sphere

attraction due to a depletion mechanism [71]. In particular, the former was suggested to promote microphase formation, while the latter bulk phase separation. According to our observation, here we speculate that an effective rod-sphere attraction is prevalent for a bulk mixture of rods and spheres, so that a sedimentation experiment results in the formation of a binary smectic configuration. However, a sphere-sphere attraction seemingly dominates in spherical confinement conditions, so that segregation of spheres is preferred to micro-phase separation.

5.4 Conclusion

In this chapter we investigated the self-assembly of mixture of spherocylinders and spheres. By preparing a thick sediment of silica rods and spherical colloidal particles, a peculiar configuration consisting in alternating layers of spheres and smectic ordered rods was observed. The configuration is consistent with the formation of a binary smectic structure which had been already reported from members of the group [72]. However, in here we observed for the first time that the proposed configuration is compatible with the disposition of spheres in a FCC pattern. This particular organization was allowed due to the low degree of polydispersity of sphere dimensions.

Subsequent Brownian Dynamics simulations were performed to study the self-assembly of rods and spheres in spherical confinement. A novel order parameter τ_{sph} was additionally introduced for quantifying the formation of the discussed binary smectic configuration. Remarkably, our study revealed that the simulated conditions caused bulk segregation of spheres from a rod-rich phase already at modest molar fractions of spheres X. In particular, simulated dynamics showed spheres preferentially direct to the spherical confinement and toward one pole of the supraparticle. Meantime, smectic order for rod nucleates close to the confinement on exactly the opposite pole with respect to the spheres. This behaviour was explained by considering that sphere-sphere effective attraction dominates in a spherical confinement, thus promoting shape-like bulk separation. The proposed mechanism is believed to originate due to depletion effect considerations.

Finally, the quantitative data analysis eventually revealed the introduced order parameter correctly reflected the qualitatively observed trend in the formation of the binary smectic configuration.

Chapter 6

Conclusion and Outlook

In this thesis, self-assembly of colloidal particles was investigated using two complementary approaches: experimental observations and computer simulations studies. Our attention was directed toward spherocylindrical and spherical particles and our interest mainly pointed to uncover the effect of a spherical confinement on the particle organization. Brownian Dynamics simulations were first performed on a model consisting of strongly repulsive spheres segregated in a repulsive spherical shrinking cavity. The study revealed the confinement conditions dramatically affect the phase behaviour by favouring a five-fold icosahedral configuration over the FCC structure of bulk systems. Our results agreed with both reported observation on analogous experimental and simulated systems, thus confirming the quality of our simulation method. After synthesis of fluorescent-labelled colloidal silica spheres of 541 nm in size (polydispersity $\delta = 0.03$), self-assembly in spherical confinement was experimentally explored by dispersing colloidal particles in water and creating a water-in-oil emulsion. The shrinking behaviour of the cavity was then reproduced by slowly evaporating the water content from the sample. Although the proposed experimental method successfully provided well-shaped spherical supraparticles of size between 2 μm and 9 μm, inspection of the internal structure via laser scanning confocal microscopy (LSCM) and data analysis over the reconstructed configuration did not reveal the expected icosahedral-like crystalline structure. The divergence from preceding results and simulated outcomes can be ascribed to the tight crystalline identification conditions (see Section 3.1.2) as well as too fast evaporation rates.

Following a similar procedure, we explored self-assembly of rod-shaped particles in spherical confinement. In order to quantitatively analyse outcomes from both simulations and experiments, a rod smectic order parameter τ was introduced together with a novel algorithm for identification of smectic domains. Brownian Dynamics simulations of spherocylinders in

a spherical cavity first revealed particles locally order into smectic layers due to the presence of the confinement. Interestingly, the dynamics revealed a liquid-crystalline structure first nucleates close to the interface and then spreads to the entire volume of the cavity. A similar pattern had also been detected in the case of spheres. Moreover, the confinement was observed to frustrate the formation of a single smectic domain, which conversely separated into smaller ones. In general, a tendency in forming a smectic domain occupying the centre of the cavity was noted. Other additional smectic layers preferentially formed at the opposed poles of the supraparticles and perpendicularly to the central domain. In some cases, the whole structure of the supraparticle was mainly determined by the creation of com-penetrating C-shaped smectic domains of comparable extension, which we referred to as a "baseball" configuration.

After synthesis of fluorescent-labelled silica rods (L= 3.00 μm, D= 598 nm), self-assembly in bulk was explored by producing a thick sediment of colloidal particles. The experiment revealed that for long times rods at the bottom of the sediment spontaneously organize to form an extended smectic ordered domain. Self-assembly in spherical confinement in real systems was subsequently studied by using the same experimental method as outlined above. Despite the formation of well-shaped spherical supraparticles, our first experiments failed in providing smectic ordered supraparticles. By decreasing the evaporation rate of water, smectic order within the system appeared to moderately increase. However, by further decrease of the water evaporation rate, hollow supraparticles displaying a 2D smectic ordering at the surface eventually formed. This peculiar structure was revealed by using confocal microscopy technique and likely originated due to attractive interactions between particles and the water-oil interface. Finally, a different setup involving the use of a rotating stage was preliminary explored for the self-assembly of rods. The method seemingly provided more smectic ordered supraparticles, while scanning electron microscopy (SEM) revealed no evidence of the existence of cavity in the structure. However, inspection of the internal configuration through confocal microscopy was not feasible due to time constrains.

We finally considered a mixture of colloidal rods and spheres. Experimental investigation over a thick sediment remarkably revealed the system can organize so that layers of spheres alternate between layers of smectic ordered rods. A similar configuration had already been reported and ascribed to the formation of a different phase, referred to as binary smectic. A novel order parameter for the quantification of the binary smectic order was then introduced. The order parameter - which was eventually employed in the data analysis of simulated mixtures of spheres and spherocylinders in a spherical shrinking cavity - apparently captured

the order within the system. In general, our study revealed that considered particles in spherical confinement conditions spontaneously separate into a sphere-rich and a rod-rich phases. In particular, spheres appeared to preferentially migrate toward the interface and one pole of the supraparticle, while rod smectic order originates close to the confinement at the opposite pole. This behaviour, which becomes more and more evident by increasing the molar faction of spheres X, was ascribed to the rising of effective sphere-sphere attraction due to depletion effect. A modest formation of the considered binary smectic configuration was eventually observed in the case of low values of X.

Future experiments should shine new light over the self-assembly of rods and mixtures of rods and spheres in spherical confinement. In particular, experimental methods aimed to slowing down the evaporation rate of water should be explored. In fact, we believe that this parameter is of fundamental importance for the formation of a ordered configurations within the final supraparticles. To this extend, the use of the rotating stage may be a promising technique since it allows very slow evaporation rates while apparently preventing the formation of hollowed supraparticles. A more extensive simulation study on mixture of rods and spheres may also be of great interest. By tuning input parameters such as the total number of simulated particles, the fraction of spheres and the ratio between sphere and rod dimensions, stabilizing conditions for a binary smectic configuration may be revealed. In fact, the disclosure of the supposed conditions would pave the way to the realization of stable binary smectic-structured supraparticles on either micro- or nano-size, thus allowing the realization of composite materials of potentially outstanding and still unexplored properties.

Appendix A: Gravitational Effect

The gravitational force affecting a particle immersed in a liquid can be expressed as $F(x) = mg$, where m is expressed as $m = V\delta\rho$, with V the volume of the colloidal particle and $\delta\rho$ the density difference between the particle and the fluid. Due to the gravitational force, the system experience a flux of particles, moving in the direction of the applied gravitational field. This flux, often refered to as *drift flux*, can be expressed as the particle concentration in a certain position times the average velocity:

$$J_{drift} = \rho(x)v(x) \tag{6.1}$$

Let as now define the mobility as the ratio between the mean velocity of the particle and the applied gravitational force:

$$\mu(x) = \frac{v(x)}{F(x)} \tag{6.2}$$

by substituing in the previous equation:

$$J_{drift} = \rho(x)\mu(x)F(x) = -\rho(x)\mu(x)\nabla U(x) \tag{6.3}$$

where we used the relation $F(x) = -\nabla U(x)$.

In general, the drift of a particle immersed in a fluid is balanced by the drag force, which is the fluid resistance to the particle motion. The drag force could be related to diffusional random motion through the *fluctuation-dissipation theorem* (FDT). Generally speaking, the theorem states that in a system at equilibrium the response to a small perturbation is the same as a response to a spontaneous fluctuation. In our case, assuming the systems is in thermal equilibrium, the perturbative drag force generates heat, and therefore Brownian motion, which could be treated as a thermal fluctuation within the system. The flux of particles generated by diffusion can be expressed by *Fick's law*:

$$J_{diff} = -D\nabla\rho(x) \tag{6.4}$$

where D is the diffusional constant.

As the system is at equilibrium, diffusional flux balance the drift flux and we can so write the relation:

$$0 = J_{diff} + J_{drift} = -\rho(x)\mu(x)\nabla U(x) - D\nabla\rho(x) \tag{6.5}$$

Now, using the chain rule, we can substitute:

$$\nabla\rho(x) = \frac{d\rho(x)}{dU(x)}\nabla U(x) \tag{6.6}$$

and obtain:

$$0 = J_{diff} + J_{drift} = \left(-\rho(x)\mu(x) - D\frac{d\rho(x)}{dU(x)}\right)\nabla U(x) \tag{6.7}$$

from which we can derive:

$$D = \frac{-\rho(x)\mu(x)}{\frac{d\rho(x)}{dU}} \tag{6.8}$$

Finally, by using Maxwell-Boltzmann statistics we can write:

$$\rho(x) = Ae^{-\frac{U(x)}{k_B T}} \tag{6.9}$$

and obtain the *Einstein-Smoluchowski relation* [18]:

$$D = \mu(x)k_B T \tag{6.10}$$

From this equation, we can calculate the velocity of the colloidal particle where diffusional flux and gravitational drift are in equilibrium, usually called *terminal velocity*:

$$D = \mu(x)k_B T = \frac{v(x)k_B T}{F(x)} \quad \text{and} \quad v(x) = \frac{F(x)D}{k_B T} = \frac{Dmg}{k_B T} \tag{6.11}$$

Remarkably, known the mobility μ of a certain particle, the *Einstein-Smoluchowski relation* let us calculate the diffusional coefficient. For spherical particles, translational and rotational mobility can be obtained by solving *Stokes equation*.

$$\mu_t(x) = \frac{1}{6\pi\eta R} \rightarrow D_t = \frac{k_b T}{6\pi\eta R} \tag{6.12}$$

$$\mu_r(x) = \frac{1}{8\pi\eta R^3} \rightarrow D_r = \frac{k_b T}{8\pi\eta R^3} \tag{6.13}$$

where η is the dynamic viscosity of the system. This relations are usually referred to as the *Stokes-Einstein equation*.

Bibliography

[1] T. Graham, "On liquid diffusion applied to analysis," *Philosophical transactions of the Royal Society of London*, vol. 151, pp. 183–224, 1861.

[2] K. D. Weiss, "Paint and coatings: A mature industry in transition," *Progress in Polymer Science (Oxford)*, 1997.

[3] R. Brown, "A brief account of microscopical observations made in the months of June, July and August, 1827, on the particles contained in the pollen of plants; and on the general existence of active molecules in organic and inorganic bodies," *The Philosophical Magazine*, vol. 4, no. 21, pp. 161–173, 1828.

[4] A. Van Blaaderen and P. Wiltzius, "Real-space structure of colloidal hard-sphere glasses," *Science*, vol. 270, pp. 1177–1179, 1995.

[5] D. Frenkel, "Order through entropy," *Nature Materials*, vol. 14, p. 9, 2015.

[6] J. Israelachvili, *Intermolecular and Surface forces*. 1985.

[7] F. London, "The general theory o f molecular forces.," *Trans. Faraday Soc.*, vol. 33, pp. 8b–26, 1937.

[8] H. C. Hamaker, "The London-van der Waals attraction between spherical particles," *Physica*, vol. 4, pp. 1058–1072, 1937.

[9] O. Stewrn, "Zur theorie der elektrolytischen doppelschicht," *Zeitschrift für Elektrochemie und angewandte physikalische Chemie*, pp. 508–516, 1924.

[10] J. Riley, *Charge in Collidal Systems,*. Blackwell Publishing, 2005.

[11] T. Tadros, "General Principles of Colloid Stability and the Role of Surface Forces," in *Colloids and Interface Science Series*, 2010.

[12] B. Derjaguin and L. Landau, "Theory of the stability of strongly charged lyophobic sols and of the adhesion of strongly charged particles in solutions of electrolytes," *Acta Physicochim*, vol. 14, pp. 633–662, 1941.

[13] E. J. Verwey and J. T. G. Overbeek, "Theory of the stability of lyophobic colloids," *Journal of Colloid Science*, vol. 51, pp. 631–636, 1955.

[14] J. C. Maxwell, "Illustrations of the dynamical theory of gases. Part I. On the motions and collisions of perfectly elastic spheres.," *Dublin Philosophical Magazine and Journal of Science*, vol. 19, no. 236, 1860.

[15] L. Boltzmann, *Lectures on Gas Theory.* 1964.

[16] A. Einstein, "Über die von der molekularkinetischen theorie der wärme geforderte bewegung von in ruhenden flüssigkeiten suspendierten teilchen.," *Ann. Phys. (Leipzig)*, vol. 322, pp. 549–560, 1905.

[17] J. B. Perrin, "Mouvement Brownien et réalité moléculaire," *Ann. Chim. Phys.*, vol. 18, pp. 5–114, 1909.

[18] K. Dill and S. Bromberg, *Molecular Driving Forces: Statistical Thermodynamics in Chemistry and Biology. By K. A. Dill, S. Bromberg.* 2003.

[19] S. Broersma, "Rotational diffusion constant of a cylindrical particle," *The Journal of Chemical Physics*, vol. 32, p. 1626, 1960.

[20] M. M. Tirado, C. L. Martínez, and J. G. de la Torre, "Comparison of theories for the translational and rotational diffusion coefficients of rod like macromolecules. Application to short DNA fragments," *The Journal of Chemical Physics*, vol. 81, p. 2047, 1984.

[21] N. Metropolis, A. W. Rosenbluth, M. N. Rosenbluth, A. H. Teller, and E. Teller, "Equation of state calculations by fast computing machines," *The Journal of Chemical Physics*, vol. 21, no. 6, pp. 1087–1092, 1953.

[22] P. N. Pusey and W. Van Megen, "Phase behaviour of concentrated suspensions of nearly hard colloidal spheres," *Nature*, vol. 320, no. 6060, pp. 340–342, 1986.

[23] B. J. Alder and T. E. Wainwright, "Phase transition for a hard sphere system," *The Journal of Chemical Physics*, vol. 27, p. 1208, 1957.

[24] W. W. Wood and J. D. Jacobson, "Preliminary results from a recalculation of the Monte Carlo equation of state of hard spheres," *The Journal of Chemical Physics*, vol. 27, p. 1207, 1957.

[25] P. G. Bolhuis, D. Frenkel, S. C. Mau, D. A. Huse, and L. V. Woodcock, "Entropy difference between crystal phases," *Nature*, vol. 388, p. 235, 1997.

[26] V. J. Anderson and H. N. Lekkerkerker, "Insights into phase transition kinetics from colloid science," 2002.

[27] A. Kuijk, D. V. Byelov, A. V. Petukhov, A. Van Blaaderen, and A. Imhof, "Phase behavior of colloidal silica rods," *Faraday Discussions*, vol. 159, p. 181, 2012.

[28] P. G. de Gennes and J. Prost, *The Physics of Liquid Crystals*. Oxford University Press, 1995.

[29] P. Bolhuis and D. Frenkel, "Tracing the phase boundaries of hard spherocylinders," *The Journal of Chemical Physics*, vol. 106, p. 666, 1997.

[30] H. N. W. Lekkerkerker and G. J. Vroege, "Liquid crystal phase transitions in suspensions of mineral colloids: new life from old roots.," *Philosophical transactions. Series A, Mathematical, physical, and engineering sciences*, vol. 371, no. 1988, 2013.

[31] V. N. Manoharan, M. T. Elsesser, and D. J. Pine, "Dense packing and symmetry in small clusters of microspheres," *Science*, vol. 301, pp. 483–487, 2003.

[32] B. De Nijs, S. Dussi, F. Smallenburg, J. D. Meeldijk, D. J. Groenendijk, L. Filion, A. Imhof, A. Van Blaaderen, and M. Dijkstra, "Entropy-driven formation of large icosahedral colloidal clusters by spherical confinement," *Nature Materials*, vol. 14, no. 1, pp. 56–60, 2015.

[33] F. C. Frank, "Supercooling of liquids," *Proceeding of the Royal Society of London*, vol. 215, p. 1120, 1952.

[34] J. H. Conway, *Spheres packings, lattices and groups*. New York: Springer-Verlag, 1998.

[35] D. Frenkel and B. Smit, "Understanding Molecular Simulation," 2002.

[36] B. Leimkuhler and C. Matthews, *Molecular Dynamics with Deterministic and Stochastic Numerical Methods*. Spinger, 2014.

[37] E. Purcell, "Life at low Reynolds number," *American Journal of Physics*, vol. 45, pp. 3–11, 1977.

[38] B. Leimkuhler and C. Matthews, "Rational construction of stochastic numerical methods for molecular sampling," *Applied Mathematics Research eXpress*, vol. 1, pp. 34–56, 2013.

[39] T. H. Besseling, *Self-assembly of colloidal spheres and rods in external fields*. PhD thesis, 2014.

[40] J. B. Pawley, *Handbook of biological confocal microscopy: Third edition*. 2006.

[41] A. Janeković and E. Matijević, "Preparation of monodispersed colloidal cadmium compounds," *Journal of Colloid And Interface Science*, vol. 103, pp. 436–447, 1985.

[42] D. Seo, C. P. Ji, and H. Song, "Polyhedral gold nanocrystals with Oh symmetry: From octahedra to cubes," *Journal of the American Chemical Society*, vol. 46, pp. 14863–14870, 2006.

[43] S. I. R. Castillo, S. Ouhajji, S. Fokker, B. H. Erné, C. T. W. M. Schneijdenberg, D. M. E. Thies-Weesie, and A. P. Philipse, "Silica cubes with tunable coating thickness and porosity: From hematite filled silica boxes to hollow silica bubbles," *Microporous and Mesoporous Materials*, vol. 195, pp. 75–86, 2014.

[44] P. M. Johnson, C. M. Van Kats, and A. Van Blaaderen, "Synthesis of colloidal silica dumbbells," *Langmuir*, vol. 24, pp. 11510–11517, 2005.

[45] F. Hagemans, E. B. Van Der Wee, A. Van Blaaderen, and A. Imhof, "Synthesis of Cone-Shaped Colloids from Rod-Like Silica Colloids with a Gradient in the Etching Rate," *Langmuir*, vol. 32, pp. 3970–3976, 2016.

[46] F. Hagemans, W. Vlug, C. Raffaelli, A. Van Blaaderen, and A. Imhof, "Sculpting Silica Colloids by Etching Particles with Nonuniform Compositions," *Chemistry of Materials*, vol. 29, pp. 3304–3313, 2017.

[47] W. Stöber, A. Fink, and E. Bohn, "Controlled growth of monodisperse silica spheres in the micron size range," *Journal of Colloid And Interface Science*, vol. 26, pp. 62–69, 1968.

[48] A. K. Van Helden, J. W. Jansen, and A. Vrij, "Preparation and characterization of spherical monodisperse silica dispersions in nonaqueous solvents," *Journal of Colloid And Interface Science*, vol. 81, no. 2, pp. 354–368, 1981.

[49] G. H. Bogush, M. A. Tracy, and C. F. Zukoski IV, "Preparation of monodisperse silica particles: Control of size and mass fraction," *Journal of Non-Crystalline Solids*, vol. 104, no. 1, pp. 95–106, 1988.

[50] A. Van Blaaderen, J. Van Geest, and A. Vrij, "Monodisperse colloidal silica spheres from tetraalkoxysilanes: Particle formation and growth mechanism," *Journal of Colloid And Interface Science*, vol. 154, pp. 481–501, 1992.

[51] A. Kuijk, A. Van Blaaderen, and A. Imhof, "Synthesis of monodisperse, rodlike silica colloids with tunable aspect ratio," *Journal of the American Chemical Society*, vol. 133, pp. 2346–2349, 2011.

[52] S. Dussi, *When shape is enough: from colloidal spheres to twisted polyhedra, from icosahedral to chiral order*. Phd thesis, University of Utrecht, 2016.

[53] P. J. Steinhardt, D. R. Nelson, and M. Ronchetti, "Bond-orientational order in liquids and glasses," *Physical Review B*, vol. 28, no. 2, pp. 784–805, 1983.

[54] N. a. M. Verhaegh and A. V. Blaaderen, "Dispersions of Rhodamine-Labeled Silica Spheres: Synthesis, Characterization, and Fluorescence Confocal Scanning Laser Microscopy," *Langmuir*, vol. 10, pp. 1427–1438, 1994.

[55] A. Kuijk, A. Imhof, M. H. W. Verkuijlen, T. H. Besseling, E. R. H. Van Eck, and A. Van Blaaderen, "Colloidal silica rods: Material properties and fluorescent labeling," *Particle and Particle Systems Characterization*, vol. 31, no. 6, pp. 706–713, 2014.

[56] C. Kennedy, *ccc3D Real-space Measurement on Colloidal Silica Rods in a Gravitational Field*. Master thesis, University of Utrecht, 2014.

[57] R. G. Lebel and D. A. Goring, "Density, Viscosity, Refractive Index, and Hygroscopicity of Mixtures of Water and Dimethyl Sulfoxide," *Journal of Chemical and Engineering Data*, vol. 7, no. 1, pp. 100–101, 1962.

[58] Glycerine Producers' Association, "Physical properties of glycerin and its solutions," p. New York : Glycerine Producers' Association, 1963.

[59] H. T. VAN DER VOORT and K. C. STRASTERS, "Restoration of confocal images for quantitative image analysis," *Journal of Microscopy*, vol. 178, no. 2, pp. 165–181, 1995.

[60] J. C. Crocker and D. G. Grier, "Methods of digital video microscopy for colloidal studies," *Journal of Colloid and Interface Science*, vol. 179, no. 1, pp. 298–310, 1996.

[61] C. Vega and S. Lago, "A fast algorithm to evaluate the shortest distance between rods," *Computers and Chemistry*, vol. 18, no. 1, pp. 55–59, 1994.

[62] A. Cuetos and M. Dijkstra, "Kinetic pathways for the isotropic-nematic phase transition in a system of colloidal hard rods: A simulation study," *Physical Review Letters*, vol. 98, no. 9, 2007.

[63] M. Cifelli, G. Cinacchi, and L. De Gaetani, "Smectic order parameters from diffusion data," *Journal of Chemical Physics*, vol. 125, no. 16, 2006.

[64] M. van der Linden, *Real-space structure of colloidal hard-sphere glasses in experiments and simulations*. PhD thesis, 2008.

[65] T. H. Besseling, M. Hermes, A. Kuijk, B. De Nijs, T. S. Deng, M. Dijkstra, A. Imhof, and A. Van Blaaderen, "Determination of the positions and orientations of concentrated rod-like colloids from 3D microscopy data," in *Journal of Physics Condensed Matter*, vol. 27, 2015.

[66] M. A. Bates and D. Frenkel, "Influence of polydispersity on the phase behavior of colloidal liquid crystals: A Monte Carlo simulation study," *Journal of Chemical Physics*, vol. 109, p. 6193, 1998.

[67] H. Yuen, J. Princen, J. Illingworth, and J. Kittler, "Comparative study of Hough Transform methods for circle finding," *Image and Vision Computing*, 1990.

[68] J. C. Loudet, A. M. Alsayed, J. Zhang, and A. G. Yodh, "Capillary Interactions Between Anisotropic Colloidal Particles," *Phys. Rev. Lett.*, vol. 94, no. 1, p. 18301, 2005.

[69] D. El Masri, T. Vissers, S. Badaire, J. C. Stiefelhagen, H. R. Vutukuri, P. Helfferich, T. H. Zhang, W. K. Kegel, A. Imhof, and A. Van Blaaderen, "A qualitative confocal microscopy study on a range of colloidal processes by simulating microgravity conditions through slow rotations," *Soft Matter*, vol. 8, no. 26, pp. 6979–6990, 2012.

[70] T. Koda, M. Numajiri, and S. Ikeda, "Smectic-A Phase of a Bidisperse System of Parallel Hard Rods and Hard Spheres," *Journal of the Physical Society of Japan*, vol. 65, no. 11, pp. 3551–3556, 1996.

[71] M. Adams, Z. Dogic, S. L. Keller, and S. Fraden, "Entropically driven microphase transitions in of colloidal rods and spheres," *Nature*, vol. 393, no. 6683, pp. 349–352, 1998.

[72] H. E. Bakker, S. Dussi, B. L. Droste, T. H. Besseling, C. L. Kennedy, E. I. Wiegant, B. Liu, A. Imhof, M. Dijkstra, and A. Van Blaaderen, "Phase diagram of binary colloidal rod-sphere mixtures from a 3D real-space analysis of sedimentation-diffusion equilibria," *Soft Matter*, vol. 12, pp. 9238–9245, nov 2016.